Diploma Thesis

Global-Local Finite Element Analysis

Konstantinos Tatsis

Supervisor: Professor Manolis Papadrakakis

INSTITUTE OF STRUCTURAL ANALYSIS AND SEISMIC RESEARCH
SCHOOL OF CIVIL ENGINEERING
NATIONAL TECHNICAL UNIVERSITY OF ATHENS

Athens, Greece
May, 2014

Diploma Thesis

Global-Local Finite Element Analysis

Konstantinos Tatsis

Supervisor: Professor Manolis Papadrakakis

Athens, Greece
May, 2014

Konstantinos Tatsis (2014).
Diploma Thesis
Global Local Finite Element Analysis
Institute of Structural Analysis and Seismic Research
School of Civil Engineering
National Technical Univarsity of Athens, Greece

Contents

List of Figures

List of Tables

Περίληψη

Η αναλυτική επίλυση πολύπλοκων προβλημάτων της μηχανικής στις μέρες μας καθίσταται δυσχερής έως αδύνατη χωρίς την εφαρμογή αριθμητικών μεθόδων και τη χρήση ηλεκτρονικού υπολογιστή. Η μέθοδος των πεπερασμένων στοιχείων αποτελεί σήμερα ένα ισχυρό εργαλείο για την επίλυση τέτοιων προβλημάτων και εξελίσσεται με μεγάλη ταχύτητα τόσο σε ακαδημαικό όσο και σε επαγγελματικό επίπεδο. Ενδεικτικά, αν και επινοήθηκε και εφαρμόστηκε για τη στατική ανάλυση φορέων, έχει καθολικότερη εφαρμογή σε μία ευρύτερη κατηγορία προβλημάτων του μηχανικού όπως στη ρευστομηχανική, στη μεταφορά θερμότητας, στην ακουστική, στον ηλεκτρομαγνητισμό και στην εμβιομηχανική. Επιπλέον, η εξέλιξη των Η/Υ με τις ολοένα και μεγαλύτερες δυνατότητες διαχείρισης όγκου δεδομένων αλλά και με την αύξηση της ταχύτητας εκτέλεσης των αριθμητικών πράξεων κατέστησε εφικτή την επίλυση σύνθετων προβλημάτων τα οποία θεωρούνταν απροσπέλαστα πριν μερικά χρόνια.

Στην κατηγορία αυτή, των προβλημάτων αυξημένου υπολογιστικού κόστους, ανήκει και η καταστατική περιγραφή πολυφασικών υλικών. Είναι γεγονός ότι το μεγαλύτερο μέρος των παραγόμενων δομικών υλικών σήμερα παρουσιάζει κάποιο είδος ανομοιογένειας, διακριτή ή μη στην κλίμακα των δομικών έργων. Χαρακτηριστικά παραδείγματα αποτελούν τα κράματα μετάλλων, τα πορώδη, τα πολυκρυσταλλικά και τα σύνθετα υλικά στα οποία το μέγεθος, το σχήμα και οι ιδιότητες των συστατικών τους μερών καθορίζουν άμεσα τη συνολική τους μηχανική συμπεριφορά.

Διάφορες τεχνικές έχουν αναπτυχθεί για την προσομοίωση και την περιγραφή της απόκρισης ανομοιογενών υλικού. Η παρούσα εργασία επικεντρώνεται στη μέθοδο ομογενοποίησης πολλαπλών κλιμάκων (first-order computational homogenization) η οποία συνίσταται στην επίλυση δύο εμφωλευμένων προβλημάτων συνοριακών τιμών, για τη μακροκλίμακα και την μικροκλίμακα αντίστοιχα. Τα βασικά χαρακτηριστικά μιας τέτοιας μεθόδου είναι ότι

- Δεν απαιτείται η περιγραφή των καταστατικών νόμων του μακροφορέα.
- Παρέχει τη δυνατότητα ενσωμάτωσης μεγάλων παραμορφώσεων και στροφών τόσο στην προσομοίωση της μικροκλίμακας όσο και του μακροφορέα.
- Παρέχει τη δυνατότητα λεπτομερούς προσομοίωσης των συστατικών μερών

της μικροκλίμακας.

- Επιτρέπει οποιαδήποτε τεχνική προσομοίωσης στην κλίμακα του μικροφορέα.

Αναλυτικά, σύμφωνα με τη μέθοδο αυτή, υπολογίζεται το διάνυσμα ανηγμένων παραμορφώσεων σε κάθε υλικό σημείο του μακροφορέα το οποίο στη συνέχεια χρησιμοποιείται για τη μόρφωση των συνοριακών συνθηκών του αντιπροσωπευτικού μικροφορέα (RVE - Representative Volume Element) στο αντίστοιχο σημείο. Μετά την επίλυση του προβλήματος συνοριακών τιμών της μικροκλίμακας, το διάνυσμα των τάσεων του μακροφορέα υπολογίζεται μέσα από τη διαδικασία ομογενοποίησης του πεδίου των τάσεων και κατά τον τρόπο αυτό υπολογίζεται η σχέση τάσεων-παραμορφώσεων για κάθε υλικό σημείο.

Ωστόσο, υπάρχουν κάποιοι περιορισμοί στην εφαρμογή της εν λόγω υπολογιστικής τεχνικής. Συγκεκριμένα, παρά το ότι κατά την προσομοίωση λαμβάνονται υπ' όψην οι διάφορες παράμετροι της μικροκλίμακας όπως το ποσοστό όγκου, η κατανομή και η μορφολογία των συστατικών μερών του υλικού, τα αποτελέσματα της μεθόδου είναι αναξάρτητα από το απόλυτο μέγεθος του αντιπροσωπευτικού όγκου της μικροκλίμακας (RVE).

Παρ' όλα αυτά, η τεχνική ομογενοποίησης στα πλαίσια ανάλυσης πολλαπλών κλιμάκων αποτελεί ένα σημαντικό εργαλείο για τον υπολογισμό των καταστατικών σχέσεων πολυφασικών υλικών στα οποία είναι αδύνατη η εφαρμογή οποιασδήποτε άλλης μεθόδου.

Abstract

Nowadays, analysis of complicated problems in the domain of mechanics constitutes a hard and even impossible task without the implementation of numerical methods and the employment of computational machines. Finite element method is a powerful tool for the solution of such problems and is rapidly developed in an academic and professional sense. Even if it was developed and implemented for structural analysis, it is widely employed in several domains such as in fluid mechanics, heat transfer, acoustics and electromagnetism. Furthermore, the development of computer hardware in terms of data processing, has significantly contributed to the solution of problems that were considered inaccessible a few years ago.

Most of the materials produced in industry are heterogeneous on one or another spatial scale. Typical examples include metal alloy systems, porous media and polycrystalline materials and composites. The overall response of these micro-heterogeneous materials depends strongly on the size, shape properties and spatial distribution of the microstructural components.

Several techniques have been developed for the prediction of the macroscopic behavior of such materials. The present work is concentrated on the first order homogenization technique in the framework of a multi-scale approach which consists of the solution of two nested boundary value problems, for the macro-scale and the micro-scale respectively. Methods of this type

- Do not require any constitutive assumption with respect to the overall material behavior.
- Enable the incorporation of large deformations and rotations on both micro and macrolevel.
- Provide the possibility to introduce detailed microstructural information.
- Allow the use of any modelling technique at the microlevel.

Concretely, according to this approach, the macroscopic deformation tensor is calculated for every integration point of the macrostructure and then is used to

formulate the kinematic boundary conditions for the associated microstructural representative volume element (RVE). After the solution of the microstructural boundary value problem, the macroscopic stress tensor is computed by averaging the resulting microstructural stress field over the volume of the RVE and as a result, we obtain the stress-strain relation at every macroscopic point.

However, there is a major disadvantage of the existing first-order computational homogenization. More specifically, this technique can account for the volume fraction, distribution and morphology of the micro-components however, it cannot take into account the absolute size of the microstructure making it thus impossible to treat microstructural size effects.

Nevertheless, computational homogenization provides a significant strategy to obtain micro-macro structure-property relations for materials for which the overall macroscopic response cannot be computed by any other method.

Chapter 1

Introduction

1.1 Multi-phase Materials

The heterogeneous nature of industrial and engineering materials has an important impact on their macroscopic response. Several phenomena of the macrolevel derive from the mechanical behavior of the underlying microstructure. In other words, the microstructural morphology, that is size, shape, spatial distribution and properties of the microstructural components, has a significant influence over the response of multi-phase materials. Consequently, these microstructural influences are important for the life performance of the material and products made thereof.

Determination of the macroscopic properties of heterogeneous materials is a requirement in many engineering problems. This relation between microstructural phenomena and macroscopic response also enables the design of a material microstructure such that the obtained macroscopic behavior presents the required characteristics. Furthermore, performing straightforward experimental measurements on a number of material samples of different sizes, for various geometrical and physical properties, volume fractions and loading paths is a hardly feasible task in terms of time and costs. Consequently, there is a clear need for numerical approaches that provide a better understanding of property relations between micro and macro scales for multiphase materials.

Among several techniques for homogenization of engineering materials, a promising one, namely the multiscale computational homogenization or also called global-local analysis, has been developed in recents years, with its basic ideas presented in various papers as mentioned in [2]. According to this approach, the constitutive equations are not obtained in a closed-form but the stress-strain relationship is computed at every point of interest of the macrostructure by detailed modelling of the microstructure assigned to that point. Hence, such method (i) do not require any constitutive assumption with respect to the overall material behavior, (ii) enable the incorporation of large deformations and rotations on both micro and macrolevel, (iii) provide the possibility to introduce detailed microstructural information, and (iv) allow the use of any modelling technique at the microlevel, sush as the finite element method.

Although the fully nested multiscale method is still computationally expensive, it seems that this can be overcome by parallel computation techniques. Moreover, a selective version can be empolyed where non-critical regions are modelled by continuum closed-form homoge-

nized constitutive relations or by the constitutive tangents obtained from the microstructural analysis but kept constant in the elastic domain, while in the critical regions the multi-scale analysis of the microstructure is fully performed. Despite the required computational efforts, the numerical homogenization approach seems to be a versatile tool to establish micro-macro structure-property relations in materials, where the collective behaviour of an evolving multi-phase heterogeneous material is not yet possible to predict by any other method. Furthermore, this technique can also be used to evaluate and verify other homogenization methods and constitutive models.

Finally, it should be noted that there is a major disadvantage of the existing first-order computational homogenization. More specifically, this technique can account for the volume fraction, distribution and morphology of the micro-components but it cannot take into account the absolute size of the microstructure making it thus impossible to treat microstructural size effects. However, it still provides a significant strategy to obtain micro-macro structure-property relations when other methods cannot be employed.

1.2 Scope and Outline

The aim of this thesis is the code developement of computational homogenization techniques for the multi-scale modelling of non-linear deformation processes of evolving components. In the framework of this purpose, MATLAB is used as the link element between mathematical approach and numerical examples where the mathematical formulations of the following chapters are entirely programmed in the aforementioned environment.

In **Chapter 2** the first-order computational homogenization approach is introduced. The basic assumptions of the technique are remarked and a detailed description of the formulation using finite element method is given. The scale bridging theorems are discussed for the case of kinematic boundary conditions and the nested solution scheme of a multiscale analysis is presented. Finally, in the last part of this chapter, two different approaches, namely lagrange multipliers and direct condensation, are illustrated and extensively described for the incorporation of boundary conditions into the microscale problem.

Chapter 3 is concentrated on the fundamentals of non-linear solid mechanics and namely in elasto-plastic model. A von-Mises criterion is employed in the framework of this work, using two different schemes, and the integration procedures of the stress-strain relations are presented in detail, through an incremental strain approach. Based on these formulations, the developed algorithm is then illustrated and presented through tables and figures.

In **Chapter 4** the non-linear analysis methods are developed. More specifically, the first part of this chapter describes the load control version of the Newton-Raphson scheme, including full, modified and initial methods, while in the second part, the displacement control version is illustrated and a comparison of the two approaches is performed.

In **Chapter 5** the modeling techniques of the performed analyses are explained, in the framework of the finite element method. Emphasis is given on the simulation of the microstructural components of the investigated Representative Volume Element (RVE), concentrating thus on the surrounding polymer, the reinforcing fibers and their interfacial mechanism.

Chapter 6 contains the numerical results of the performed analyses. A nested procedure

is examined in the first part, where an L-shaped domain constitutes the macrostructural model and a fiber reinforcing material is assigned to the microlevel. The same RVE is then further investigated in terms of microstructural mechanics, where the influence of non-linear effects is taken into account. Concretely, an elasto-plastic model is employed for the behavior of the surrounding polymer and four different cases of interfacial mechanisms are examined and the response of the microstructure is obtained for the imposed normal strains in x and y directions.

Finally, **Chapter 7** gives a brief summary of the conclusions of the present work and remarks on some perspectives of future research.

Chapter 2

First-order Homogenization

2.1 Introduction

The description of the macroscopic overall response of a heterogeneous material with complex microstructure in an averaged or homogenized sense, constitutes an important component of continuum micromechanics. Analytical approaches are restricted in many cases, especially with respect to the geometry of the representative microstructure and its constitutive response. In this sense, various numerical methods have been developed in recent years which produce fine-scale fields on the representative microstructure.

Computational homogenization is one of these multi-scale techniques, which is based on the description of the local macroscopic constitutive response through the appropriate definition and solution of a boundary value problem in the micro-scale. The fundamental principles of the first-order homogenization can be included in the following four points: (i) definition of the microstructural representative volume element (RVE), of which the constitutive response of its components is assumed to be known; (ii) definition of the microscopic boundary conditions through the macro-to-micro transition; (iii) calculation of the macroscopic output variables through the micro-to-macro transition; (iv) prevail the numerical and constitutional relation between the macroscopic input and output variables.

2.2 Basic Assumptions

As mentioned in [2] we assume that the considered material configuration is macroscopically homogeneous, or sufficiently homogeneous, but microscopically heterogeneous consisted of several perceptible components. Either we assume a statistical homogeneity or a spatial periodicity for the employed materials, we need to define a subvolume $\Omega \subset \Re^d$ (d = 2,3), of length l, the aforementioned representative volume element (RVE), which will describe properly the material heterogeneities. This subvolume Ω, in the context of the principle of separation of scales, has to be small enough in order to be regarded as a point at the coarse-scale level ($l << l_M$ where l_M is the length of the macrocontinuum).

In the following homogenization scheme (first order homogenization), the macroscopic deformation tensor ϵ_M is calculated for every material point of the macrostructure, that is the integration points of the macroscopic mesh. From now on, the subscript "M" will denote

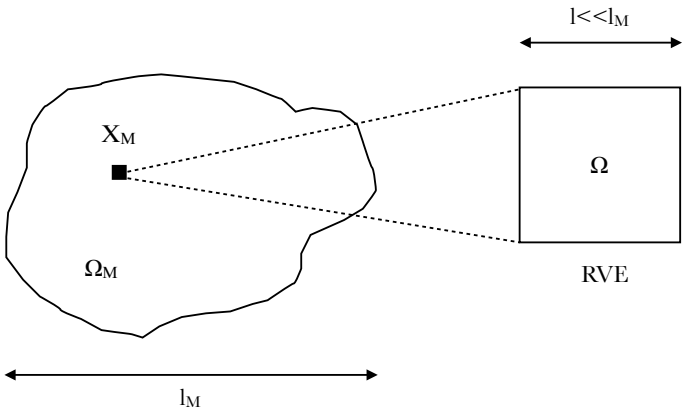

Figure 2.1: Macrostructure and microstructure associated with the macroscopic position X_M

macroscale while the subscript "m" will refer to the macroscale. Then the deformation tensor ϵ_M is employed to define the boundary conditions on the RVE that is assigned to this point and through the boundary value problem solution of the RVE, the macrostress tensor σ_M is calculated as the average stress field of the RVE. As a result, we obtain the stress-deformation relationship at the macroscopic scale and the consistent tangent of the macroscale through the microstructural stiffness.

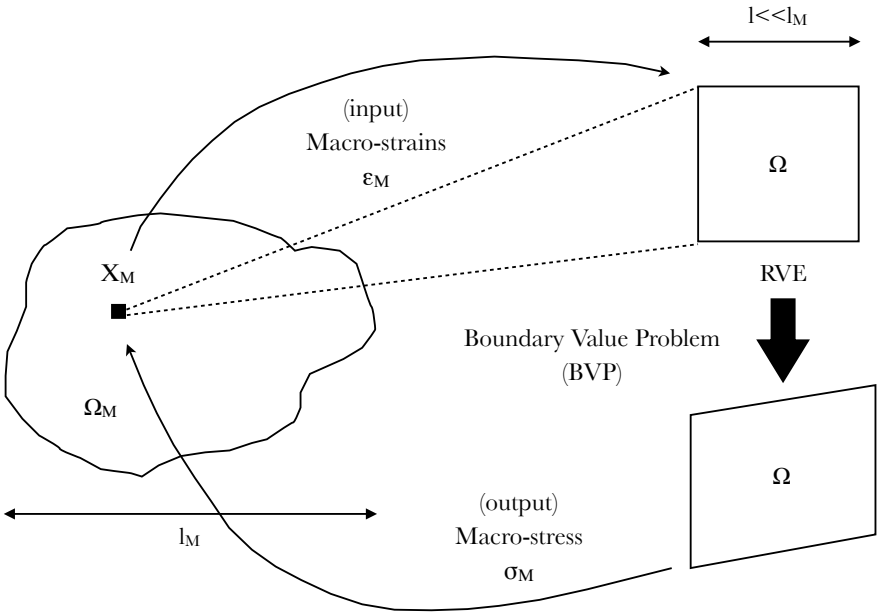

Figure 2.2: First-order homogenization

This formulation is called strain-driven since microstructural response is driven by the macro-strains and the problem is defined as follows: given a macroscopic deformation tensor ϵ_M, calculate the macro stress σ_M and the constitutive tangent, according to the response of

the associated microstructure.

2.3 The Microscale Problem

As already mentioned in Section 2.1, the constitutive behavior of the macrostructure is not a priori defined, but it is computed through the averaged microstructural response. Hence, the first step of a multiscale scheme is the definition of the microscale problem, that is the description of the representative volume element (RVE). Such a task, requires the geometrical properties and the constitutive laws for each micro-component, specifying a stress deformation relatioship

$$\sigma_m^i = f(\epsilon_m^i), \qquad i = 1, 2, ...n \tag{2.1}$$

where i denotes the index of the microstructural components to be distinguished. A further theoretical discussion over the employed constitutive laws for this thesis is presented in Chapter 3, which deals with material non-linearity.

Once defined the representative volume element, the next step includes the imposition of the macroscale output (deformation gradient tensor ϵ_M) on the RVE. Various approaches have been proposed for this task (including stress-driven formulations) however, in the present project only the strain-driven boundary conditions will be implemented and concretely, the prescribed displacements and the prescribed periodicity.

In the first case, where linear displacements are imposed as boundary conditions, the displacements of a point A on the boundary are given by

$$u(x,t) = \overline{\epsilon}_M(t)x, \quad x \in \partial\Omega \tag{2.2}$$

From the opposing point of view, prescribed periodicity on the boundary can be expressed by the following relations

$$u(x^+,t) - u(x^-,t) = \overline{\epsilon}_M(t)(x^+ - x^-), \quad x^+, x^- \in \partial\Omega \tag{2.3}$$

Here, we need to declare that, for this type of conditions, the boundary $\partial\Omega$ is decomposed into two parts, $\partial\Omega^+$ and $\partial\Omega^-$, so that $\partial\Omega = \partial\Omega^+ \cup \partial\Omega^-$. Hence, the position vectors x^+ and x^- denote the position vectors of boundary points of parts $\partial\Omega^+$ and $\partial\Omega^-$ respectively.

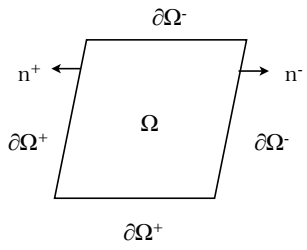

Figure 2.3: Schematic decomposition of the boundary into $\partial\Omega^+$ and $\partial\Omega^-$ parts

2.4 The Scale Bridging

The scale bridging, that is the connection of the two scales, is completed through average relations depending on the involved averaged quantities. In the present work, due to the implemented coupling quantities, that is the strains, two of the averaging theorems, the deformation and the internal work, will be presented along with the consistency of the employed boundary conditions. For the sake of generality, it should be noted that the stress averaging relation can also be employed as a coupling theorem however, only in a stress-driven formulation.

2.4.1 Deformation

This averaging relation is implemented for the connection of kinematic quantities between the micro and macro structure. More specifically, according to this theorem the deformation gradient tensor ϵ_M of the macrostructure must equal to the volume average of the corresponding deformation gradient tensor ϵ_m of the microstructure

$$\epsilon_M = \frac{1}{|\Omega|}\int_\Omega \epsilon_M d\Omega = \frac{1}{|\Omega|}\int_{\partial\Omega} u(x)\vec{n}dS \tag{2.4}$$

where in order to transform the volume integral over Ω to a surface integral of the RVE we use the divergence theorem. Now, if we substitute equation 2.2 into 2.4 we can easily verificate that linear displacements, as boundary conditions, satisfy the previous averaging relation

$$\epsilon_M = \frac{1}{|\Omega|}\int_{\partial\Omega} (\epsilon_M x)\vec{n}dS = \frac{1}{|\Omega|}\epsilon_M \int_{\partial\Omega} x\vec{n}dS$$

$$= \frac{1}{|\Omega|}\epsilon_M \int_\Omega (\nabla x)d\Omega = \epsilon_M \tag{2.5}$$

In the same way, the validation of the periodic boundary conditions can be verificated through the substitution of equation 2.3 into 2.4

$$\epsilon_M = \frac{1}{|\Omega|}\Big(\int_{\partial\Omega^+} u(x^+)\vec{n}dS + \int_{\partial\Omega^-} u(x^-)\vec{n}dS\Big) = \frac{1}{|\Omega|}\int_{\partial\Omega^+}\Big(u(x^+) - u(x^-)\Big)\vec{n}^+dS$$

$$= \frac{1}{|\Omega|}\epsilon_M \int_{\partial\Omega^+}(x^+ - x^-)\vec{n}^+dS = \frac{1}{|\Omega|}\epsilon_M\int_{\partial\Omega} x\vec{n}dS = \epsilon_M \tag{2.6}$$

while this time the surface integral must be decomposed into the two parts concerning the boundary $\partial\Omega^+$ and $\partial\Omega^-$ respectively. Consequently, both the linear and periodic displacements are formulated consistent with the deformation averaging theorem.

2.4.2 The Energy Averaging Theorem

The energy theorem, also know as the *Hill-Mandel* principle of macrohomogeneity, states that the stress work at any point x_M of the macrostructure must equal to the volume average work of the corresponding RVE, so that fine- and coarse-scale are energetically equivalent. The variational statement of this principle is as follows: let σ be an admissible micro-scale stress field and σ_M the associated macroscopic stress tensor, then the realtion

$$\sigma_M^T \delta\epsilon_M = \frac{1}{|\Omega|}\int_\Omega \sigma_m^T \delta\epsilon_m d\Omega \tag{2.7}$$

must hold for any kinematically admissible strain change $\delta\epsilon_m$. Now, if we transform the right-hand side of equation 2.7 into a surface integral, we obtain

$$\delta W_\Omega = \frac{1}{|\Omega|}\int_\Omega \sigma_m^T \delta\epsilon_m d\Omega = \frac{1}{|\Omega|}\int_{\partial\Omega} F\delta u(x) d\partial\Omega \tag{2.8}$$

where we take into account the equilibrium state of the microstructure and the relation

$$\nabla\big(\sigma_m^T \delta u(x)\big) = \big(\nabla\sigma_m^T\big)\delta u(x) + \sigma_m^T\big(\nabla\delta u(x)\big)$$

or

$$\sigma_m^T\big(\nabla\delta u(x)\big) = \nabla\big(\sigma_m^T\delta u(x)\big) - \big(\nabla\sigma_m^T\big)\delta u(x) \tag{2.9}$$

Consequently, as already done for the deformation theorem, we need to verify that both the kinematic boundary conditions satisfy the Hill-Mandel condition. In the first case, (linear displacements) we work as in section 1.4.1 by substituting equation 2.2 into 2.8 which gives

$$\delta W_\Omega = \frac{1}{|\Omega|}\int_{\partial\Omega} F(\delta\epsilon_M x) dS = \frac{1}{|\Omega|}\bigg(\int_{\partial\Omega} F x dS\bigg)^T \delta\epsilon_M = \sigma_M^T \delta\epsilon_M \tag{2.10}$$

Similarly, if we substitute equation 2.3 into 2.8 we take

$$\begin{aligned}
\delta W_\Omega &= \frac{1}{|\Omega|}\bigg(\int_{\partial\Omega^+} F\delta u(x^+) dS + \int_{\partial\Omega^-} F\delta u(x^-) dS\bigg) \\
&= \frac{1}{|\Omega|}\int_{\partial\Omega^+} F\big(\delta u(x^+) - \delta u(x^-)\big) dS = \frac{1}{|\Omega|}\bigg(\int_{\partial\Omega} F(x^+ - x^-) dS\bigg)^T \delta\epsilon_M \\
&= \frac{1}{|\Omega|}\bigg(\int_{\partial\Omega} F x dS\bigg)^T = \sigma_M^T \delta\epsilon_M
\end{aligned} \tag{2.11}$$

and thus we prove that periodic boundary conditions also satisfy the energy averaging theorem, where again the surface integral was decomposed into the parts $\partial\Omega^+$ and $\partial\Omega^-$.

2.5 Nested Scheme

According to the above developed theory, the entire first-order homogenization process can be described by a nested solution scheme consisted of a finite number of steps.

First of all, we need to declare that such a solution is approached through the implementation of the finite element method where both the micro and macro levels need to be discretized. Once obtained this discretization, a representative volume element (RVE) must be assigned to each integration point, that is a Gauss-point, and an incremental procedure must be defined for the imposition of the external load. Hence, the non-linear system of macro-equations is solved in an iterative manner through the employment of the Newton-Raphson method.

The first step of this algorithm consists in the initialization of the tangent macrostructural stiffness matrix $\partial F/\partial d$, required for the first load-increment. At this point, it should be clear that load-increment may refer to either the external forces or the prescribed displacements increment. Consequently, an infinitesimal micro-strain increment is produced for each RVE and the computed consitutive tangent is obtained through the overall microstructural response and then assigned to the corresponding integration point. As a result, the tangent stiffness matrix for the macrostructure can be initialized and implemented for iterative process.

Once initialized the stiffness matrix, the first load-increment, that is the first iteration of the first step of the Newton-Raphson method, is produced on the macro level and the nodal displacements are computed through the linearized equations. Now, the deformation state within each finite element is obtained and hence, the deformation gradient tensor $\delta\epsilon_M$ is calculated for each integration point through the deformation matrix B_{Mi}. Thus, each Gauss-point's deformation gradient tensor is assigned to the corresponding RVE as an input variable (called macro-to-micro transition) and the problem is then transferred to the micro level.

Now, for each RVE, the obtained input quantities are trasformed into the equivalent displacement values and imposed as boundary conditions, either linear or periodic. Thus, a displacement control non-linear analysis takes place for the computation of the overall RVE's response until an equilibrium state is reached. Here, it should be noted that each macro-iteration of the Newton-Raphson method equals to a micro-step for each Gauss-point. Hence, each macro-to-micro transition requires a full step of the iterative process within the RVEs, until a converged equilibrium state is achieved. The overall response of the microstructure is then averaged and the required quantities, averaged stress and constitutive tangent, are assigned to the corresponding integration point (micro-to-macro transition). When the computation of all microstructural RVEs is obtained, the problem is again transferred to the macro level.

At this point, the stress tensor and the constitutive tangent is available for every Gauss-point and thus the internal forces of the macrostructure can be computed. The convergence is then checked and if the external forces are in balance with the internal forces the next increment is produced. From the opposing point of view, if convergence is not achieved, the next iteration is produced in order to achieve an updated estimation of the macrostructural displacements and consequently, a new macro-to-micro transition is generated. The procedure now returns to the micro level and continues until a converged state is obtained.

Macro-scale		**Micro-scale**
A. Initialization		
• Initialize the macroscopic structure		
• Define the microstructure and assign an RVE to every integration point		
• Loop over all integration points	ε_M	
impose an infinitesimal strain	$\longrightarrow$	RVE Analysis
		• Impose boundary conditions
		• Solve the Boundary Value Problem
assign the tangent moduli to the integration point	$\longleftarrow$ C_{tM}	• Compute the tangent moduli C_{tM}
• End integration point loop		
B. Increment		
• Apply increment of the macro load		
C. Iteration		
• Get the macroscopic tangent stiffness		
• Solve the macroscopic system		
• Loop over all integration points	ε_M	
Compute ε_M	$\longrightarrow$	RVE Analysis
		• Impose boundary conditions
		• Solve the Boundary Value Problem
assign the stress and the tangent moduli to the integration point	$\longleftarrow$ C_{tM}	• Compute the stress σ_M and the tangent moduli C_{tM}
• End integration point loop		
• Compute the internal forces		
D. Convergence		
• If not converged $\Rightarrow$ return to C		
• Else go to B		

Table 2.1: Nested multi-scale scheme solution for the first-order homogenization

2.6 The Microequilibrium State

This section is focused on the equilibrium state of the microstructure and the required procedures for the computation of the overall stress σ_{Mij} and modular C_{Mij} at the integration points. In this sense, we consider a discretization of the RVE in terms of a mesh with N nodal points and a partition into those of the surface $\partial\Omega$ and those of the interior Ω where $B < N$ nodal points lie on the boundary. Now, the force vector

$$F = \begin{bmatrix} F_i \\ F_b \end{bmatrix} = \begin{bmatrix} T_i F \\ T_b F \end{bmatrix} \tag{2.12}$$

and the displacement vector

$$D = \begin{bmatrix} d_i \\ d_b \end{bmatrix} = \begin{bmatrix} T_i d \\ T_b d \end{bmatrix} \tag{2.13}$$

are partitioned according to this direction where T_i and T_b are boolean matrices which define the interior contributions and the contribution of the boundary, respectively. Similarly, we need to decompose the total stiffness matrix into the contributions associated with the interior and the boundary

$$K = \begin{bmatrix} K_{ii} & K_{ib} \\ K_{bi} & K_{bb} \end{bmatrix} = \begin{bmatrix} T_i K_{ii} T_i^T & T_i K_{ib} T_b^T \\ T_b K_{bi} T_i^T & T_b K_{bb} T_b^T \end{bmatrix} \tag{2.14}$$

so that the form of the equilibrium equations facilitate the imposition of the boundary conditions. Once obtained this partition, the next step includes the solution of the boundary value problem (BVP) and the computation of the averaged quantities.

2.6.1 Linear Displacements

According to this formulation, a linear mapping of the macrostrain ϵ_m into equivalent nodal displacement is imposed as constraint for each node i of the boundary $\partial\Omega$

$$d_n = \epsilon_M x_n \tag{2.15}$$

where $n = 1, 2, ..., B$ denotes the identity of the supported nodes, that is the boundary nodes. Now, if we express the above involved quantities in matrix form we obtain

$$\epsilon_M = \begin{bmatrix} \epsilon_{xx} \\ \epsilon_{yy} \\ \gamma_{xy} \end{bmatrix} \quad \text{and} \quad d_n = \begin{bmatrix} d_x \\ d_y \end{bmatrix}_n \tag{2.16}$$

where we assume a plane stress problem and thus the strain quantities are reduced to ϵ_{xx}, ϵ_{yy} and γ_{xy}. Hence, a more compact form of equation 2.14 takes the following form

$$d_n = P_n^T \epsilon_M \tag{2.17}$$

where P_n^T denotes the position matrix of the i-th node depending on the global node coordinates and in the case of plane stress it is given by the relation

$$P_n = \frac{1}{2} \begin{bmatrix} 2x_n & 0 \\ 0 & 2y_n \\ y_n & x_n \end{bmatrix} \tag{2.18}$$

Then, the global form of matrix P associated with all, K in number, boundary nodes is obtained through the assembled relation

$$P = \begin{bmatrix} P_1 & P_2 & ... & P_B \end{bmatrix} = \frac{1}{2} \begin{bmatrix} 2x_1 & 0 & 2x_2 & 0 & \cdots & 2x_B & 0 \\ 0 & 2y_1 & 0 & 2y_2 & \cdots & 0 & 2y_B \\ y_1 & x_1 & y_2 & x_2 & \cdots & y_K & x_B \end{bmatrix} \tag{2.19}$$

Consequently, a compact relation for the application of these constraints takes the following form

$$d_b - P^T \epsilon_M = 0 \tag{2.20}$$

and they can be incorporated into the equilibrium equations through the implementation of the Lagrange multiplier method or simply imposed as prescribed displacements if a displacement control analysis is employed. Thus, the microequilibrium state is obtained from the set of equations

$$F_i = 0 \tag{2.21a}$$
$$F_b - \lambda_1 = 0 \tag{2.21b}$$
$$d_b - P^T \epsilon_M = 0 \tag{2.21c}$$

where the Lagrange multiplier λ_1 denotes the external forces on the nodes of the boundary. The solution of the above set of equations is obtained within a Newton-Raphson iterative solution through the linearized relations

$$F_i + K_{ii}\delta d_i + K_{ib}\delta d_b = 0 \tag{2.22a}$$
$$F_b - \lambda_1 + K_{bi}\delta d_i + K_{bb}\delta d_b - \delta\lambda_1 = 0 \tag{2.22b}$$
$$d_b - P^T \epsilon_M + \delta d_b - P^T \delta\epsilon_M = 0 \tag{2.22c}$$

In order to approach the solution, a number of finite steps is produced, starting from the

displacement increment δd_b on the boundary. Assuming an equilibrium state, we get from 2.22c

$$\delta d_b = P^T \delta\epsilon \tag{2.23}$$

the displacement increments on the boundary and from 2.22a

$$\delta d_i = -K_{ii} K_{ib} \delta d_{ib} \tag{2.24}$$

the internal displacements increment. Then the increment of the internal forces is determined by equation 2.22a in terms of the condensed stiffness matrix K_{bb}^C

$$\delta\lambda_1 = K_{bb}^C P^T \delta\epsilon, \qquad \text{with} \qquad K_{bb}^C = K_{bb} - K_{bi} K_{ii}^{-1} K_{ib} \tag{2.25}$$

and the balance of internal and external forces is checked. If there is no convergence, a next iteration is produced, the displacements in the interior of the domain are updated using equation 2.22a

$$\delta d_i \leftarrow \delta d_i + \delta d_i', \qquad \text{where} \qquad \delta d_i' = -K_{ii}^{-1} F_i \tag{2.26}$$

and the iterative procedure is performed until a converged equilibrium state, in terms of internal forces, that is $\|F_i\| \leq tolerance$. Now, using equation 2.22b, we compute the surface forces of the RVE through

$$\lambda_1 = F_b(d) \tag{2.27}$$

Finally, expressing the nodal forces and stress in a matrix form

$$F_n = \begin{bmatrix} F_{nx} \\ F_{ny} \end{bmatrix}, \text{ and stresses } \quad \sigma_M = \begin{bmatrix} \sigma_{xx} \\ \sigma_{yy} \\ \tau_{xy} \end{bmatrix} \tag{2.28}$$

we obtain the overall macrostress of the representative volume in relation with the coordinate matrix of the boundary nodes

$$\sigma_M = \frac{1}{|\Omega|} \sum_{n=1}^{B} P_n \lambda_{n1} = \frac{1}{|\Omega|} \sum_{n=1}^{B} P_n F_{nb} \tag{2.29}$$

or in a more compact form, by using the total coordinate matrix P of the boundary

$$\sigma_M = \frac{1}{|\Omega|} P \lambda_1 = \frac{1}{|\Omega|} P F_b \tag{2.30}$$

Consequently, the stress sensitivity $\partial\sigma_M / \partial\epsilon_M$ is expressed through a differential form of the equation 2.30 which gives

$$\delta\sigma_M = \frac{1}{|\Omega|} P \delta\lambda_1 = \frac{1}{|\Omega|} P \delta F_b \tag{2.31}$$

and now if we substitute equation 2.25 into equation 2.31 we obtain

$$\delta\sigma_M = \frac{1}{|\Omega|} P\delta\lambda_1 = \frac{1}{|\Omega|} P\big(K_{bb}^C P^T \delta\epsilon_M\big) = \frac{1}{|\Omega|}\big(PK_{bb}^C P^T\big)\delta\epsilon_M \tag{2.32}$$

and thus the tangent constitutive modular matrix is given by

$$C_{Mt} = \frac{1}{|\Omega|} PK_{bb}^C P^T \tag{2.33}$$

in terms of the condensed stiffness matrix K_{bb}^C. In total, the above procedure is summarized in the presented algorithm of table 2.2

1. For each RVE, get the corresponding macrostrain ϵ_M and set the nodal displacements on the boundary
$$d_b = P^T \epsilon_M$$
2. Calculate the internal force vector F and the stiffness matrix K according to the partition of interior and boundary nodes
$$F = \begin{bmatrix} F_i \\ F_b \end{bmatrix}, \quad K = \begin{bmatrix} K_{ii} & K_{ib} \\ K_{bi} & K_{bb} \end{bmatrix}, \quad D = \begin{bmatrix} d_i \\ d_b \end{bmatrix}$$
3. Update the interior displacements using equation 2.22a
$$\delta d_i \leftarrow \delta d_i + \delta d_i', \qquad \text{where} \qquad \delta d_i' = -K_{ii}^{-1} F_i$$
and check the convergence.
4. If $\|F_i\|$ >tolerance, return to step 2, else go to 5.
5. Calculate the condensed stiffness matrix of the surface $\partial\Omega$
$$K_{bb}^C = K_{bb} - K_{bi} K_{ii}^{-1} K_{ib}$$
6. Compute the overall stress and tangent constitutive matrix
$$\sigma_M = \frac{1}{|\Omega|} PF_b, \quad C_{Mt} = \frac{1}{|\Omega|} PK_{bb}^C P^T$$
7. Assign the averaged quantities to the corresponding integration point of the macrostructure.

Table 2.2: Linear displacements' scheme

2.6.2 Periodic Displacements

In the case of periodic displacements, a kinematic constraint is also imposed on the boundary nodes, only this time a pair discretization of the surface need to be generated. Thus, the boundary is decomposed into nodes x^+ belonging to $\partial\Omega^+$ and x^- of $\partial\Omega^-$ as illustraded in figure 2.3 and the macro-to-micro transition is obtained through

$$d_n^+ - d_n^- = \epsilon_M(x^+ - x^-) \tag{2.34}$$

where now index $n = 1, 2, ..., P$ denotes the identity of the supported pair of nodes. Working in the same way as in the linear displacement formulation, we can rewrite equation 2.34 in a more compact form, using matrix notations

$$d_n^+ - d_n^- = \big(P_n^{+T} - P_n^{-T}\big)\epsilon_M, \quad \text{or} \quad Q_n d_b = P_n^T \epsilon_M \tag{2.35}$$

where Q_n is a topology matrix consited of (0,1,-1) values which expresses the connection between the n-th pair of nodes and hence we obtain constraint relation

$$Qd_b - P^T\epsilon_M = 0 \tag{2.36}$$

where again the assembled form of matrix $P = P^+ - P^-$ is constructed. Then, the method of Lagrange multipliers is adopted for the incorporation of the constraint equations into the equilibrium

$$F_i = 0 \tag{2.37a}$$
$$F_b - Q^T\lambda_2 = 0 \tag{2.37b}$$
$$Qd_b - P^T\epsilon_M = 0 \tag{2.37c}$$

where the multiplier λ_2 expresses the force acting on the node pairs of the surface. Now the solution is produced through an iterative procedure within the Newton-Raphson method from the following set of equations

$$F_i + K_{ii}\delta d_i + K_{ib}\delta d_b = 0 \tag{2.38a}$$
$$F_b - Q^T\lambda_2 + K_{bi}\delta d_i + K_{bb}\delta d_b + Q^T\delta\lambda_2 = 0 \tag{2.38b}$$
$$Qd_b - P^T\epsilon_M + Q\delta d_b - P^T\delta\epsilon_M = 0 \tag{2.38c}$$

however, this time the final equations need to be transformed in terms of the condensed stiffness matrix. Thus, we eliminate the internal displacements δd_i through equation 2.38a

$$\delta d_i = -K_{ii}^{-1}\big(F_i + K_{ib}\delta d_b\big) \tag{2.39}$$

and we substitute 2.39 into equation 2.38b in order to obtain the reduced set of equations

$$F_b^C - Q^T\lambda_2 + K_{bb}^C\delta d_b + Q^T\delta\lambda_2 = 0 \tag{2.40a}$$
$$Qd_b - P^T\epsilon_M + Q\delta d_b - P^T\delta\epsilon_M = 0 \tag{2.40b}$$

in terms of condensed force vector and stiffness matrix

$$F_b^C = F_b - K_{bi}K_{ii}^{-1}F_i, \quad K_{bb}^C = K_{bb} - K_{bi}K_{ii}^{-1}K_{ib} \tag{2.41}$$

Following the same direction as presented in Section 1.6.1, we obtain the solution of system 2.40 through an iterative process. Concretely, as a first step we compute from equation 2.40a the displacement increment

$$\delta d_b = -\big(K_{bb}^C\big)^{-1}\big(F_b^C - Q^T\lambda_2 + Q^T\delta\lambda_2\big) \tag{2.42}$$

and substituting into 2.40b we obtain the change of Lagrange multiplier

$$\delta\lambda_2 = \Big(Q\big(K_{bb}^C\big)^{-1}Q^T\Big)^{-1}\Big(Qd_b - P^T\epsilon_M - Q\big(K_{bb}^C\big)^{-1}\big(F_b^C - Q^T\lambda_2\big) - P^T\delta\epsilon_M\Big) \tag{2.43}$$

Now, in the framework of the Newton-Raphson method, the invloved quantities are updated into a typical iteration step according to the relations

$$\lambda_2 \leftarrow \lambda_2 + \delta\lambda_2, \quad \text{and} \quad d_b \leftarrow d_b + \delta d_b \tag{2.44}$$

and hence, the update of the internal displacement field is performed through

$$d_i \leftarrow d_i + \delta d_i \tag{2.45}$$

where δd_i is obtained after the calculation of δd_b through equation 2.39. When a converged state is reached, the averaged values must be produced and starting from the stress, we take

$$\sigma_M = \frac{1}{|\Omega|}\sum_{n=1}^{P} P_n\lambda_{n2} = \frac{1}{|\Omega|}\sum_{n=1}^{P} P_nF_{nb} \tag{2.46}$$

or using a global notation instead of the sum of the nodal quantities

$$\sigma_M = \frac{1}{|\Omega|}P\lambda_2 = \frac{1}{|\Omega|}PF_b \tag{2.47}$$

The tangent constitutive matrix is then expressed as the sensitivity of the macro-stress with respect to the macro-deformation. In other words, it is given through a differential form of equation 2.47

$$\delta\sigma_M = \frac{1}{|\Omega|} P \delta\lambda_2 = \frac{1}{|\Omega|} P \delta F_b \tag{2.48}$$

where the change of Lagrange multiplier $\delta\lambda_2$ or δF_b is taken from equation 2.43, written in an equilibrium point, and substituted in the previous formula

1. Calculate the current internal force vector F and the stiffness matrix K according to the partition of interior and boundary nodes

$$F = \begin{bmatrix} F_i \\ F_b \end{bmatrix}, \quad K = \begin{bmatrix} K_{ii} & K_{ib} \\ K_{bi} & K_{bb} \end{bmatrix}, \quad D = \begin{bmatrix} d_i \\ d_b \end{bmatrix}$$

2. Compute the condensed force vector and stiffness matrix from equation 2.41

$$F_b^C = F_b - K_{bi} K_{ii}^{-1} F_i, \quad K_{bb}^C = K_{bb} - K_{bi} K_{ii}^{-1} K_{ib}$$

3. Get the update of the Lagrange parameter using equations 2.43 and 2.44

$$\lambda_2 \leftarrow \lambda_2 + \delta\lambda_2, \quad \text{where}$$

$$\delta\lambda_2 = \Big(Q \big(K_{bb}^C\big)^{-1} Q^T \Big)^{-1} \Big(Q d_b - P^T \epsilon_M Q \big(K_{bb}^C\big)^{-1} \big(F_b^C - Q^T \lambda_2\big) - P^T \delta\epsilon_M \Big)$$

4. Get the displacement increments and their update using 2.39 and 2.42

$$d \leftarrow d + \delta d, \quad where$$

$$\delta d_i = -K_{ii}^{-1} \big(F_i + K_{ib} \delta d_b\big), \quad and \quad \delta d_b = -\big(K_{bb}^C\big)^{-1} \big(F_b^C - Q^T \lambda_2 + Q^T \delta\lambda_2\big)$$

5. Check convergence, if $\|F_i\|$ >tolerance, return to step 1, else go to 6.

6. Compute the overall stress and tangent constitutive matrix

$$\sigma_M = \frac{1}{|\Omega|} P F_b, \quad C_{tM} = \frac{1}{|\Omega|} P \Big(Q \big(K_{bb}^C\big)^{-1} Q^T \Big)^{-1} P^T$$

7. Assign the averaged quantities to the corresponding integration point of the macrostructure.

Table 2.3: Periodic displacements' scheme

$$\delta\lambda_2 = \Big(Q\big(K_{bb}^C\big)^{-1}Q^T\Big)^{-1}P^T\delta\epsilon_M \tag{2.49}$$

and thus the sensitivity of σ_M is given from

$$\delta\sigma_M = \frac{1}{|\Omega|}P\Big(Q\big(K_{bb}^C\big)^{-1}Q^T\Big)^{-1}P^T\delta\epsilon_M \tag{2.50}$$

where the overall constitutive relation is

$$C_{tM} = \frac{1}{|\Omega|}P\Big(Q\big(K_{bb}^C\big)^{-1}Q^T\Big)^{-1}P^T \tag{2.51}$$

In total, the summarized steps for the periodic displacements formulation are presented in table 2.3 according to the developed theory and the proposed matrix representations.

2.7 A Computational Approach

The previous developed procedure, employs the relation between the forces acting on the RVE boundary and the associated boundary displacements in order to compute the averaged stress and tangent moduli. Furthermore, the incorporation of the invloved constraints into the equations of equilibrium is realized through the Lagrange multipliers method. On the contrary, in this section an alternative procedure which employs the direct condensation of the constrained degrees of freedom will be developed, in order to take into account the boundary constraints. For this purpose, the following scheme will be partitioned into two directions. The first one consists in the computation of the overall stress of the RVE while the second approaches the calculation of the macroscopic tangent moduli.

2.7.1 Macroscopic Stress

As already discussed and developed in Section 2.4 and according to the averaging theorems, the macroscale quantities are obtained through the corresponding volume averaged values of the RVE. Consequently, the overall RVE stress is extracted from the surface integral

$$\sigma_M = \frac{1}{|\Omega|}\int_\Omega \sigma_m d\Omega \tag{2.52}$$

which for linear prescribed displacements is simply transformed into a surface integral and finally computed as

$$\sigma_M = \frac{1}{|\Omega|}\sum_{n=1}^{B} P_n F_n \tag{2.53}$$

where $n = 1, 2, ..., B$ denotes the boundary nodes, while F_n and P_n express the force and coordinate vector of the n-th node respectively. On the other hand, when the periodic

boundary conditions are implemented, the macrostress is in a similar way obtained from the relation

$$\sigma_M = \frac{1}{|\Omega|} \sum_{k=1}^{3} P_k F_k^C \tag{2.54}$$

where now $k = 1, 2, 3$ denotes the three independent corner nodes and F_m^C expresses the external forces at these nodes, in terms of the condensed force vector.

2.7.2 Macroscopic Moduli

According to this approach, the extract of the constitutive matrix is achieved by the condensation of the constrained degrees of freedom. Then, a transformation is necessary for the derivation of the expression relating macroscopic stress and deformation tensors. Thus, in tha case of linear displacements, the linearized equations are partitioned as

$$\begin{bmatrix} K_{ss} & K_{sf} \\ K_{fs} & K_{ff} \end{bmatrix} \begin{bmatrix} \delta d_s \\ \delta d_f \end{bmatrix} = \begin{bmatrix} \delta F_s \\ \delta F_f \end{bmatrix} \tag{2.55}$$

where indices s and f denote the boundary and the inernal degrees of freedom respectively. Next, the internal displacement vector δd_f is eliminated from 2.55 and the condensed equation is obtained

$$K^C \delta d_s = \delta F_s \quad \text{where } K^C = K_{ss} - Ksf\big(K_{ff}\big)^{-1} K_{fs} \tag{2.56}$$

which will then be employed for the formation of the overall tangent moduli.At this point, it should be noted that the above notation corresponds to the previous developed one, where indices b and i were used instead of s and f respectively. However, in the following formulation index i will be employed to denote the *independent* degrees of freedom and hence it is replaced in order to avoid any confusion. Now, a similar procedure is followed in the case of periodic displacements, only this time an additional condensation must be produced for the treatment of periodicity.

More specifically, apart from the equilibrium equations, a constraint relation is imposed through

$$d_T = d_B + d_4 - d_1 \tag{2.57a}$$

$$d_R = d_L + d_2 - d_1 \tag{2.57b}$$

where the bottom and the left side nodes are considered to be independent as illustrated in figure 2.4. A more compact form of equations 2.57 is obtained through the relation

$$C d_s = 0 \tag{2.58}$$

where C is a matrix containing the coefficients of the involved degrees of freedom.

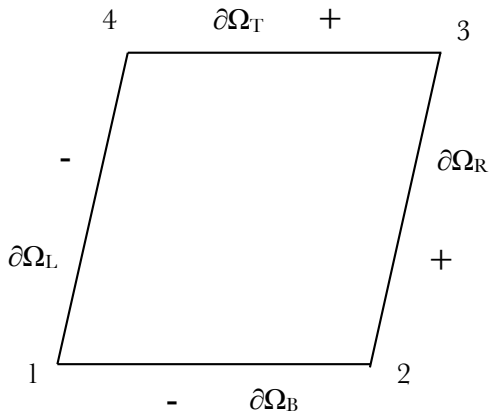

Figure 2.4: Schematic representation of the RVE discretization

Equation 2.58 is then partitioned according to

$$\begin{bmatrix} C_i & C_d \end{bmatrix} \begin{bmatrix} d_i \\ d_d \end{bmatrix} = 0 \tag{2.59}$$

where d_i and d_d are the vectors of the independent and dependent degrees of freedom respectively. In order to eliminate the latter, we take from 2.59

$$d_d = C_{di} d_i \quad \text{where } C_{di} = -C_d^{-1} C_i \tag{2.60}$$

or in more compact form, equation 2.59 can be written as

$$\begin{bmatrix} d_i \\ d_d \end{bmatrix} = \begin{bmatrix} I \\ C_{di} \end{bmatrix} d_i = T d_i \tag{2.61}$$

where T is a transformation matrix which is employed for the transformation of the linear system $Kd = F$ into $K'd' = F'$. This is achieved through the common relations $K' = T^T K T$, $d' = T^T d$ and $F' = T^T F$ and hence, the transformation is applied in the partitioned system

$$\begin{bmatrix} K_{ii} & K_{id} \\ K_{di} & K_{dd} \end{bmatrix} \begin{bmatrix} \delta d_i \\ \delta d_d \end{bmatrix} = \begin{bmatrix} \delta F_i \\ \delta F_d \end{bmatrix} \quad \text{or } K' \delta d_i = \delta F' \tag{2.62}$$

Once applied the transformation, equation 2.62 can be expanded as

$$\begin{bmatrix} K_{ii} + K_{id} C_{di} + C_{di} K_{di} + C_{di} K_{dd} C_{di} \end{bmatrix} \delta d_i = \begin{bmatrix} \delta F_i + C_{di} \delta F_d \end{bmatrix} \quad \text{or } K' \delta d_i = \delta F' \tag{2.63}$$

where the nodes of the boundary $\partial\Omega^+$ are considered as independent in the present work. Noting that the boundary conditions will be imposed on the corner nodes of the RVE, a further elimination of 2.63 is necessary according to

$$\begin{bmatrix} K'_{ss} & K'_{sf} \\ K'_{fs} & K'_{ff} \end{bmatrix} \begin{bmatrix} \delta d_s \\ \delta d_f \end{bmatrix} = \begin{bmatrix} \delta F'_s \\ \delta F'_f \end{bmatrix} \tag{2.64}$$

where condensation of δd_f leads to

$$K'^C \delta d_s = \delta F'_s \quad \text{where } K'^C = K'_{ss} - K'_{sf}\big(K'_{ff}\big)^{-1} K'_{fs} \tag{2.65}$$

which constitutes a [6x6] system concerning the corner degrees of freedom in a two-dimensional case. Now, the overall moduli will be produced using equations 2.56 and 2.65 for linear and periodic displacements respectively or generaly from the relation

$$K^C \delta d_s = \delta F_s \tag{2.66}$$

which expresses a NxN system of equations where N denotes the supported or boundary degrees of freedom and to equals to nodes 1,2 and 4 in the case of periodic displacements. Next, the expression of stress related to the displacements is obtained from the expression

$$\delta\sigma_M = \frac{1}{|\Omega|} P \delta F_s = \frac{1}{|\Omega|} P\Big(K^C \delta d_s\Big) \tag{2.67}$$

after the substitution of δF_s from equation 2.66. Finally, substitution of the equation $\delta d_s = P^T \delta\epsilon_M$ into 2.67 gives

$$\delta\sigma_M = \frac{1}{|\Omega|} P K^C \delta d_s = \frac{1}{|\Omega|} P K^C P^T \delta\epsilon_M \tag{2.68}$$

and thus we obtain the expression relating the variation of the macroscopic stress and macroscopic strain. Consequently, the consistent constitutive tangent is identified as

$$C_{tM} = \frac{1}{|\Omega|} P K^C P^T \tag{2.69}$$

for both linear and periodic displacements with matrices P and K^C refering to the corresponding degrees of freedom. That is, in the first case, P and K^C are expressed in terms of all the boundary degrees of freedom while in the case of periodicity only the three corner degrees of freedom are involved in their computation. In conclusion, comparing the above developed formulations we observe that this second approach expresses the micro-to-macro transition, and hence the averaged quantities, for both cases of BC, in a more compact form through equations 2.53 and 2.69.

Chapter 3

Theory of Plasticity

3.1 Introduction

The main objective of this chapter is to concentrate on the numerical formulation of theory of plasticity through the implementation of elasto-plastic von Mises materials. In mathematical terms, the concept of plasticity is defined through a function Ψ, called yield function or yield criterion, whose interior describes the elastic domain and its boundary is the yield limit:

$$\Psi(\sigma, \sigma_o) = \sigma_{eff} - \sigma_o \tag{3.1}$$

In this sense, an admissible stress may lie either on the elastic domain where $\Psi < 0$ or on the yield limit where $\Psi = 0$.

$$\Psi(\sigma, \sigma_o) \leq 0 \tag{3.2}$$

Consequently, it should be noted that for stresses within the elastic domain, only elastic straining may occur while for stresses on the boundary either plastic loading or elastic unloading may be produced.

Concerning the von Mises materials, the yield function takes the following form for three dimensional elasticity:

$$\Psi = \sqrt{\frac{1}{2}[(\sigma_{xx} - \sigma_{yy})^2 + (\sigma_{yy} - \sigma_{zz})^2 + (\sigma_{zz} - \sigma_{xx})^2 + 6(\tau_{xy}^2 + \tau_{yz}^2 + \tau_{zx}^2)]} - \sigma_o \tag{3.3}$$

and

$$\Psi = \sqrt{\frac{1}{2}[\sigma_{xx}^2 - \sigma_{xx}\sigma_{yy} + \sigma_{yy}^2 + 3\tau_{xy}^2]} - \sigma_o = \sigma_{eff} - \sigma_o \tag{3.4}$$

for plain stress problems, where σ_{eff} and σ_o denote the von Mises stress and the yield stress respectively. In the context of the present thesis both the aforementioned cases are developed however, the following theory will be expressed in terms of plain stress due to the fewer involved components.

Furthermore, in this direction, a range of algorithms is developed in order to incorporate the material non-linearities into the first order homogenization scheme (FE^2) where the fundamental concepts are summarized in the folowing points:

- the construction of the standard tangent modular matrix in order to be used in the incremental tangent stiffness matrix.
- the integration of the stress/strains laws.
- the formation of a "consistent" tangent modular matrix appropriate for the Newton-Raphson iterations.

3.2 Iterative and Incremental Strains

For the employment of an iterative scheme, two different procedures, the iterative and the incremental strains, are proposed in the framework of multiscale simulation and for the sake of completeness, they are both presented and described in the following steps:

Iterative strains algorithm:

1. The iterative displacements δp are computed.
2. The iterative strains $\delta\epsilon$ are obtained, through δp, where $\delta\epsilon = f(\delta\text{p})$.
3. The iterative stresses are calculated using the relation $\delta\sigma = C_t(\sigma)\delta\epsilon$ or by the integration of the rate equations.
4. The stresses are updated, $\sigma_n = \sigma_o + \delta\sigma$ where σ_o are the old stresses.

Incremental strains procedure:

1. The iterative displacements δp are computed.
2. The incremental displacements are updated through the relation $\Delta\text{p}_n = \Delta\text{p}_o + \delta\text{p}$ where Δp_o is the incremental displacement vector at the end of the last iteration.
3. The incremental strains $\Delta\epsilon$ are obtained, through Δp, where $\Delta\epsilon = f(\Delta\text{p})$.
4. The incremental stresses are calculated using $\Delta\sigma = C_t(\sigma)$ or by the integration of the rate equations.
5. The stresses are updated, $\sigma_n = \sigma_o + \Delta\sigma$ where σ_o are the old stresses.

As illustraded in the example of figure 3.1, both the procedures will take the stress from point A, expressing an equilibrium state, to B when a positive displacement occurs. However, if at this stage a negative displacement and hence a negative strain is produced, the incremental argorithm will take the stress to point C, as shown in figure 3.1, using the total

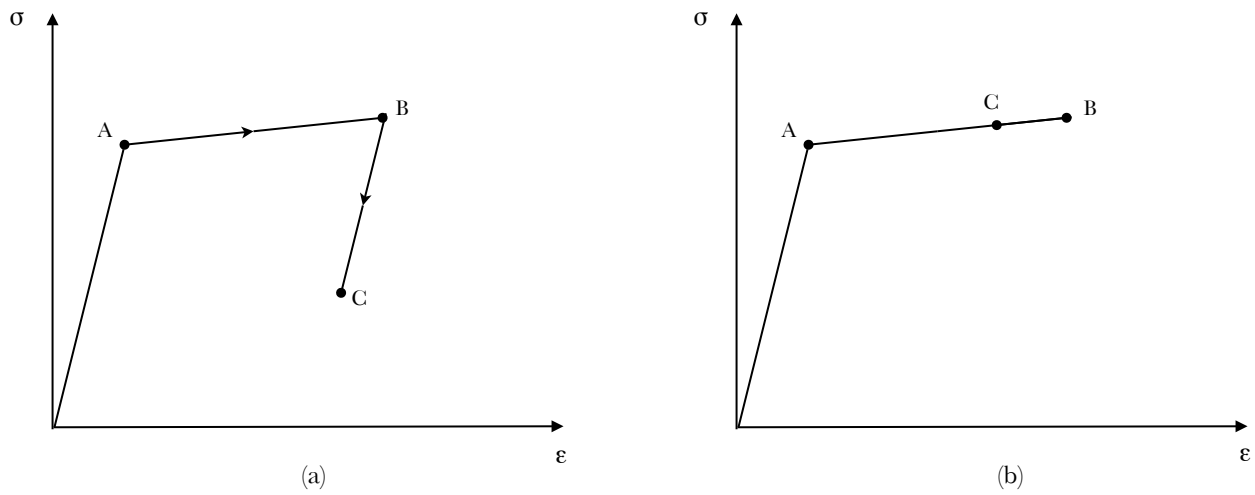

Figure 3.1: Description of the (a) Iterative and (b) Incremental algorithms

strain increment while the iterative algorithm will produce an elastic unloading at this point and will take the stress to point C, as shown in figure 3.1. This misleading unloading which constitutes the main disadvantage of the iterative algorithm and may lead to entirely different results, acted as a catalyst for the developement and the implementation of the incremental solution, as also recommended in [4].

3.3 The Standard Tangent Modular Matrix

According to the main assumption of the small strain theory of plasticity, the total strain ϵ is decomposed into the sum of a fully reversible elastic component ϵ_e and a plastic non-reversible (permanent) component ϵ_p:

$$\epsilon = \epsilon_e + \epsilon_p \tag{3.5}$$

where the elastic component ϵ_e is defined as:

$$\epsilon_e = \epsilon - \epsilon_p \tag{3.6}$$

Consequently, through the latter and taking into account the constitutive law which relates the elastic strain with the stress we obtain:

$$\sigma = E\epsilon_e = E(\epsilon - \epsilon_p) \tag{3.7}$$

Now, in order to calculate the permanent component ϵ_p also known as flow rules, the Prandtl-Reuss law is implemented:

$$\epsilon_p = \begin{pmatrix} \epsilon_{px} \\ \epsilon_{py} \\ \epsilon_{pxy} \end{pmatrix} = \lambda\alpha = \frac{\lambda}{2\sigma_{eff}} \begin{pmatrix} 2\sigma_x - \sigma_y \\ 2\sigma_y - \sigma_x \\ 6\tau_{xy} \end{pmatrix} \tag{3.8}$$

where, as shown in figure 3.2 , α is the normal vector to the yield surface and λ is a constant also referred to as the plastic strain-rate multiplier.

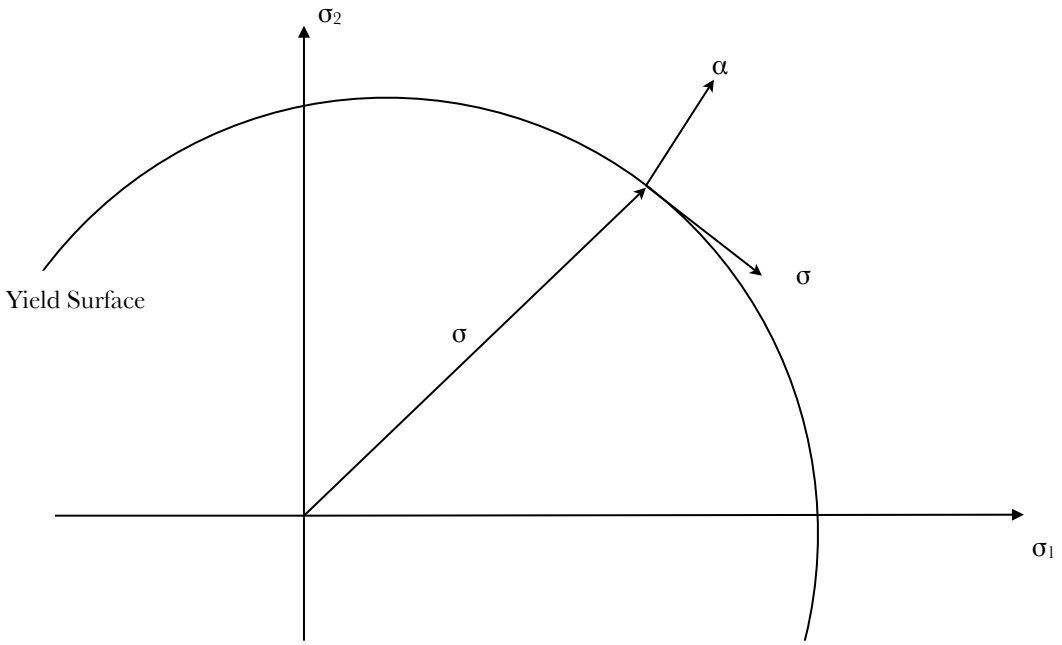

Figure 3.2: Plastic flow illustration in terms of principal stresses

Substituting the plastic strain into equation 3.7, we obtain the relation between the small strain changes and the small changes in stress:

$$\sigma = \begin{pmatrix} \sigma_x \\ \sigma_y \\ \sigma_{xy} \end{pmatrix} = C \begin{pmatrix} \epsilon_x - \epsilon_{px} \\ \epsilon_y - \epsilon_{py} \\ \epsilon_{xy} - \epsilon_{pxy} \end{pmatrix} = C(\epsilon - \epsilon_p) = C(\epsilon - \lambda\alpha) \tag{3.9}$$

where C denotes the isotropic elastic modular matrix:

$$C = \frac{E}{1-v^2} \begin{bmatrix} 1 & \mathrm{v} & 0 \\ v & 1 & 0 \\ 0 & 0 & \dfrac{1-v}{2} \end{bmatrix} \tag{3.10}$$

Now, for plastic flow to occur, we need to assure that the stress remain on the yield surface, and consequently the inner product of the normal vector to the surface α and the stress vector must be zero:

$$\delta\Psi = \frac{\partial\Psi}{\partial\sigma}^T \delta\sigma = \alpha^T \delta\sigma = 0 \tag{3.11}$$

This equation is scematically presented in the figure 3.2 and shows that when plastic flow

occurs the stress changes σ must move tangentially to the yield surface and hence the stress changes vector must be orthogonal to the vector α. In order to calculate the plastic strain-rate multiplier λ, equation 3.9 is substituted into equation 3.11 and the following expression is obtained in terms of strain changes:

$$\delta\lambda = \frac{\alpha^T C \delta\epsilon}{\alpha^T C \alpha} \tag{3.12}$$

and hence, using equation 3.9 the stress changes are expressed through the relation:

$$\delta\sigma = C_t \delta\epsilon = C\left(I - \frac{\alpha\alpha^T C}{\alpha^T C \alpha}\right)\delta\epsilon \tag{3.13}$$

where C_t denotes the tangential modular matrix and consitutes a function of the material properties, E and v, but also of the normal vector α.

3.4 Isotropic Strain Hardening

In the case of hardening, the fixed yield stress σ_o need to be expressed as a function of the plastic strain so that equation 3.1 takes the form

$$\Psi(\sigma, \sigma_o) = \sigma_{eff} - \sigma_o(\epsilon_p) \tag{3.14}$$

where ϵ_p denotes the total plastic strain

$$\epsilon_p = \sum \delta\epsilon_p = \int \epsilon_p \tag{3.15}$$

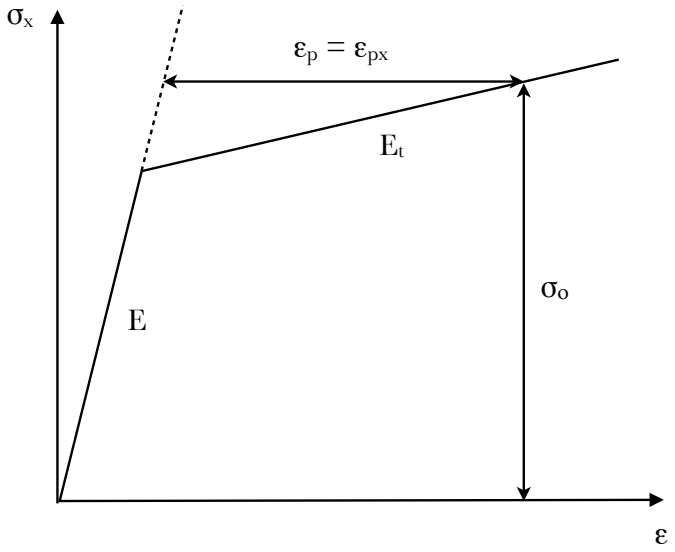

Figure 3.3: One-dimensional

and in the case of plane stress, the total plastic strain is given from

$$\epsilon_p = \frac{2}{\sqrt{3}}\left(\epsilon_{px}^2 + \epsilon_{py}^2 + \epsilon_{px}\epsilon_{py} + \frac{1}{4}\gamma_{pxy}\right) \tag{3.16}$$

Now, for uniaxial stress, $\epsilon_{py} = \epsilon_{pz} = -\frac{1}{2}\epsilon_{px}$ so that no plastic volume occurs and $\epsilon_p = \epsilon_{px}$ while $\sigma_{eff} = \sigma_o = \sigma_x$. As a result, the form relating σ_o and ϵ_{ps} can be obtained from the uniaxial stress/plastic strain relationship where

$$\frac{\partial \sigma_o}{\partial \epsilon_p} = H = \frac{\partial \sigma_x}{\partial \epsilon_{px}} = \frac{E_t}{1 - E_t/E} \tag{3.17}$$

as illustrated in figure 3.3. Then, the plastic flow relation 3.11 is modified to

$$\delta\Psi = \frac{\partial \Psi}{\partial \sigma}^T \delta\sigma + \frac{\partial \Psi}{\partial \sigma_o}\frac{\partial \sigma_o}{\partial \epsilon_p}\delta\epsilon_p = \alpha^T \delta\sigma - H\delta\epsilon_p = 0 \tag{3.18}$$

and substitution from 3.8 into equation 3.18 gives

$$\delta\Psi = \alpha^T \delta\sigma - H\alpha\delta\lambda = \alpha^T \delta\sigma - A'\delta\lambda = 0. \tag{3.19}$$

Solving now for $\delta\lambda$ we obtain

$$\delta\lambda = \frac{\alpha^T C \delta\epsilon}{\alpha^T C \alpha + A'} \tag{3.20}$$

and equation 3.13 is also modified to

$$\delta\sigma = C_t \delta\epsilon = C\left(I - \frac{\alpha\alpha^T C}{\alpha^T C\alpha + A'}\right)\delta\epsilon \tag{3.21}$$

For linear hardening, as shown in figure 3.3, A' is a single measurable constant while for non-linear hardening, A' constitutes a function of ϵ_p or more generally, of σ_o which vary with ϵ_p.

3.5 Integration of the Stress-strain Relation

In order to apply the previous tangential formulation for the calculation of the strain and stress in a structure, we should require that the strain increments are infinitesimally small, so such a procedure would be computationally inefficient since it would lead to an accumulative error. Consequently, we need to advance to the integration of the flow rules through the loading path, a procedure that requires some additional steps in order to assure that the final stress do not lie outside the yield surface. In this sense, a more precise expression of the yield function change should be achieved and is obtained if we add a high-order term in the von-Mises criterion

$$\delta\Psi = \alpha^T \delta\sigma + \frac{1}{2}\delta\sigma^T + \frac{\partial\alpha}{\partial\sigma}\delta\sigma \tag{3.22}$$

where differentiation of the normal vector α gives

$$\frac{\partial\alpha}{\partial\sigma} = \frac{1}{2\sigma_{eff}} \begin{bmatrix} 2 & -1 & 0 \\ -1 & 2 & 0 \\ 0 & 0 & 6 \end{bmatrix} - \frac{1}{\sigma_{eff}}\alpha\alpha^T = \frac{1}{2\sigma_{eff}}A - \frac{1}{\sigma_{eff}}\alpha\alpha^T \tag{3.23}$$

It becomes now evident that the omission of the second order terms in the expression of the yield function change will lead to error. Now, in this direction we need to adopt a scheme whose aim is to update the stress at a Gauss point given (i) the old stress, strains and (ii) the new strains. Such a scheme includes as a first step the elastic prediction for the updated stresses and secondly the verification of the predicted position. That is, if the stresses lie within the yield surface, which means that the Gauss-point remained in the elastic domain, or that it was elastically unloaded, there is no need for integration. On the other hand, if the stresses are found outside the yield limit we need to adopt one of the following procedures:

- Implementation of a return to the "forward-Euler" scheme.
- Employment of a form of "backward-Euler" scheme.

In the context of the present project, both the aforementioned algorithms were developed and tested however, only the backward-Euler scheme was adopted in the framework of the Newton-Raphson method, for the solution of the non-linear equilibrium equations. A more schematical view of this method can be found at the final part of this chapter which refers to the algorithmic formulation of the material non-linearity. Though, for the sake of generality, it should be mentioned that the implementation of sub-increments throughout the integration procedure could also be an alternative approach for the preservation of the stress within the yield surface.

3.5.1 A forward-Euler Scheme

According to a forward integration scheme, the location of the intersection of the stress vector with the yield surface is required and it is obtained through the following equation:

$$\Psi(\sigma_A + \alpha\Delta\sigma) = 0 \tag{3.24}$$

where α is a constant expressing the required part of the elastic stress increments $\Delta\sigma$ in order to reach the yield surface and σ_A is the initial stress such that

$$\Psi(\sigma_A) < 0 \tag{3.25}$$

In addition, with $\alpha = 1$ the elastic predicted stress $\sigma_A + \alpha\Delta\sigma$ give

$$\Psi(\sigma_B) = \Psi(\sigma_A + \Delta\sigma) > 0 \tag{3.26}$$

which means that the elastic predicted stress lies outside the yield limit.

For some yield functions, like von Mises, we can easily obtain the solution of equation 3.24 through an analytical expression. Concretely, re-expressing equation 3.4 in squared form and substituting the effective stress with $\sigma_A + \alpha\Delta\sigma$ gives

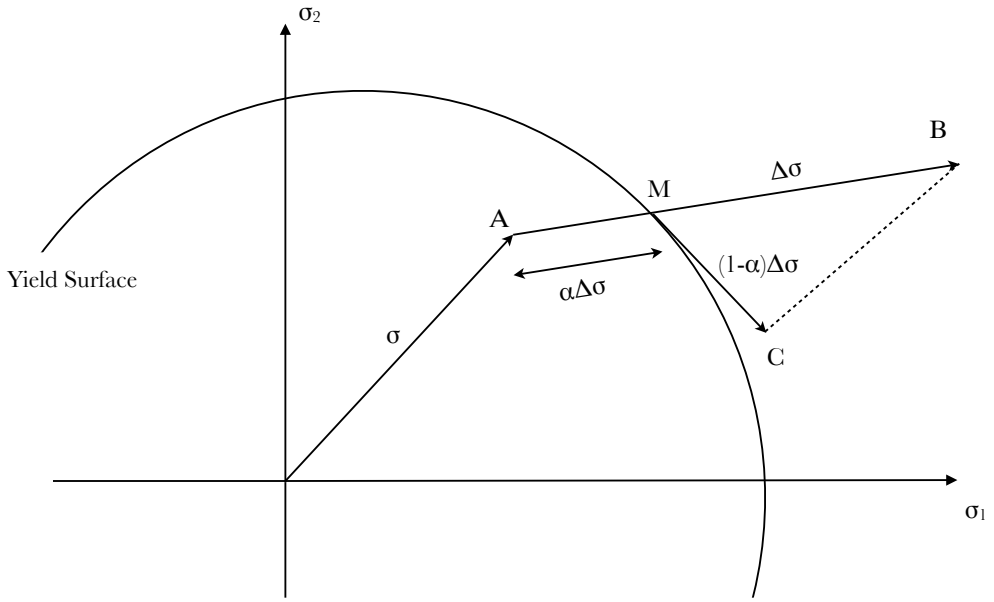

Figure 3.4: The forward Euler procedure

$$\Psi = \alpha^2\sigma_{eff}(\Delta\sigma)^2 + \alpha\Delta\sigma^T A\sigma_A + \sigma_{eff}(\sigma_A)^2 - \sigma_o^2 = 0 \tag{3.27}$$

where matrix A is obtained through the derivative of the normal vector α and as shown before, it takes the following form for plane stress problems:

$$A = \begin{bmatrix} 2 & -1 & 0 \\ -1 & 2 & 0 \\ 0 & 0 & 6 \end{bmatrix} \tag{3.28}$$

Finally, the positive root of 3.27 produces the intersection point M as illustrated in figure 3.4. Alternatively, a more computational approach could be adopted when a general yield criterion is used and the analytical solution is unfeasible. More specifically, we can use a short Taylor series of 3.27, with a as the only variable, to set up the iterative scheme and the initial estimate

$$\alpha_o = \frac{-\Psi_A}{\Psi_B - \Psi_A} \tag{3.29}$$

Then, the Taylor series takes the form

$$\Psi_n = \Psi_o + \frac{\partial \Psi}{\partial \sigma}\frac{\partial \sigma}{\partial \alpha}\delta\alpha = \Psi_o + \alpha^T \Delta\sigma_{eff}\delta\alpha = 0 \tag{3.30}$$

and gives the first change $\delta\alpha_o$ where the "old" yield function Ψ_o is computed from the stress $\sigma = \sigma_A + \alpha_o \Delta\sigma_{eff}$ and the scalar a is updated according to $\alpha_1 = \alpha_o + \delta\alpha_o$. Next, a second iteration would give

$$\delta\alpha_1 = \frac{-\Psi_1}{\alpha^T \Delta\sigma_{eff}} \tag{3.31}$$

where the normal vector a and the yield function value are computed at α_1. Thus, having computed the intersection point, the stress is updated by the portion $\sigma_A + \alpha\Delta\sigma$ to point M using the elastic properties and by the portion $(1-\alpha)\Delta\sigma$ to point C in an elasto-plastic manner. More specifically, the forward-Euler scheme is equivalent to a forward elastic step from point A to point B and a return from point B to C through the normal vector of point M

$$\sigma_C = \sigma_A + \Delta\sigma - \Delta\lambda C\alpha_M = \sigma_B - \Delta\lambda C\alpha_M \tag{3.32}$$

A schematic representation of this process and equation 3.32 is presented and explained in figure 3.4.

An alternative procedure could avoid the necessity of computing the intersection point M and as a result the return step could be produced through the normal vector at the elastic point B. Thus, a Taylor expansion of yield function about point B produces

$$\Psi = \Psi_B + \frac{\partial \Psi}{\partial \sigma}^T \Delta\sigma + \frac{\partial \Psi}{\partial \epsilon_p}\Delta\epsilon_p = \Psi_B - \Delta\lambda\alpha_B^T C\alpha_B - \Delta\lambda A' \tag{3.33}$$

As a result, if the new yield-function value Ψ equals to zero, equation 3.33 gives

$$\Delta\lambda = \frac{\Psi_B}{\alpha_B^T C\alpha_B + A'_B} \tag{3.34}$$

and hence the final stress σ_C is given by

$$\sigma_C = \sigma_A + \Delta\sigma - \Delta\lambda C\alpha_B = \sigma_B - \Delta\lambda C\alpha_B \tag{3.35}$$

At this point, it should be noted that both of the previous algorithms produce stresses that lie outside the yield surface and hence it is necessary to apply a return technique in order to approach the yield surface and minimize the generated error.

3.5.2 The forward-Euler Return to the Yield Surface

As an extension of the previous return process we can produce an iterative loop using equation 3.35, this time starting from point C:

$$\sigma_D = \sigma_C - \delta\lambda_C C\alpha_C \tag{3.36}$$

where

$$\delta\lambda_C = \frac{f_C}{\alpha_C^T C\alpha_C + A'} \tag{3.37}$$

If the obtained stress at point D lies outside the yield limit, further relaxation can be applied until a sufficiently small divergence. Consequently, the general procedure can be expressed by the following relation either for the forward or the bacward prediction:

$$\Delta\sigma = C\Delta\epsilon - \Delta\lambda_o C\alpha_o - \delta\lambda_B C\alpha_B - \delta\lambda_C C\alpha_C \tag{3.38}$$

In this general form, α_o denotes the normal vector at the intersection point M when the forward-Euler scheme is employed while for the backward-Euler it denotes the normal vector at point B.

3.5.3 The backward-Euler Return to the Yield Surface

From the opposing point of view, the backward-Euler scheme derives from the following equation

$$\sigma_C = \sigma_B - \Delta\lambda C\alpha_C \tag{3.39}$$

where an estimate for σ_C must be obtained in order to produce an iterative loop able to approach the yield surface. Hence, the whole process is based on the reduction of a vector v which represents the difference between the current stress and the backward-Euler stress

$$v = \sigma - (\sigma_B - \Delta\lambda C\alpha_C) \tag{3.40}$$

Now, if we express this equation in a short Taylor form we obtain

$$v = v_o + \delta\sigma + \delta\lambda C\alpha + \Delta\lambda C\frac{\partial a}{\partial\sigma}\delta\sigma \tag{3.41}$$

where we require that the vector v is equal to zero and solving for the stress change $\delta\sigma$ we take

$$\delta\sigma = -\left(I + \Delta\lambda C\frac{\partial a}{\partial\sigma}\right)^{-1}(v_o + \delta\lambda C\alpha) = -P^{-1}v_o - \delta\lambda P^{-1}C\alpha \tag{3.42}$$

In the same way, we obtain a Taylor form for the yield function of point C, which should satisfy the yield criterion $\Psi = 0$

$$\Psi = \Psi_o + \frac{\partial f}{\partial \sigma}^T \delta\sigma + \frac{\partial \Psi}{\partial \epsilon_p}\delta\epsilon_p = \Psi_o + \alpha_C^T \delta\sigma + A'_c \delta\lambda = 0 \tag{3.43}$$

where solving for the change $\delta\lambda$ in $\Delta\lambda$ gives

$$\delta\lambda = \frac{\Psi_o - \alpha^T P v_o}{\alpha^T P^{-1} C \alpha + A'} \tag{3.44}$$

As a result, the iterative stress change $\delta\sigma$ is calculated through equation 3.42 and the final stress is updated until a sufficiently small value of the yield function is reached.

3.6 The Consistent Tangent Modular Matrix

For the efficient implementation of Newton-Raphson method, a consistent tangent modular matrix needs to be produced in order to be employed along with the backward-Euler scheme of Section 2.4.3. In this sense, the characteristics of the overall equilibrium iterations will be improved and a faster convergence rate will be achieved.

As expressed in Section 2.4.2, the backward-Euler scheme is described by equation 3.36 and hence, differentiation produces

$$\delta\sigma = C\delta\epsilon - \delta\lambda C\alpha - \Delta\lambda C\frac{\partial \alpha}{\partial \sigma}\delta\sigma \tag{3.45}$$

and solving for $\delta\sigma$ we obtain

$$\delta\sigma = \left(I + \Delta\lambda C\frac{\partial \alpha}{\partial \sigma}\right)^{-1} C(\delta\epsilon - \delta\lambda\alpha) = P^{-1}C(\delta\epsilon - \delta\lambda\alpha) \tag{3.46}$$

Again, for plastic flow to occur, we need to assure that the stress remain on the yield surface, and hence, as in Section 2.3, we obtain

$$\alpha^T\delta\sigma = 0 \implies \alpha^T P^{-1} C\delta\epsilon - \delta\lambda\alpha^T P^{-1} C\alpha + A'\delta\lambda = 0 \tag{3.47}$$

and solving for $\delta\sigma$ gives

$$\delta\sigma = \left(P^{-1}C - \frac{P^{-1}C\alpha\alpha^T(P^{-1}C)^T}{\alpha^T P^{-1} C\alpha + A'}\right)\delta\epsilon = C_{ct}\delta\epsilon \tag{3.48}$$

Consequently, in contrast to the standard modular matrix, the consistent modular matrix constitutes a function not only of the material properties and the normal vector α but also of the plastic strain-rate multiplier $\Delta\lambda$.

3.7 The Algorithmic Formulation

As already mentioned in the previous development, theory of plasticity is mathematically incorporated into the Newton-Raphson method through a total langrangian scheme, since the incremental strains are employed in the framework of the solution process. Taking into account this incremental form, the stress-strain relation is considered to be

$$\Delta\sigma_i = C_t(\sigma_{i-1})\Delta\epsilon \quad or \;\; \Delta\sigma_i = f(\sigma_{i-1}, \Delta\epsilon) \tag{3.49}$$

where C_t is not only a function of the material properties, but also of the current stress. As a result, the Gauss-point stress is obtained at the end of each iteration within an incremental step however, it is only updated at a converged equilibrium state, that is at the end of the step. In mathematical terms,

$$\sigma_i = \sigma_{i-1} + \Delta\sigma_i(\Delta\epsilon_i) \tag{3.50}$$

where σ_i and σ_{i-1} denote the final stress at the end of the incremental steps i and $i-1$ respectively and $\Delta\sigma_i$ and $\Delta\epsilon_i$ express the incremental stress and strain within the step i. Then, in order to obtain the incremental stress $\Delta\sigma_i$, the incremental displacements ΔD_i must be calculated as

$$\Delta d_i = \delta d_i^1 + \delta d_i^2 + ... + \delta d_i^n \tag{3.51}$$

so that incremental strains are finally obtained through

$$\Delta\epsilon_i = \delta\epsilon_i^1 + \delta\epsilon_i^2 + ... + \delta\epsilon_i^n \tag{3.52}$$

where $\delta\epsilon_i^j$ denotes the strain change within the iteration j of the incremental step i.

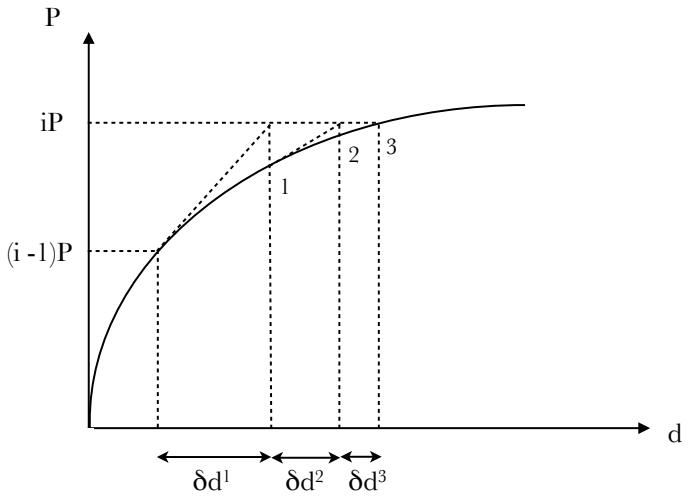

Figure 3.5: Schematic representation of the incremental displacements

In the following table, the summarized steps of the iterative total Lagrange process within a Newton-Raphson increment are schematically presented, according to the self developed program.

1. Enter with
   (a) d_o : old displacement vector at the end of last increment
   (b) d_n : new displacement vector
   (c) σ_o : old stress vector at the end of last increment
   (d) ϵ_o : old strain vector at the end of last increment
2. Loop over all elements and for every integration point
   (a) compute $\epsilon_n = f(d_n)$
   (b) compute $\Delta\sigma = f(\sigma_o, \epsilon_n - \epsilon_o)$
   (c) update the stress $\sigma_n = \sigma_o + \Delta\sigma$
   (d) update the tangent costitutive matrix $C_n = f(\sigma_n)$
3. Compute the internal forces f_{int} and the tangent stiffness K_t
4. Assemble f_{int} and K_t for all the elements
5. Check convergence
   (a) if $\|f_{int} - f_{ext}\| >$ tolerance, go to 5
   (b) else go to 7
6. Solve for the residual forces $\|f_{int} - f_{ext}\|$ and compute the displacement change δd
7. Update the displacement vector $d_n \leftarrow d_n + \delta d$ and return to 2
8. Update the stress, the strain and the tangent constitutive matrix
   (a) $\sigma_o \leftarrow \sigma_n$
   (b) $\epsilon_o \leftarrow \epsilon_n$
   (c) $C_o \leftarrow C_n$
9. Get the next increment and go to 1

Table 3.1: Algorithm for elasto-plastic update

At this point, it should be noted that the computation of $\Delta\sigma$ constitutes a quite delicate task since it does not simply arise through $f(\sigma_o, \epsilon_n - \epsilon_o)$, as simply mentioned in step 2(b). Consequently, once obtained the strain increment $\Delta\epsilon = \epsilon_n - \epsilon_o$, an elastic prediction for the stress change is produced according to

$$\Delta\sigma^{ep} = E\Delta\epsilon \tag{3.53}$$

and as a result, the elastically predicted final stress is obtained as

$$\sigma_n^{ep} = \sigma_o + \Delta\sigma^{ep} \tag{3.54}$$

where four cases are distinguished, depending on the relation between σ_o and σ_n^{ep} with the yield stress σ_y. These are presented in the following points in terms of uniaxial stress, so that thay can be easily illustrated and schematically comprehensible.

A. Elastic Loading

$\sigma_o < \sigma_y \quad \& \quad \sigma_n^{ep} < \sigma_y \implies \sigma_n = \sigma_n^{ep}$

B. Elasto-plastic Loading

$\sigma_o < \sigma_y \quad \& \quad \sigma_n^{ep} > \sigma_y \implies \sigma_n = \sigma_y + E_T\big(\epsilon_n - \epsilon_y\big)$

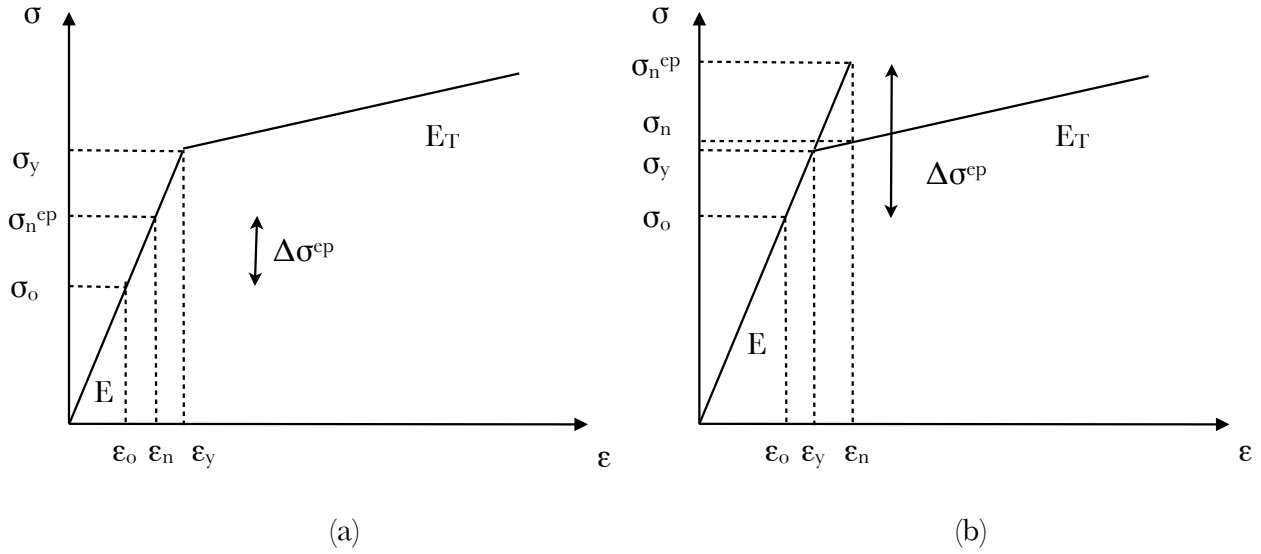

Figure 3.6: Elastic Loading (a) and Elasto-plastic Loading (b)

C. Plastic Loading

$$\sigma_o > \sigma_y \quad \& \quad \sigma_n^{ep} > \sigma_o \implies \sigma_n = \sigma_o + E_T\big(\epsilon_n - \epsilon_o\big)$$

D. Elastic Unloading

$$\sigma_o > \sigma_y \quad \& \quad \sigma_n^{ep} < \sigma_o \implies \sigma_n = \sigma_n^{ep}$$

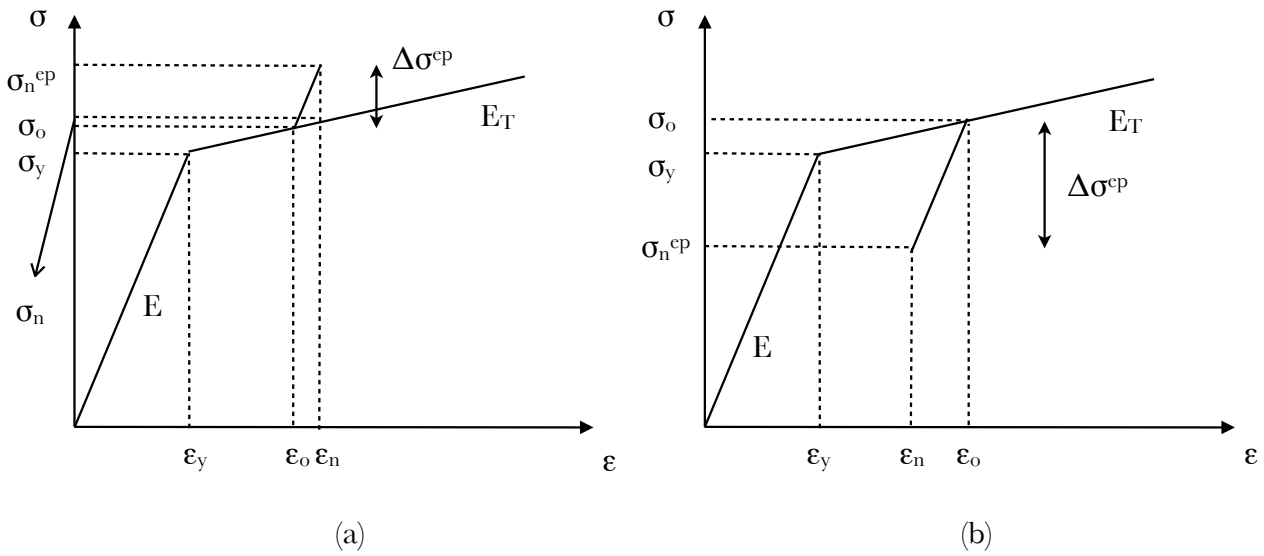

Figure 3.7: Plastic Loading (a) and Elastic Unloading (b)

Apart from the new stress σ_n, the constitutive matrix must also be updated according to the final stress position. This task includes some similar steps which are distinguished this time in two cases. If the final stress lies within the elastic domain, the constitutive matrix equals to the elastic mudular matrix otherwise, the tangent matrix must be implemented, as developed in the previous section, for the production of the next increment.

Chapter 4

Non-linear Finite Element Analysis

In order to incorporate the non-linear constitutve relations into the finite element analysis, a pure displacement version is employed in the framework of this project, since it constitutes the most convenient discretization method. Furthermore, its formulation is simple and allows for a straightforward implementation of complicated constitutive relations. Consequently, in the following sections, the solution procedure will be developed according to the Newton-Raphson method, including its full, modified and initial versions. However, due to the multi-scale requirements which demand the solution of a strain-driven boundary value problem, not only the load-control but also the displacement-control formulation will be developed for the case of quasi-static problems. Hence, the present chapter is divided into two parts. The first one is concentrated on the load-control formulation of the full Newton-Raphson method and the modified and the initial versions while the second part, is dedicated to the displacement control formulation.

4.1 Load Control

The general equilibrium equation takes the form

$$f_{ext} - f_{int} = 0 \tag{4.1}$$

for quasi-static processes, where time plays no role. Yet, also then we need a parameter to order the sequence of events. For this reason the concept of time will also be used in static mechanical processes to form the loading sequence. In particular, the concept of time can be employed to apply the external load in a number of loading steps (or increments). It would be possible to impose the entire external load f_{ext} in a single step, but this is not a sensible approach due to:

1. The fact that the system of equations produced from the discretization of a non-linear continuum model is non-linear and as a result, the solution must be obtained through an iterative procedure. For very large loading steps, it is usually difficult to obtain a properly converged solution, if a solution can be obtained at all. Indeed, the convergence radius is limited for most commonly used iterative procedures, including the NewtonRaphson method.

2. As shown by experiments, most materials exhibit a path-dependent behaviour. In other words, the obtained stress values are dependending on the followed strain path. For instance, the resulting stress can be different when we first apply tension on a panel followed by a shear strain increment or when the same strain increments are imposed in the reverse order. Consequently, the strain increments must be relatively small, in order to obtain the correct structural behaviour, so that the strain path is followed as closely as possible.

In this sense, the vector of unknow stress components is decomposed into $\sigma^{t+\Delta t}$ and σ^t instead of using the "new" and "old" notation respectively. Hence, the stress components are related through

$$\sigma^{t+\Delta t} = \sigma^t + \Delta\sigma \tag{4.2}$$

where again $\Delta\sigma$ denotes the unknown change within the incremental step. Now, substituting into 4.1, we obtain

$$f_{ext}^{t+\Delta t} - \sum_{e=1}^{n_e} Q_e^T \int_{Ve} B^T \sigma^{t+\Delta t} dV = 0 \tag{4.3}$$

and expanding according to 4.2

$$f_{ext}^{t+\Delta t} - \sum_{e=1}^{n_e} Q_e^T \int_{Ve} B^T \sigma^t dV - \sum_{e=1}^{n_e} Q_e^T \int_{Ve} B^T \Delta\sigma dV = 0 \tag{4.4}$$

or

$$f_{ext}^{t+\Delta t} - f_{int}^t = \sum_{e=1}^{n_e} Q_e^T \int_{Ve} B^T \Delta\sigma dV \tag{4.5}$$

where Q_i is the location matrix. Then, if we relate the stress change $\Delta\sigma$ in a linearized form with the displacement change Δd, as shown in Chapter 3, we obtain the following linearized set of equations

$$f_{ext}^{t+\Delta t} - f_{int}^t = \sum_{e=1}^{n_e} Q_e^T \left(\int_{Ve} B^T C B dV \right) Q_e \Delta d \tag{4.6}$$

where

$$K = \sum_{e=1}^{n_e} Q_e^T \left(\int_{Ve} B^T C B dV \right) Q_e \tag{4.7}$$

is the tangential stiffness matrix of the structure upon a small increment of the loading. As a result, equation 4.6 obtains the simplified form

$$f_{ext}^{t+\Delta t} - f_{int}^{t} = K\Delta d \tag{4.8}$$

Due to the above linearization of the constitutive equations, a drift-away from the true solution will be produced, especially if relatively large loading steps are employed. A graphical illustration of this tendancy is provided in figure 4.1.

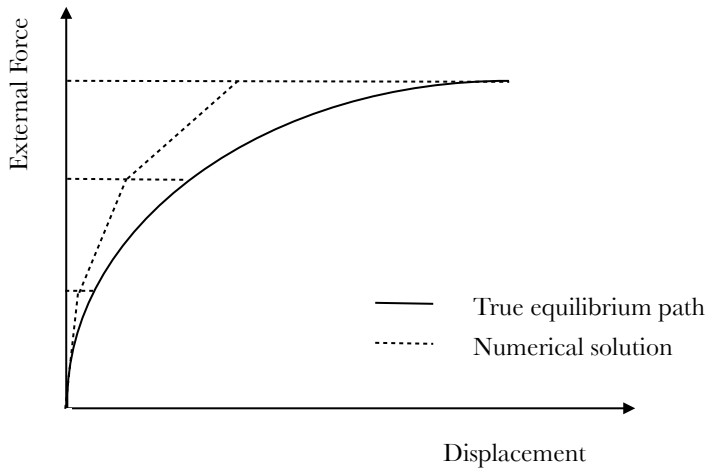

Figure 4.1: Purely incremental solution scheme

In order to prevent this gradual departure of the numerical solution from the true solution, or at least make it smaller, we need to add equilibrium iterations within each loading step. Now, we obtain an incremental-iterative procedure instead of a pure incremental procedure. In such a procedure, a first estimate for the displacement increment Δd is made through

$$\Delta d_1 = K_0^{-1} r_0 \tag{4.9}$$

where

$$r_0 = f_{ext}^{t_1} - f_{int,0} \tag{4.10}$$

is the residual vector at the beginning of the load increment and the subscript 1 of Δd denotes the estimate in the first iteration for the incremental displacement vector. In the same way, the subscript 0 of the internal force vector relates to the fact that this vector is calculated using the stresses at the beginning of the loading step, i.e. that are left behind at the end of the previous iteration ($\sigma_0 = \sigma_t$)

$$f_{int,0} = \sum_{e=1}^{n_e} Q_e^T \left(\sum_{i=1}^{n_i} w_i \big(\det J_i\big) B_i^T \sigma_{i,0} \right) \tag{4.11}$$

From the incremental displacement vector Δd_1 a first estimate for the strain increment $\Delta\epsilon_1 1$

can be calculated, whereupon, using the stressstrain law, the stress increment $\delta\sigma_1$ can be computed. The stresses after the first iteration are then given by

$$\sigma_1 = \sigma_0 + \Delta\sigma_1 \tag{4.12}$$

where a more extensive discussion over this update can be found in Chapter 3, concerning the material non-linearity.

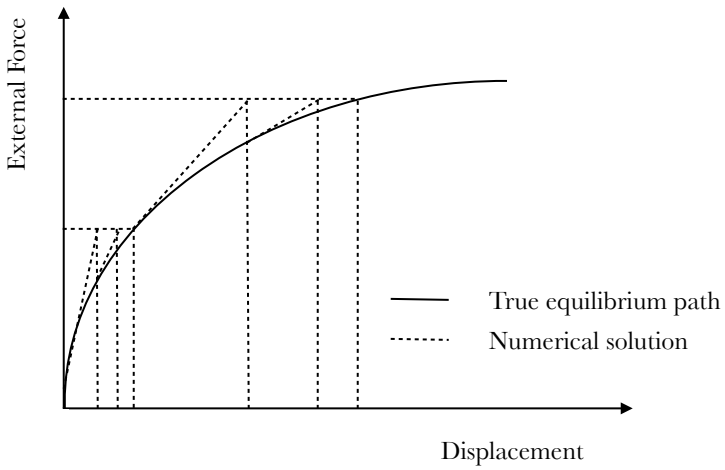

Figure 4.2: Incremental-iterative solution scheme

Generally, the first estimation of the internal force vector $f_{int,1}$ that is computed on the basis of the stress σ_1 is not in equilibrium with the external force vector $f_{ext,1}$ that have been added up to and including this loading step. As a result, a correction to the displacement vector is necessary and is obtained through

$$\delta d_2 = K_1^{-1} r_1 \quad \text{where} \quad r_1 = f_{ext}^{t_1} - f_{int,1} \tag{4.13}$$

and K_1 is the updated tangential stiffness matrix. After the second iteration in the loading step, the displacement increment follows from

$$\Delta d_2 = \Delta d_1 + \delta d_2 \tag{4.14}$$

Then, the stress and strain increments $\Delta\sigma_2$ and $\Delta\epsilon_2$ are calculated in a similar fashion and hence a better approximation for the internal forces can be produced so that

$$\begin{aligned} r_j &= f_{ext}^{t_1} - f_{int,j} \\ \delta d_{j+1} &= K_j^{-1} r_j \\ \Delta d_{j+1} &= \Delta d_j + \delta d_{j+1} \\ \Delta\epsilon_{i,j+1} &= \Delta\epsilon_i\big(\Delta d_{j+1}\big) \end{aligned}$$

$$\begin{aligned}\Delta\sigma_{i,j+1} &= \Delta\sigma_i\big(\Delta\epsilon_{i,j+1}, \sigma_{i,0}\big) \\ \sigma_{i,j+1} &= \sigma_{i,0} + \Delta\sigma_{i,j+1} \\ f_{int,j+1} &= \sum_{e=1}^{n_e} Q_e^T \left(\sum_{i=1}^{n_i} w_i \big(\det J_i\big) B_i^T \sigma_{i,j+1} \right)\end{aligned} \tag{4.15}$$

where index i denotes that the operations have to be done for every integration point and the above procedure is continued until a converged equilibrium state.

Table 4.1: Non-linear finite element analysis procedure

For each loading step

1. Initialize the data, set Δd_0=0
2. Get the new external force vector $f_{ext}^{t+\Delta t}$
3. Get the tangential stiffness matrix
$$K_i = \sum_{e=1}^{n_e} Q_e^T \left(\sum_{i=1}^{n_i} w_i \big(\det J_i\big) B_i^T C_{i,j} B_i \right) Q_e$$
4. Solve the linear system of equations
$$K_j \delta d_{j+1} = f_{ext}^{t+\Delta t} - f_{int,j}$$
5. Compute the incremental displacement vector
$$\Delta d_{j+1} = \Delta d_j + \delta d_{j+1}$$
6. Compute the incremental strain vector for each integration point
$$\Delta\epsilon_{i,j+1} = \Delta\epsilon_i\big(\Delta d_{j+1}\big)$$
7. Compute the final the incremental stress vector for each integration point
$$\sigma_{i,j+1} = \sigma_{i,0} + \Delta\sigma_{i,j+1}$$
8. Compute the internal force vector
$$f_{int,j+1} = \sum_{e=1}^{n_e} Q_e^T \left(\sum_{i=1}^{n_i} w_i \big(\det J_i\big) B_i^T \sigma_{i,j+1} \right)$$
9. Check convergence, if $\| f_{ext}^{t+\Delta t} - f_{int,j+1} \|$ <tolerance, go to the next loading step, else return to 3.

An issue that has not been discussed yet, is the implicit assumption that the tangential stiffness matrix K_j is updated after each iteration. Indeed, it is not necessary to update and decompose the stiffness matrix in every iteration, as is being done within the full Newton-Raphson process, since alternative methods that obviate the need to construct a tangential stiffness matrix in every iteration have been developed.

Consequently, we could adopt a scheme where tha stiffness matrix is obtained simply by setting up a new tangential stiffness only every few iterations, or only once within a loading step. The stiffness matrix is assumed to vary so slowly that its set up in an iteration serves as a reasonably accurate approximation of the tangential stiffness for a couple of subsequent iterations. Hence, it is estimated that the slowing down of the convergence speed is off set by the gain in computer time within each iteration.

A first method along this direction is the modified Newton-Raphson, which sets up and decomposes the stiffness matrix only once within every loading step and usually at the beginning of the loading step. An advantage of this process is that all state variables are computed on the basis of an equilibrium state (presuming of course that a converged solution has been obtained in the preceding load increment). The alternative approach in which the stiffness matrix is only updated at the beginning of the second iteration of each load increment lacks in this advantage, but also does no suffer from the drawback of the first variant, namely that none of the non-linearities that arise during the loading step are incorporated in the stiffness matrix that is being used in the majority of the iterations. However, it should be noted that the implementation of the modified Newton-Rapshon method can cause convergence difficulties, since it cannot cope well with either local or global stiffening of structural behaviour

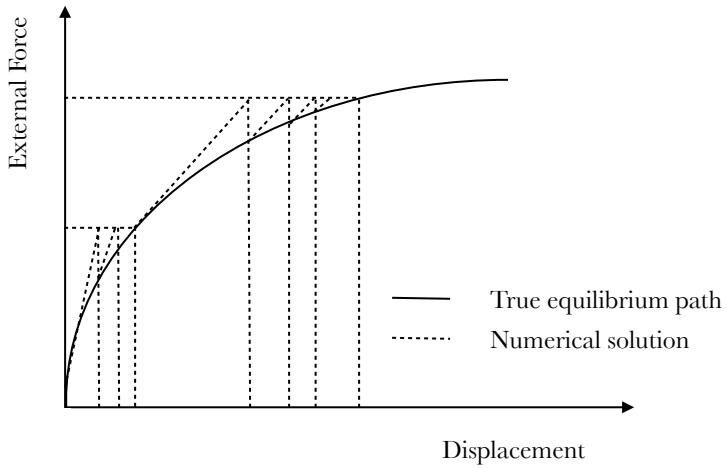

Figure 4.3: Modified Newtion-Rapshon

A more simple variant of this iterative procedures, is the initial stiffness method, as illustrated in 4.4. According to this method, the stiffness matrix is set up and decomposed only at the beginning of the first loading step. It is evident that, when the failure load is approached and the current stiffness matrix remains at the same initial value, convergence becomes slow and a large number of iterations are required to obtain a reasonable accuracy. As a result, a less tight convergence tolerance must be adopted in order to achieve a sutisfactory number of iterations and thus, the failure load will be overestimated. However, by

continuing the calculation beyond the limit point of the loaddeflection curve the proper failure load can sometimes be obtained, since the additional iterations that are added in these post-peak increments result in a levelling out of the loaddeflection path until the true failure load has been reached.

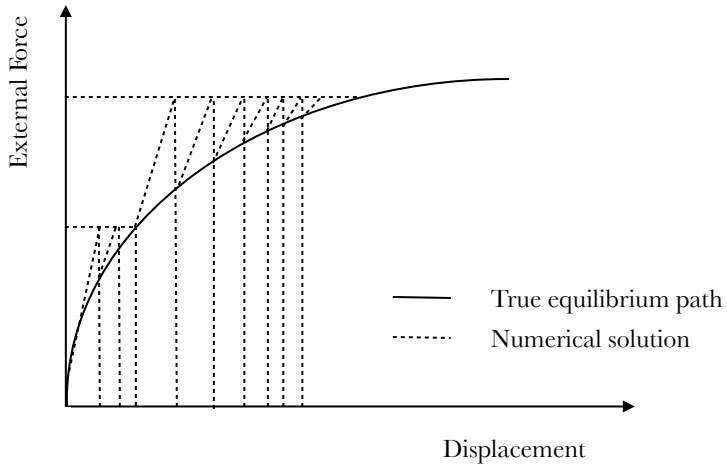

Figure 4.4: Initial stiffness method

For the sake of generality, it should be mentioned that a second class of method could be used, including the so-called Quasi-Newton methods or Secant-Newton methods. These methods apply updates on existing tangential stiffness matrices such that the stiffness in the subsequent iteration is computed using a multi-dimensional secant approximation.

4.2 Displacement Control

Unlike the previous section where the load is applied to the structure, in the present section, the so-called displacement control procedure will be developed where prescribed displacements are imposed on the structure. Thus, a stress is produced within the specimen which in turn results in nodal forces at the nodes where the displacements are prescribed. The sum of these forces produces the total reaction force which describes the equivalent external load that would be caused by the prescribed displacements.

Concerning the comparison, when the physics do not explicitly dictate which type of solution is the most appropriate, the displacement control procedure is often preferred according to the following reasons

1. The tangential stiffness matrix is better conditioned for displacement control than for load control. This tends to result in a faster convergence behaviour of the iterative procedure.

2. Under load control, the tangential stiffness matrix becomes singular at a limit point in the loaddeflection diagram, not only when global failure occurs, but also when we have a local maximum along this curve. The tangential stiffness matrix of the displacement

controlled problem, on the other hand, does not become singular. An illustration of this phenomenon is presented in figure 4.5.

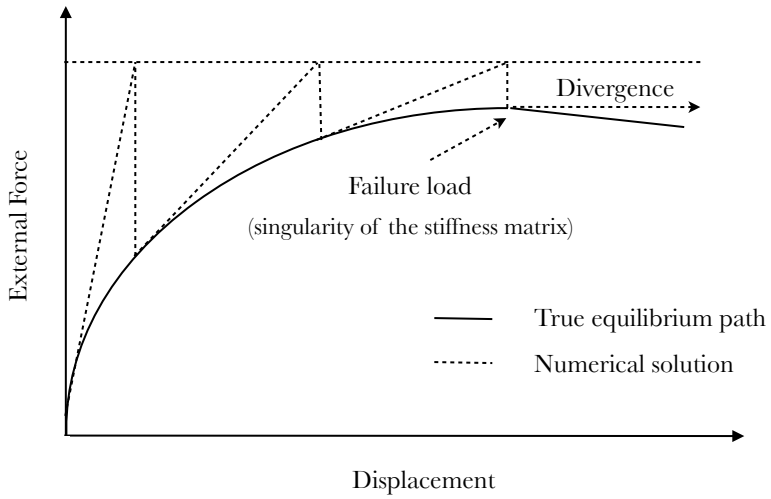

Figure 4.5: Singularity of tangential stiffness matrix at limit point and divergence of iterative procedure

The above statements are best clarified from equation 4.8 which has been produced for load control and the prescribed external load is contained explicitly in the vector f_{ext}. Now, instead of the external forces, a number of non-zero displacements are imposed in an incremental procedure. Thus, we decompose the incremental displacement and force vectors Δd and into a vector that contains only degrees of freedom that are free Δd_f and displacement increments that have been assigned a certain non-zero value Δd_p, so that

$$\Delta d = \begin{bmatrix} \Delta d_f \\ \Delta d_p \end{bmatrix} \quad \text{and} \quad f_{int,0} = \begin{bmatrix} (f_f)_{int,0} \\ (f_p)_{int,0} \end{bmatrix} \tag{4.16}$$

In a similar fashion the stiffness matrix is partitioned as

$$K = \begin{bmatrix} K_{ff} & K_{fp} \\ K_{pf} & K_{pp} \end{bmatrix} \tag{4.17}$$

and finally the equilibrium equation 4.8 receives the following form

$$\begin{bmatrix} K_{ff} & K_{fp} \\ K_{pf} & K_{pp} \end{bmatrix} \begin{bmatrix} \Delta d_f \\ \Delta d_p \end{bmatrix} = - \begin{bmatrix} (f_f)_{int,0} \\ (f_p)_{int,0} \end{bmatrix} \tag{4.18}$$

where it has been assumed that, apart from the prescribed displacements, no other forces act on the structure.
Then, the free displacement increments can be computed by eliminating Δd_p. Consequently, from 4.17 we obtain the elimination formula for the first iteration

$$\Delta d_{f,1} = -K_{ff}^{-1}\Big(K_{fp}\Delta d_p + \big(f_f\big)_{int,0}\Big) \tag{4.19}$$

while for the next iterations the formula changes to

$$\delta d_{f,1} = -K_{ff}^{-1}\big(f_f\big)_{int,j} \tag{4.20}$$

since the increment δd_p is imposed only on the first iteration. Comparison of 4.8 and 4.19, shows that for the first iteration the external load $f_{ext}^{t+\Delta t}$ must be replaced by the equivalent force vector $K_{fp}\Delta d_p$ when switching from load to displacement control. In the next iterations this contribution vanishes altogether for displacement control.

Chapter 5

Modeling of the Microstructure

This chapter is concentrated on the microstructural simulation within a multiscale approach, using the finite element method. A fiber-reinforced material, and concretely a carbon nanotube composite, is investigated in the present work and as a result the following development will be directed according to this approach. For this purpose, the present chapter is divided into three parts concerning the components of the polymer and their mechanical interaction. In the first section, the isoparametric formulation of the quadrilateral element, which is used for the discretization of the surrounding matrix, is extensively presented, while the second section is concentrated on the finite element simulation of the carbon nanotubes. The first part of this section presents the carbon fibers random geometries which are dirived from processing scanning electron microscope images according to [7]. Finally, in the third section the interaction of these components is further discussed and presented in mathematical and computational terms.

5.1 Polymer Simulation

The first step for the discretization of the microstructure concerns the polymer simulation, which is achieved through the employment of the linear quadrilateral element. Furthermore, for the production of the stiffness matrix the isoparametric formulation is adopted.

5.1.1 Isoparametric Formulation

The isoparametric elements were invented by Taig and Irons for the purpose of the simulation of curved boundaries using non-rectangular elements. According to this approach, the production of isoparametric elements is based on two coordinate systems

1. The Cartesian Coordinate System and
2. The Natural Coordinate System which constitutes a mapping of the Cartesian Coordinate System

The bridging of these systems is achieved through the transformation matrix $[J]$, the so-called Jacobian matrix which, in general, relates the partial derivatives of a function f expressed in two coordinate systems, (x, y, z) and (ξ, η, ζ) respectively.

The transformation formula is expressed as

$$\begin{bmatrix} \dfrac{\partial f}{\partial \xi} \\ \dfrac{\partial f}{\partial \eta} \\ \dfrac{\partial f}{\partial \zeta} \end{bmatrix} = \begin{bmatrix} \dfrac{\partial x}{\partial \xi} & \dfrac{\partial y}{\partial \xi} & \dfrac{\partial z}{\partial \xi} \\ \dfrac{\partial x}{\partial \eta} & \dfrac{\partial y}{\partial \eta} & \dfrac{\partial z}{\partial \eta} \\ \dfrac{\partial x}{\partial \zeta} & \dfrac{\partial y}{\partial \zeta} & \dfrac{\partial z}{\partial \zeta} \end{bmatrix} \begin{bmatrix} \dfrac{\partial f}{\partial x} \\ \dfrac{\partial f}{\partial y} \\ \dfrac{\partial f}{\partial z} \end{bmatrix} \tag{5.1}$$

where the 3x3 matrix denotes the Jacobian matrix

$$J = \begin{bmatrix} \dfrac{\partial x}{\partial \xi} & \dfrac{\partial y}{\partial \xi} & \dfrac{\partial z}{\partial \xi} \\ \dfrac{\partial x}{\partial \eta} & \dfrac{\partial y}{\partial \eta} & \dfrac{\partial z}{\partial \eta} \\ \dfrac{\partial x}{\partial \zeta} & \dfrac{\partial y}{\partial \zeta} & \dfrac{\partial z}{\partial \zeta} \end{bmatrix} \tag{5.2}$$

It should be noted that the term "Isoparametric" derives from the fact that both the displacements u, v, w and the coordinates x, y, z are interpolated through the same rule, namely the interpolation or shape functions.

As a first step for the computation of the stiffness matrix, we need to obtain the transformation of the cartesian system as

$$\begin{aligned} x &= x\big(\xi, \eta, \zeta\big) \\ y &= y\big(\xi, \eta, \zeta\big) \\ z &= z\big(\xi, \eta, \zeta\big) \end{aligned} \qquad \text{or} \qquad \begin{aligned} \xi &= \xi\big(x, y, z\big) \\ \eta &= \eta\big(x, y, z\big) \\ \zeta &= \zeta\big(x, y, z\big) \end{aligned} \tag{5.3}$$

Then for the integration of the stiffness matrix relations, we obtain the following formula, using equation 5.1

$$dV = \begin{vmatrix} \dfrac{\partial x}{\partial \xi} & \dfrac{\partial y}{\partial \xi} & \dfrac{\partial z}{\partial \xi} \\ \dfrac{\partial x}{\partial \eta} & \dfrac{\partial y}{\partial \eta} & \dfrac{\partial z}{\partial \eta} \\ \dfrac{\partial x}{\partial \zeta} & \dfrac{\partial y}{\partial \zeta} & \dfrac{\partial z}{\partial \zeta} \end{vmatrix} d\xi d\eta d\zeta = \det\big(J\big) d\xi d\eta d\zeta \tag{5.4}$$

which relates the infinitesimal volume dV of the cartesian coordinate system with the natural coordinate system. A more simplified form is obtained for the transformation of the infinitesimal area dA into the natural system

$$dA = \begin{vmatrix} \dfrac{\partial x}{\partial \xi} & \dfrac{\partial y}{\partial \xi} \\ \dfrac{\partial x}{\partial \eta} & \dfrac{\partial y}{\partial \eta} \end{vmatrix} d\xi d\eta = \det\big(J\big) d\xi d\eta \tag{5.5}$$

Similarly, for the case of the one-dimensional mapping, the above relation is further simplified by eliminating the corresponding rows and columns of the initial formula 5.1.

5.1.2 Shape Functions

In the following figure, the four-node quadrilateral element is illustrated in both the cartesian and the natural systems.

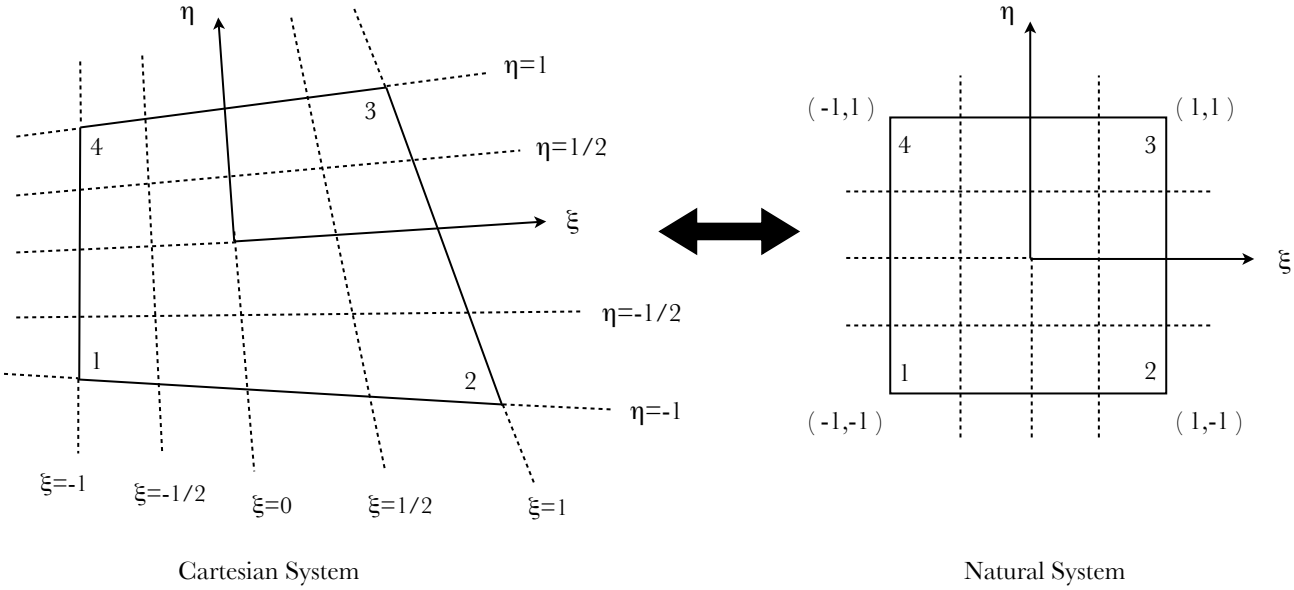

Figure 5.1: Four-node isoparametric quadrilateral element

Now, in order to obtain the transformation, the cartesian coordinates are given as

$$\begin{aligned} x &= a_1 + a_2\xi + a_3\eta + a_4\xi\eta \\ y &= a_5 + a_6\xi + a_7\eta + a_8\xi\eta \end{aligned}$$

or using a matrix notation

$$x = \begin{bmatrix} 1 & \xi & \eta & \xi\eta \end{bmatrix} \begin{bmatrix} a_1 \\ a_2 \\ a_3 \\ a_4 \end{bmatrix}, \qquad y = \begin{bmatrix} 1 & \xi & \eta & \xi\eta \end{bmatrix} \begin{bmatrix} a_5 \\ a_6 \\ a_7 \\ a_8 \end{bmatrix} \tag{5.6}$$

In the same fashion, and according to the isoparametric formulation, the displacement field is obtained through the same interpolation functions

$$u = \begin{bmatrix} 1 & \xi & \eta & \xi\eta \end{bmatrix} \begin{bmatrix} b_1 \\ b_2 \\ b_3 \\ b_4 \end{bmatrix}, \qquad v = \begin{bmatrix} 1 & \xi & \eta & \xi\eta \end{bmatrix} \begin{bmatrix} b_5 \\ b_6 \\ b_7 \\ b_8 \end{bmatrix} \tag{5.7}$$

where now, applying the boundary conditions we take

$$\begin{aligned} x_1 &= a_1 - a_2 - a_3 + a_4 \quad (\xi = -1, \eta = -1) \\ x_2 &= a_1 + a_2 - a_3 - a_4 \quad (\xi = 1, \eta = -1) \\ x_3 &= a_1 + a_2 + a_3 + a_4 \quad (\xi = 1, \eta = 1) \\ x_4 &= a_1 - a_2 + a_3 - a_4 \quad (\xi = -1, \eta = 1) \end{aligned} \tag{5.8}$$

or using matrix notation

$$\begin{bmatrix} x_1 \\ x_2 \\ x_3 \\ x_4 \end{bmatrix} = \begin{bmatrix} 1 & -1 & -1 & 1 \\ 1 & 1 & -1 & -1 \\ 1 & 1 & 1 & 1 \\ 1 & -1 & 1 & -1 \end{bmatrix} \begin{bmatrix} a_1 \\ a_2 \\ a_3 \\ a_4 \end{bmatrix} \tag{5.9}$$

and solving for the coefficients a_i we obtain

$$\begin{bmatrix} a_1 \\ a_2 \\ a_3 \\ a_4 \end{bmatrix} = \begin{bmatrix} 1 & 1 & 1 & 1 \\ -1 & 1 & 1 & -1 \\ -1 & -1 & 1 & 1 \\ 1 & -1 & 1 & -1 \end{bmatrix} \begin{bmatrix} x_1 \\ x_2 \\ x_3 \\ x_4 \end{bmatrix} \tag{5.10}$$

Substituting equation 5.10 into 5.6, we take the formula relating the natural coordinates of any point with the cartesian system. Similarly, if we repeat the above procedure for y we obtain

$$x = \begin{bmatrix} N_1 & N_2 & N_3 & N_4 \end{bmatrix} \begin{bmatrix} x_1 \\ x_2 \\ x_3 \\ x_4 \end{bmatrix}, \qquad y = \begin{bmatrix} N_1 & N_2 & N_3 & N_4 \end{bmatrix} \begin{bmatrix} y_1 \\ y_2 \\ y_3 \\ y_4 \end{bmatrix} \tag{5.11}$$

where

$$
\begin{aligned}
N_1 &= \frac{1}{4}(1-\xi)(1-\eta) \\
N_2 &= \frac{1}{4}(1+\xi)(1-\eta) \\
N_3 &= \frac{1}{4}(1+\xi)(1+\eta) \\
N_4 &= \frac{1}{4}(1-\xi)(1-\eta)
\end{aligned}
\tag{5.12}
$$

are the shape functions of the element. Now, writting 5.11 in a more compact form we take

$$
\begin{bmatrix} x \\ y \end{bmatrix} = \begin{bmatrix} N_1 & 0 & N_2 & 0 & N_3 & 0 & N_4 & 0 \\ 0 & N_1 & 0 & N_2 & 0 & N_3 & 0 & N_4 \end{bmatrix} \begin{bmatrix} x_1 \\ y_1 \\ x_2 \\ y_2 \\ x_3 \\ y_3 \\ x_4 \\ y_4 \end{bmatrix} \tag{5.13}
$$

the transformation of the natural coordinate system into the cartesian. In a similar manner, and taking into account the isoparametric formulation, in order to obtain the displacement field, we use the above shape functions and hence we take

$$
\begin{bmatrix} u \\ v \end{bmatrix} = \begin{bmatrix} N_1 & 0 & N_2 & 0 & N_3 & 0 & N_4 & 0 \\ 0 & N_1 & 0 & N_2 & 0 & N_3 & 0 & N_4 \end{bmatrix} \begin{bmatrix} u_1 \\ v_1 \\ u_2 \\ v_2 \\ u_3 \\ v_3 \\ u_4 \\ v_4 \end{bmatrix} \quad \text{or} \quad \{u\} = [N]\{d\} \tag{5.14}
$$

where u_i, v_i denote the nodal displacements in direction x and y respectively. Consequently, in order to calculate the coordinates x, y or the displacements u, v of any point, we simply substitute the coordinates ξ and η into equations 5.13 and 5.14 respectively.

5.1.3 Deformation Matrix

Once obtained the deformation field and the coordinate transformation, the next step includes the computation of the deformation matrix B which relates the strain at any point with the nodal displacements u and v. According to the continuum mechanics, the strain vector for plane stress problems is obtained through

$$\begin{bmatrix} \epsilon_{xx} \\ \epsilon_{yy} \\ \gamma_{xy} \end{bmatrix} = \begin{bmatrix} \dfrac{\partial u}{\partial x} \\ \dfrac{\partial v}{\partial y} \\ \dfrac{\partial u}{\partial y} + \dfrac{\partial v}{\partial x} \end{bmatrix} = \begin{bmatrix} \dfrac{\partial}{\partial x} & 0 \\ 0 & \dfrac{\partial}{\partial y} \\ \dfrac{\partial}{\partial y} & \dfrac{\partial}{\partial x} \end{bmatrix} \begin{bmatrix} u \\ v \end{bmatrix} \tag{5.15}$$

However, the displacement field u, v is expressed in the natural coordinate system and as a result the above derivatives cannot be directly computed through equation 5.14. Generally, in such a case, where a function f, defined in two coordinate systems (x, y) and (ξ, η), is not possible to be expressed in terms of (x, y), we obtain first the expression

$$\frac{\partial f}{\partial \xi} = \frac{\partial f}{\partial x}\frac{\partial x}{\partial \xi} + \frac{\partial f}{\partial y}\frac{\partial y}{\partial \xi} \tag{5.16}$$

or

$$\begin{bmatrix} \dfrac{\partial f}{\partial \xi} \\ \dfrac{\partial f}{\partial \eta} \end{bmatrix} = \begin{bmatrix} \dfrac{\partial x}{\partial \xi} & \dfrac{\partial y}{\partial \xi} \\ \dfrac{\partial x}{\partial \eta} & \dfrac{\partial y}{\partial \eta} \end{bmatrix} \begin{bmatrix} \dfrac{\partial f}{\partial x} \\ \dfrac{\partial f}{\partial y} \end{bmatrix} \tag{5.17}$$

or

$$\begin{bmatrix} \dfrac{\partial f}{\partial \xi} \\ \dfrac{\partial f}{\partial \eta} \end{bmatrix} = \big[J\big] \begin{bmatrix} \dfrac{\partial f}{\partial x} \\ \dfrac{\partial f}{\partial y} \end{bmatrix} \tag{5.18}$$

where $\big[J\big]$ denotes the Jacobian matrix and derives from equation 5.13 and as a result, it takes the following form

$$\big[J\big] = \begin{bmatrix} N_{1,\xi} & N_{2,\xi} & N_{3,\xi} & N_{4,\xi} \\ N_{1,\eta} & N_{2,\eta} & N_{3,\eta} & N_{4,\eta} \end{bmatrix} \begin{bmatrix} x_1 & y_1 \\ x_2 & y_2 \\ x_3 & y_3 \\ x_4 & y_4 \end{bmatrix} = \big[D_N\big] \begin{bmatrix} x_1 & y_1 \\ x_2 & y_2 \\ x_3 & y_3 \\ x_4 & y_4 \end{bmatrix} \tag{5.19}$$

where matrix D_N is obtained through the shape functions expressed by equations 5.12

$$\big[D_N\big] = \frac{1}{4} \begin{bmatrix} -(1-\eta) & (1-\eta) & (1+\eta) & -(1+\eta) \\ -(1-\xi) & -(1+\xi) & (1+\xi) & (1-\xi) \end{bmatrix} \tag{5.20}$$

Now, in order to produce the strain vector, we need to compute the derivatives of the displacement field. Thus, equation 5.18 gives

$$\begin{bmatrix} \dfrac{\partial f}{\partial x} \\ \dfrac{\partial f}{\partial y} \end{bmatrix} = \big[J\big]^{-1} \begin{bmatrix} \dfrac{\partial f}{\partial \xi} \\ \dfrac{\partial f}{\partial \eta} \end{bmatrix} \tag{5.21}$$

where the inverse of the Jacobian matrix is obtained through the relation

$$\big[J\big]^{-1} = \begin{bmatrix} J_{11}^{*} & J_{12}^{*} \\ J_{21}^{*} & J_{22}^{*} \end{bmatrix} = \frac{1}{\det\big(J\big)} \begin{bmatrix} J_{22} & -J_{12} \\ -J_{21} & J_{11} \end{bmatrix} \tag{5.22}$$

where

$$\det\big(J\big) = J_{11}J_{22} - J_{21}J_{12} \tag{5.23}$$

J_{ij} denotes the elements of the Jacobian matrix $\big[J\big]$ and J_{ij}^{*} denotes the elements of the inverse Jacobian matrix $\big[J\big]^{-1}$. Through equation 5.21, the strain expression leads to

$$\begin{bmatrix} \epsilon_{xx} \\ \epsilon_{yy} \\ \gamma_{xy} \end{bmatrix} = \begin{bmatrix} \dfrac{\partial u}{\partial x} \\ \dfrac{\partial v}{\partial y} \\ \dfrac{\partial u}{\partial y} + \dfrac{\partial v}{\partial x} \end{bmatrix} = \frac{1}{\det\big(J\big)} \begin{bmatrix} J_{22} & -J_{12} & 0 & 0 \\ 0 & 0 & -J_{21} & J_{11} \\ -J_{21} & J_{11} & J_{22} & -J_{12} \end{bmatrix} \begin{bmatrix} \dfrac{\partial u}{\partial \xi} \\ \dfrac{\partial u}{\partial \eta} \\ \dfrac{\partial v}{\partial \xi} \\ \dfrac{\partial v}{\partial \eta} \end{bmatrix} \tag{5.24}$$

or

$$\{\epsilon\} = \big[B_1\big]\{u_\xi\} \tag{5.25}$$

where the partial derivatives of the displacement field are computed, using equation 5.14, through

$$\begin{bmatrix} \dfrac{\partial u}{\partial \xi} \\ \dfrac{\partial u}{\partial \eta} \\ \dfrac{\partial v}{\partial \xi} \\ \dfrac{\partial v}{\partial \eta} \end{bmatrix} = \begin{bmatrix} N_{1,\xi} & 0 & N_{2,\xi} & 0 & N_{3,\xi} & 0 & N_{4,\xi} & 0 \\ N_{1,\eta} & 0 & N_{2,\eta} & 0 & N_{3,\eta} & 0 & N_{4,\eta} & 0 \\ 0 & N_{1,\xi} & 0 & N_{2,\xi} & 0 & N_{3,\xi} & 0 & N_{4,\xi} \\ 0 & N_{1,\eta} & 0 & N_{2,\eta} & 0 & N_{3,\eta} & 0 & N_{4,\eta} \end{bmatrix} \begin{bmatrix} u_1 \\ v_1 \\ u_2 \\ v_2 \\ u_3 \\ v_3 \\ u_4 \\ v_4 \end{bmatrix} \tag{5.26}$$

or

$$\{u_\xi\} = \big[B_2\big]\{d\} \tag{5.27}$$

Then, combining equations 5.25 and 5.27 we obtain the expression of the strain vector

$$\{\epsilon\} = \big[B_1\big]\big[B_2\big]\{d\} \tag{5.28}$$

where the second component B_2 of the deformation matrix is

$$\big[B_2\big] = \frac{1}{4}\begin{bmatrix} -(1-\eta) & 0 & (1-\eta) & 0 & (1+\eta) & 0 & -(1+\eta) & 0 \\ -(1-\xi) & 0 & -(1+\xi) & 0 & (1+\xi) & 0 & (1-\xi) & 0 \\ 0 & -(1-\eta) & 0 & (1-\eta) & 0 & (1+\eta) & 0 & -(1+\eta) \\ 0 & -(1-\xi) & 0 & -(1+\xi) & 0 & (1+\xi) & 0 & (1-\xi) \end{bmatrix}$$

Consequently, the deformation matrix B is expressed as the product of the two components $B1$ and $B2$, so that

$$\big[B\big] = \big[B_1\big]\big[B_2\big] \quad \text{and} \quad \{\epsilon\} = \big[B\big]\{d\} \tag{5.29}$$

5.1.4 Stiffness Matrix

Once obtained the formula of the deformation matrix in the natural coordinate system, the expression of the stiffness matrix can now be transformed. In the general case, the stiffness matrix derives from the following form

$$\big[k\big] = \int_{V_e} \big[B\big]^T \big[E\big]\big[B\big] dV_e \tag{5.30}$$

while for the four-node quadrilateral element, the integration is reduced to the plane of the element and thus 5.30 gives

$$\big[k\big] = \int_{A_e} \big[B\big]^T \big[E\big]\big[B\big] t dA_e \tag{5.31}$$

where t denotes the thickness of the element and $\big[E\big]$ is the constitutive matrix which for plane stress problems is

$$\big[E\big] = \frac{E}{1-\nu^2}\begin{bmatrix} 1 & \nu & 0 \\ \nu & 1 & 0 \\ 0 & 0 & \dfrac{(1-\nu)}{2} \end{bmatrix} \tag{5.32}$$

Now, using equations 5.5 and 5.29, we obtain the transformed expression of 5.31 in the natural coordinate system

$$\big[k\big] = \int_{-1}^{1}\int_{-1}^{1} \big[B(\xi,\eta)\big]^T \big[E\big]\big[B(\xi,\eta)\big] t \det\big(J\big) d\xi d\eta \tag{5.33}$$

where the integration limits are also adapted according to the natural coordinate system, as illustrated in figure 5.1. From equations 5.25 and 5.29 we notice that $\det(J)$, constituting the denominator of B_1, contains a polynomial $a_1 + a_2\xi + a_3\eta + a_4\xi\eta$, so in order to compute the integral of 5.33 we will employ a numerical method, namely the Gauss method.

5.1.5 Numerical Integration

The Gaussian integration will be used for the computation of the stiffness integrals of 5.33 instead of a closed form integration. This quadrature rule produces an approximation of a definite integral of a function as the weighted sum of function values at specified points within the domain of integration. In general, a n-point Gaussian quadrature rule is a quadrature rule constructed to yield an exact result for polynomials of degree 2n-1 or less by a suitable choice of the points x_i , the so-called Gauss-points, and weights a_i for $i = 1, 2, ..., n$. The domain of integration for such a rule is conventionally taken as $[-1, 1]$, so the rule is stated as

$$\int_{-1}^{1} f(x)dx \approx a_1 f(x_1) + a_2 f(x_2) + ... + a_n f(x_n) = \sum_{i=1}^{n} a_n f(x_n) \tag{5.34}$$

where x_i and a_i constitute a suitable choice of points, the so-called Gauss-points, and weights respectively for i = 1,...,n. Now, in order to expand this rule for a function of two variables, we take

$$\int_{-1}^{1}\int_{-1}^{1} f(x,y)dxdy = \int_{-1}^{1} g(y)dy \tag{5.35}$$

where

$$g(y) = \int_{-1}^{1} f(x,y)dxdy = \sum_{i=1}^{n} a_i f(x_i, y) \tag{5.36}$$

or in a more compact form

$$\begin{aligned}\int_{-1}^{1}\int_{-1}^{1} f(x,y)dxdy &= \sum_{j=1}^{n} a_j \sum_{i=1}^{n} a_i f(x_i, y_j) \\ &= \sum_{j=1}^{n}\sum_{i=1}^{n} a_i a_j f(x_i, y_i)\end{aligned} \tag{5.37}$$

Similarly, this quadrature rule can be expanded for functions of three or more variables. Depending on the degree of the polynomial, an adequate order rule must be adopted for solving the integration problem. In particular, for a linear quadrilateral element a 2x2-point rule has to be employed for the accurate computation of the stiffness matrix. Now, using 5.37 we take the stiffness matrix expression

$$\begin{aligned}\big[k\big] &= \int_{-1}^{1}\int_{-1}^{1} \big[B\big(\xi,\eta\big)\big]^T \big[E\big(\xi,\eta\big)\big]\big[B\big(\xi,\eta\big)\big] t\det\big(J\big)d\xi d\eta \\ &= \sum_{j=1}^{n}\sum_{i=1}^{n} a_i a_j \big[B\big(\xi_i,\eta_j\big)\big]^T \big[E\big(\xi_i,\eta_j\big)\big]\big[B\big(\xi_i,\eta_j\big)\big] t\det\big(J(\xi_i,\eta_j)\big)\end{aligned} \tag{5.38}$$

where the constitutive matrix $[E]$ is also considered to be a function of ξ and η in the framework of a non-linear material.

Number of Points, n	**Points, x_i**	**Weights, a_i**
1	0	2
2	$\pm\sqrt{1/3}$	1
3	0	8/9
	$\pm\sqrt{3/5}$	5/9
4	$\pm\sqrt{\left(3-2\sqrt{6/5}\right)/7}$	$\frac{18+\sqrt{30}}{16}$
	$\pm\sqrt{\left(3+2\sqrt{6/5}\right)/7}$	$\frac{18-\sqrt{30}}{16}$
5	0	$\frac{128}{225}$
	$\pm\frac{1}{3}\sqrt{\left(5-2\sqrt{10/7}\right)}$	$\frac{322+13\sqrt{70}}{900}$
	$\pm\frac{1}{3}\sqrt{\left(5+2\sqrt{10/7}\right)}$	$\frac{322-13\sqrt{70}}{900}$

Table 5.1: Order rules for solving the integration problem

5.2 Fiber Simulation

5.2.1 Geometry

According to [7], random fiber waviness is modeled as a non-homogeneous stochastic field using the spectral representation method in conjunction with evolutionary power spectra. The statistical properties of this spectra are derived from processing a number of carbon nanotube geometries from scanning electron microscope images. The evolutionary power spectra depend not only on the frequency ω but also on spatial state variables. Consequently, it can be expressed as the product of a homogeneous power spectrum $S_h(x)$ and a spatial envelope function $g_h(x)$ as follows:

$$S(\omega, x) = S_h(\omega) g_h(\omega) \tag{5.39}$$

where an estimate of the first term in 5.39 can be obtained by averaging the periodograms over the ensemble:

$$\bar{S}_h(\omega) = E\left[\frac{1}{2\pi L}\left|\int_0^L f^{(i)}(x)e^{-i\omega x}dx\right|^2\right] \tag{5.40}$$

with $f^{(i)}(x)$ being the wavy geometry of the ith fiber and E denoting the mathematical expectation.

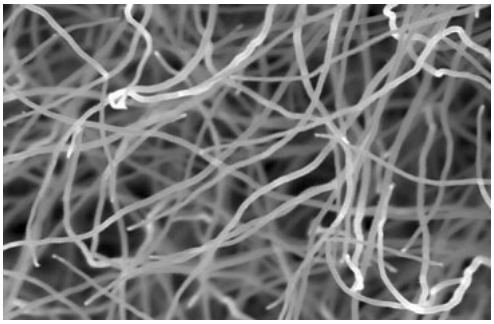

Figure 5.2: Image of wavy geometry of fibers

An estimate of the spatial envelope function can be obtained from the distribution of the mean square over the samples as

$$\bar{g}_h(x) = \frac{E\left[\left|f(x)\right|^2\right]}{2\int_0^\infty \bar{S}_h(\omega)d\omega} \tag{5.41}$$

and an estimate of the evolutionary power spectra is given by

$$\bar{S}_h(\omega, x) = E\left[\left|f^{(i)}(x)\right|^2\right]\frac{\bar{S}_h(\omega)}{2\int_0^\infty \bar{S}_h(\omega)d\omega} \tag{5.42}$$

Now, samples of wavy carbon nanotubes can be generated using equation 5.40 according to

$$f^{(j)}(x) = \sqrt{2}\sum_{n=0}^{N-1} A_n cos\left(\omega_n x + \phi_n^{(j)}\right) \tag{5.43}$$

where

$$\begin{aligned}
&A_n = \sqrt{2\bar{S}_h(\omega_n, x)\Delta\omega}, \quad n = 1, 2, ..., N-1 \\
&\omega_n = n\Delta\omega, \quad n = 1, 2, ..., N-1 \\
&\Delta\omega = \frac{\omega_{up}}{N} \\
&A_0 = 0 \\
&\bar{S}_h(\omega_0, x) = 0
\end{aligned} \tag{5.44}$$

The parameter ω_{up} refers to an upper limit of the frequency, beyond which the autocorrelation function is supposed to be zero. Parameter $\phi_n^{(j)}$ stands for random phase angles in the range $[0, 2\pi]$, for the jth sample realization.

5.2.2 Beam Element

Once obtained the geometry, according to the previous development, the fibers are then discretized using plane beam elements. The evaluation of the mechanical properties of the fibers, namely the young modulus and the stiffness properties, is achieved through the equivalent beam element for carbon nanotubes.

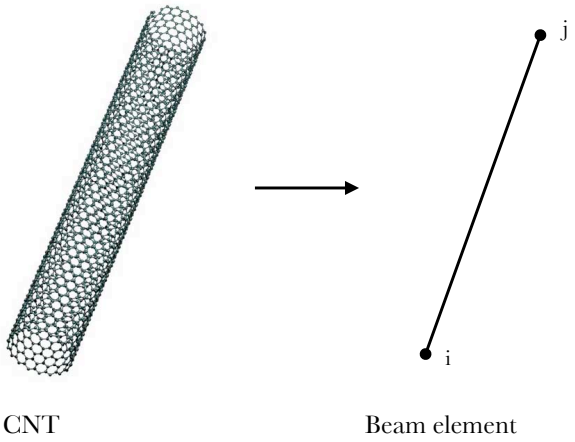

Figure 5.3: Schematic representation of the multiscale modeling

According to this approach, the carbon nanotube is first simulated as a space frame structure with the covalent bond between the atoms being represented by continuum beams. However, such a simulation is an extremely computationally demanding task and it is only used for the production of the equivalent beam properties. More specifically, the space frame model is subjected to different loading conditions in order to produce the stiffness indices, and the fibers are then simulated using beam elements with equivalent mechanical properties. Consequently, the local stiffness matrix of a fiber element is

$$\left[k_{Local}\right] = \begin{bmatrix} \frac{AE}{L} & 0 & 0 & -\frac{AE}{L} & 0 & 0 \\ 0 & \frac{12EI}{L^3} & \frac{6EI}{L^2} & 0 & -\frac{12EI}{L^3} & \frac{6EI}{L^2} \\ 0 & \frac{6EI}{L^2} & \frac{4EI}{L} & 0 & -\frac{6EI}{L^2} & \frac{2EI}{L} \\ -\frac{AE}{L} & 0 & 0 & \frac{AE}{L} & 0 & 0 \\ 0 & -\frac{12EI}{L^3} & -\frac{6EI}{L^2} & 0 & \frac{12EI}{L^3} & -\frac{6EI}{L^2} \\ 0 & \frac{6EI}{L^2} & \frac{2EI}{L} & 0 & -\frac{6EI}{L^2} & \frac{4EI}{L} \end{bmatrix} \tag{5.45}$$

where the area A and the inertia I are obtained from the assumed profile section for the equivalent beam element and the elastic moduli derives by equating the space frame results

with the corresponding stiffness indices of 5.45. An extensive development for the modeling of carbon nanotubes with equivalent beam element can be found in [7] along with the produced fiber geometry.

Now, in order to incorporate the beam element in the surrounding polymer for the finite element analysis, the embedded element technique is used. At first, the global stiffness matrix of the beam element is computed as

$$\left[k_{Global}\right] = \left[T_1\right]^T \left[k_{Local}\right] \left[T_1\right] \tag{5.46}$$

where $\left[T_1\right]$ is a transformation matrix according to

$$\left[T_1\right] = \begin{bmatrix} cos\theta & -sin\theta & 0 & 0 & 0 & 0 \\ sin\theta & cos\theta & 0 & 0 & 0 & 0 \\ 0 & 0 & 1 & 0 & 0 & 0 \\ 0 & 0 & 0 & cos\theta & -sin\theta & 0 \\ 0 & 0 & 0 & sin\theta & cos\theta & 0 \\ 0 & 0 & 0 & 0 & 0 & 1 \end{bmatrix} \tag{5.47}$$

with θ the angle between the local axis, that is the beam axis, and the global coordinate system. The global stiffness matrix can be now embedded in the quadrilateral element of the discretized polymer through a similar transformation of the global matrix given by

$$\left[k_{Embedded}\right] = \left[T_2\right]^T \left[k_{Global}\right] \left[T_2\right] \tag{5.48}$$

where $\left[T_2\right]$ is the transformation matrix containing the kinematic constraint relations. In order to obtain $\left[T_2\right]$, we need first to relate the kinematic quantities of the corresponding degrees of freedom for the involved elements.

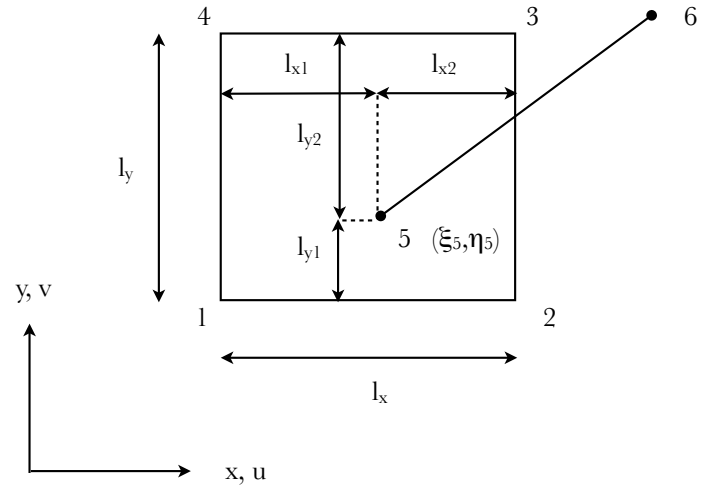

Figure 5.4: Composite element, consisted of a quadrilateral and a beam element

As illustrated in figure 5.4, the kinematic quantities of node 5 (u_5, v_5, θ_5) need to be depended on the master degrees of freedom, namely those of nodes 1,2,3 and 4. Let subscript b and q denote the quantities of the beam and the quadrilateral element respectively. We impose now that both node 5 of the beam element and point 5 of the surrounding matrix have the same displacement components

$$\begin{bmatrix} u_{5b} \\ v_{5b} \end{bmatrix} = \begin{bmatrix} u_{5q} \\ v_{5q} \end{bmatrix} \tag{5.49}$$

where u_{5q} and v_{5q} are related with the nodal displacements through the shape functions according to equation 5.14

$$\begin{bmatrix} u_{5q} \\ v_{5q} \end{bmatrix} = \begin{bmatrix} N_1 & 0 & N_2 & 0 & N_3 & 0 & N_4 & 0 \\ 0 & N_1 & 0 & N_2 & 0 & N_3 & 0 & N_4 \end{bmatrix} \begin{bmatrix} u_1 \\ v_1 \\ u_2 \\ v_2 \\ u_3 \\ v_3 \\ u_4 \\ v_4 \end{bmatrix} \tag{5.50}$$

with N_i being the shape functions at point 5, $N_i = N_i(\xi_5, \eta_5)$. Now, in order to relate rotation θ_{5b} with the degrees of freedom of nodes $1, 2, 3, 4$ we perform the following decomposition

$$\theta_{5b} = \theta_{5b}(u) + \theta_{5b}(v) \tag{5.51}$$

with

$$\theta_{5b}(u) = -\frac{l_{x2}}{l_x l_y} u_1 - \frac{l_{x1}}{l_x l_y} u_2 + \frac{l_{x1}}{l_x l_y} u_3 + \frac{l_{x2}}{l_x l_y} u_4 \tag{5.52}$$

and

$$\theta_{5b}(u) = \frac{l_{y2}}{l_y l_x} v_1 - \frac{l_{y2}}{l_y l_x} v_2 - \frac{l_{y1}}{l_y l_x} v_3 + \frac{l_{y1}}{l_y l_x} v_4 \tag{5.53}$$

or finally, in a more compact form, equation 5.51 is substituted by

$$\theta_{5b} = \begin{bmatrix} -\frac{l_{x2}}{l_x l_y} & \frac{l_{y2}}{l_y l_x} & -\frac{l_{x1}}{l_x l_y} & -\frac{l_{y2}}{l_y l_x} & \frac{l_{x1}}{l_x l_y} & -\frac{l_{y1}}{l_y l_x} & \frac{l_{x2}}{l_x l_y} & \frac{l_{y1}}{l_y l_x} \end{bmatrix} \begin{bmatrix} u_1 \\ v_1 \\ u_2 \\ v_2 \\ u_3 \\ v_3 \\ u_4 \\ v_4 \end{bmatrix} \tag{5.54}$$

where quantities l_x, l_y, l_{xi} and l_{yi} are illustrated in figure 5.4. Combining equations 5.50 and 5.54 we form the global formula for the imposition of the required kinematic constraints in order to "embed" the beam into the 4-node plane stress element.

$$\begin{bmatrix} u_{5b} \\ v_{5b} \\ \theta_{5b} \end{bmatrix} = \begin{bmatrix} N_1 & 0 & N_2 & 0 & N_3 & 0 & N_4 & 0 \\ 0 & N_1 & 0 & N_2 & 0 & N_3 & 0 & N_4 \\ -\dfrac{l_{x2}}{l_x l_y} & \dfrac{l_{y2}}{l_y l_x} & -\dfrac{l_{x1}}{l_x l_y} & -\dfrac{l_{y2}}{l_y l_x} & \dfrac{l_{x1}}{l_x l_y} & -\dfrac{l_{y1}}{l_y l_x} & \dfrac{l_{x2}}{l_x l_y} & \dfrac{l_{y1}}{l_y l_x} \end{bmatrix} \begin{bmatrix} u_1 \\ v_1 \\ u_2 \\ v_2 \\ u_3 \\ v_3 \\ u_4 \\ v_4 \end{bmatrix} \tag{5.55}$$

or

$$\{d_{5b}\} = \big[T_{2i}\big]\{d_q\} \tag{5.56}$$

and taking into account the degrees of freedom of node 6, equation 5.56 is transformed into

$$\left[\begin{array}{c} u_{5b} \\ v_{5b} \\ \theta_{5b} \\ \hdashline u_{6b} \\ v_{6b} \\ \theta_{6b} \end{array}\right] = \left[\begin{array}{ccc:ccc} & T_{2i} & & & & \\ & & & & & \\ & & & & & \\ \hdashline & & & 1 & & \\ & & & & 1 & \\ & & & & & 1 \end{array}\right] \left[\begin{array}{c} u_1 \\ v_1 \\ u_2 \\ v_2 \\ u_3 \\ v_3 \\ u_4 \\ v_4 \\ \hdashline u_{6b} \\ v_{6b} \\ \theta_{6b} \end{array}\right] \tag{5.57}$$

or

$$\{d_b\} = \big[T_2\big]\{d_q\} \tag{5.58}$$

where $\big[T_2\big]$ is the requested transformation matrix. In order to perform the above transformation, we take into account that $\big[T_2\big]$ is an orthogonal matrix so that $\big[T_2\big]^T = \big[T_2\big]^{-1}$ and we obtain the stiffness matrix through

$$\big[k_{Embedded}\big] = \big[T_2\big]^T \big[k_{Global}\big] \big[T_2\big] \tag{5.59}$$

and using equation 5.46

$$\big[k_{Embedded}\big] = \big[T_2\big]^T \big[T_1\big]^T \big[k_{Local}\big] \big[T_1\big] \big[T_2\big] \tag{5.60}$$

which now can be assembled to the stiffness matrix of the sourrounding element, that is the quadrilateral element.

5.3 The Interfacial Mechanism

5.3.1 Bond Behavior

Bond is the interaction between reinforcing fiber and surrounding material. As discussed in the previous section, the interaction of the reinforcing fiber and the surrounding polymer is assured through a perfect bond model, since we assume a complete compatibility of strains between the two components. However, a more realistic approach should be taken into account where the produced bond stress is related to the relative displacement between the fiber and the polymer. In other words, we have to consider a nonlinear bond-slip model and more specifically, a stick slip behaviour for the discription of the interfacial load transfer mechanism between the lateral surface of the carbon nanotube and the surrounding matrix. Figure 5.5 illustrates the requested stress-slip relation between the involved components.

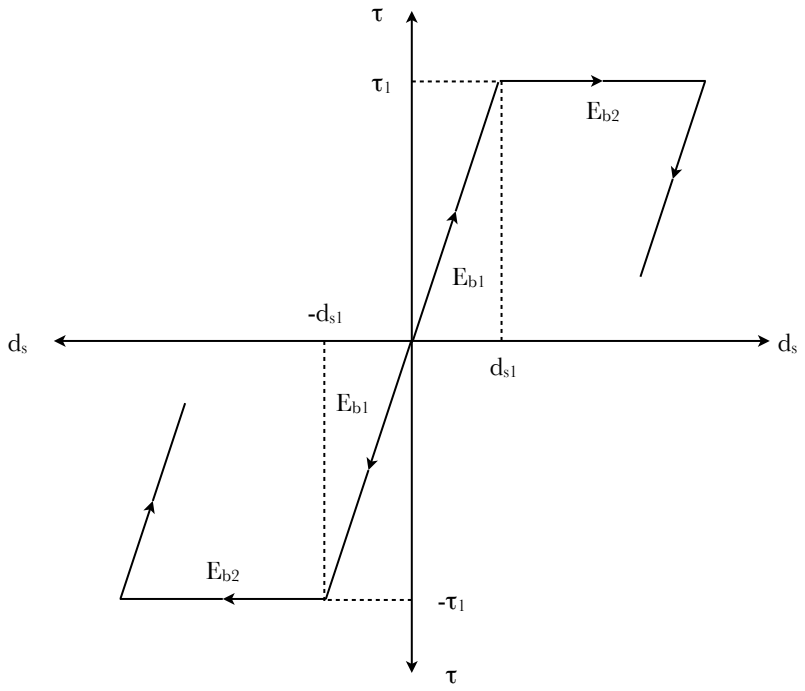

Figure 5.5: Bond stress-slip relation

If a fiber is in slip state, this means that its corresponding interface bond has failed, leading to its inability for further load-transferring. The condition of slip for a beam element is simulated by reducing its axial stiffness to a very small value. Notice that bending and shear rigidities are not affected allowing the element in slip to resist against bending and shear. In mathematical terms, it is expressed as

$$\tau = E_{b1} d_s \begin{cases} < \tau_1 & \text{fully bonded} \\ \geq \tau_1 & \text{slip} \end{cases} \tag{5.61}$$

where τ_1 denotes the interfacial shear strength, E_{b1} is the initial slip modulus and is replaced by E_{b2}, which is almost zero, when the bond-slip d_s exceeds the value d_{s1} (Figure 5.5).

5.3.2 Bond-Slip Model

For including the bond-slip in the finite element analysis of carbon reinforced structures, a bond link element will be used, consisted of an axial spring element which connect and transmit shear forces between the fiber node and the adjacent polymer node. Since the link element has no physical dimensions, the two connected nodes originally occupy the same location in the finite element mesh of the undeformed structure.

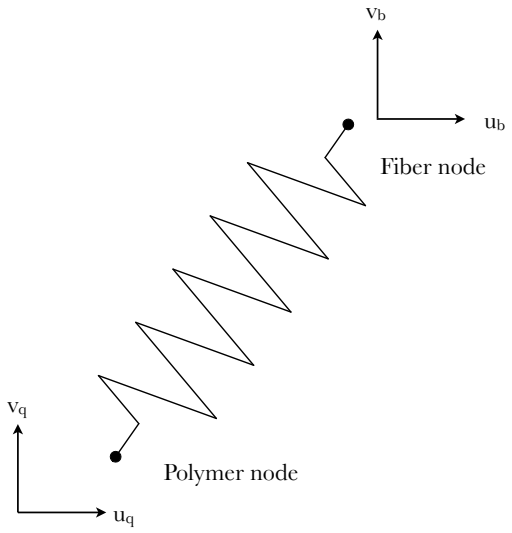

Figure 5.6: Bond link element

The element stiffness matrix relates shear force to the corresponding nodal displacements by the following relation

$$\{F_s\} = \big[k_s\big]\{d_s\} \tag{5.62}$$

where Ks is the shear stiffness of the interface and can be derived from the measured bond stress-slip relation according to the following equation

$$k_s = E_{b1} A_c \tag{5.63}$$

with E_{b1} the initial slip modulus and A is the bar circumferential area tributary to one bond link element.

A reinforcing fiber element which is embedded in a polymer element is shown in figure 5.7. The corresponding degrees of freedom of the reinforcing fiber and the polymer at each end are connected by the bond link element whose stiffness depends on the relative displacement between fiber and polymer. Since the finite element model only includes the concrete displacement degrees of freedom, the degrees of freedom which are associated with the reinforcing beam need to be condensed out from the element stiffness matrix, before it is assembled into the structure stiffness matrix.

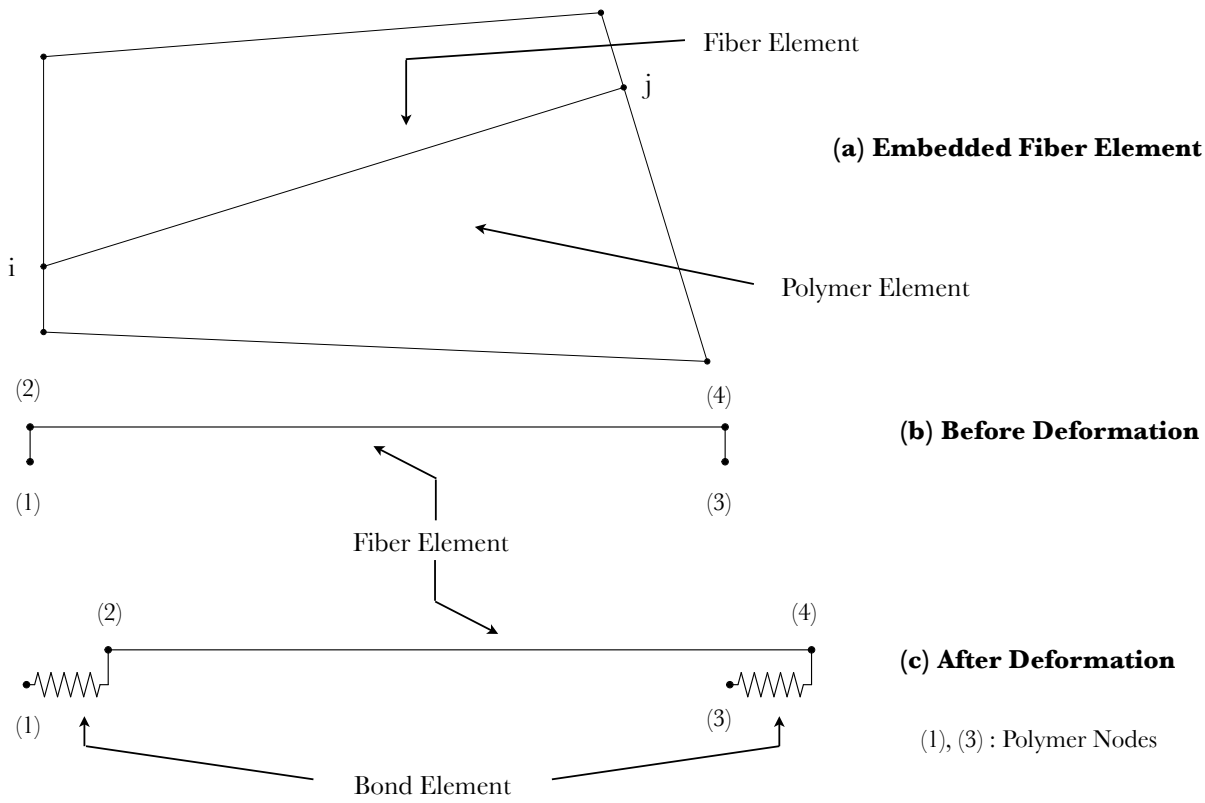

Figure 5.7: Discrete reinforcing fiber element with bond-slip

With this assumption the stiffness matrix which relates the end displacements along the axis of the reinforcing bar with the corresponding forces is given by

$$\begin{bmatrix} F_1' \\ F_1 \\ F_2 \\ M_1 \\ F_3' \\ F_3 \\ F_4 \\ M_2 \end{bmatrix} = \begin{bmatrix} k_s & -k_s & 0 & 0 & 0 & 0 & 0 & 0 \\ -k_s & \frac{AE}{L}+k_s & 0 & 0 & 0 & -\frac{AE}{L} & 0 & 0 \\ 0 & 0 & \frac{12EI}{L^3} & \frac{6EI}{L^2} & 0 & 0 & -\frac{12EI}{L^3} & \frac{6EI}{L^2} \\ 0 & 0 & \frac{6EI}{L^2} & \frac{4EI}{L} & 0 & 0 & -\frac{6EI}{L^2} & \frac{2EI}{L} \\ 0 & 0 & 0 & 0 & k_s & -k_s & 0 & 0 \\ 0 & -\frac{AE}{L} & 0 & 0 & -k_s & \frac{AE}{L}+k_s & 0 & 0 \\ 0 & 0 & -\frac{12EI}{L^3} & -\frac{6EI}{L^2} & 0 & 0 & \frac{12EI}{L^3} & -\frac{6EI}{L^2} \\ 0 & 0 & \frac{6EI}{L^2} & \frac{2EI}{L} & 0 & 0 & -\frac{6EI}{L^2} & \frac{4EI}{L} \end{bmatrix} \begin{bmatrix} u_1' \\ u_1 \\ v_1 \\ \theta_1 \\ u_2' \\ u_2 \\ v_2 \\ \theta_2 \end{bmatrix}$$

which is rearranged in order to eliminate u_1 and v_1, according to

$$\begin{bmatrix} F_e \\ F_c \end{bmatrix} = \begin{bmatrix} K_{ee} & K_{ec} \\ K_{ce} & K_{cc} \end{bmatrix} \begin{bmatrix} d_e \\ d_c \end{bmatrix} \tag{5.64}$$

where subscript e denotes the eliminated and c the condensated degrees of freedom. Consequently, equation 5.64 is expanded as

$$\{F_e\} = \big[K_{ee}\big]\{d_e\} + \big[K_{ec}\big]\{d_c\} \tag{5.65a}$$

$$\{F_c\} = \big[K_{ce}\big]\{d_e\} + \big[K_{cc}\big]\{d_c\} \tag{5.65b}$$

Now, solving 5.65a for d_c and substituting in 5.65b gives

$$\{F_c\} = \big[K_{ce}\big]\big[K_{ee}\big]^{-1}\Big(\{F_e\} - \big[K_{ec}\big]\{d_c\}\Big) + \big[K_{cc}\big]\{d_c\} \tag{5.66a}$$

or

$$\Big(\{F_c\} - \big[K_{ce}\big]\big[K_{ee}\big]^{-1}\{F_e\}\Big) = \Big(\big[K_{cc}\big] - \big[K_{ce}\big]\big[K_{ee}\big]^{-1}\big[K_{ec}\big]\Big)\{d_c\} \tag{5.66b}$$

or

$$\{F_{cc}\} = \big[K_{Equal}\big]\{d_c\} \tag{5.66c}$$

where K_{equal} is the condensed stiffness matrix and F_{cc} the condensed load vector according to equation 5.66b. As already expained in the beginning of this section, only the axial stiffness of the beam element is linked with the bond element. Hence, the remaining degrees of freedom in equation 5.66c are u_1', v_1, θ_1 and u_2', v_2, θ_2 for nodes i and j respectively.

Once obtained the above static condensation, stiffness matrix of equation 5.66c can be assembled together with the polymer element stiffness matrix to form the total stiffness of the structure. Using 5.60 we compute the transformed stiffness matrix in terms of the equal beam element

$$\big[k_{Embedded}\big] = \big[T_2\big]^T\big[T_1\big]^T\big[k_{Equal}\big]\big[T_1\big]\big[T_2\big] \tag{5.67}$$

where matrices $\big[T_1\big]$ and $\big[T_2\big]$ are the transformation matrices as developed in the previous section, only this time, the transformation is performed on the *equal* stiffness matrix which includes the bond-slip effect.

Chapter 6

Numerical Examples

In the present chapter, the performance of the formulations outlined above is demonstrated by using some representative numerical examples. The first part is concentrated on the nested solution scheme in the context of the multi-scale analysis, as presented in table 2.1. An L-shaped domain is employed as macro-specimen while a fiber-reinforced matrix is assigned as representative volume element to every integration point. The overall microstructure response is computed for both types of boundary conditions, namely linear and periodic displacements, and their influence is examined at the level of the RVE and the macroscale as well. In the second part, the numerical analyses are tranfered to the micro level where a microstructure cell is examined in terms of micromechanics, introducing bond-slip effect and material non-linearity. Their influence over the RVE's behavior is tested in different deformation modes and presented in comperative figures and numerical results.

6.1 Nested Solution Scheme

We consider an L-shaped domain for macro-scale (Figure 6.1) where both the length and the height of the sample equal 20m and the thickness is taken 1m. At the bottom side, the nodes are fixed in vertical direction while the horizontal displacement is free. In contrast, the vertical displacements of the left side are free while the horizontal degrees of freedom are fixed.

6.1.1 Macrostructural Model

The implementation of the nested solution procedure for the L-shaped domain, will be performed according to the algorithm of table 2.1. Hence, the first step consists in the initialization of the macrostructure where the aforementioned L-shaped domain of plane stress type, is discretized with 4-node quadrilateral elements. Figure 6.1 illustrates the performed finite element mesh, consisted of 1200 elements and 2562 degrees of freedom, along with the applied boundary conditions and the macro load.

As already mentioned, according to this computational homogenization approach there is no explicit form of the constitutive behaviour on the macrolevel assumed a priori. Consequently, the stiffness matrix and the overall mechanical properties of the macro-specimen

have to be determined numerically from the relation between variations of the macroscopic stress and variations of the macroscopic deformation at every integration point.

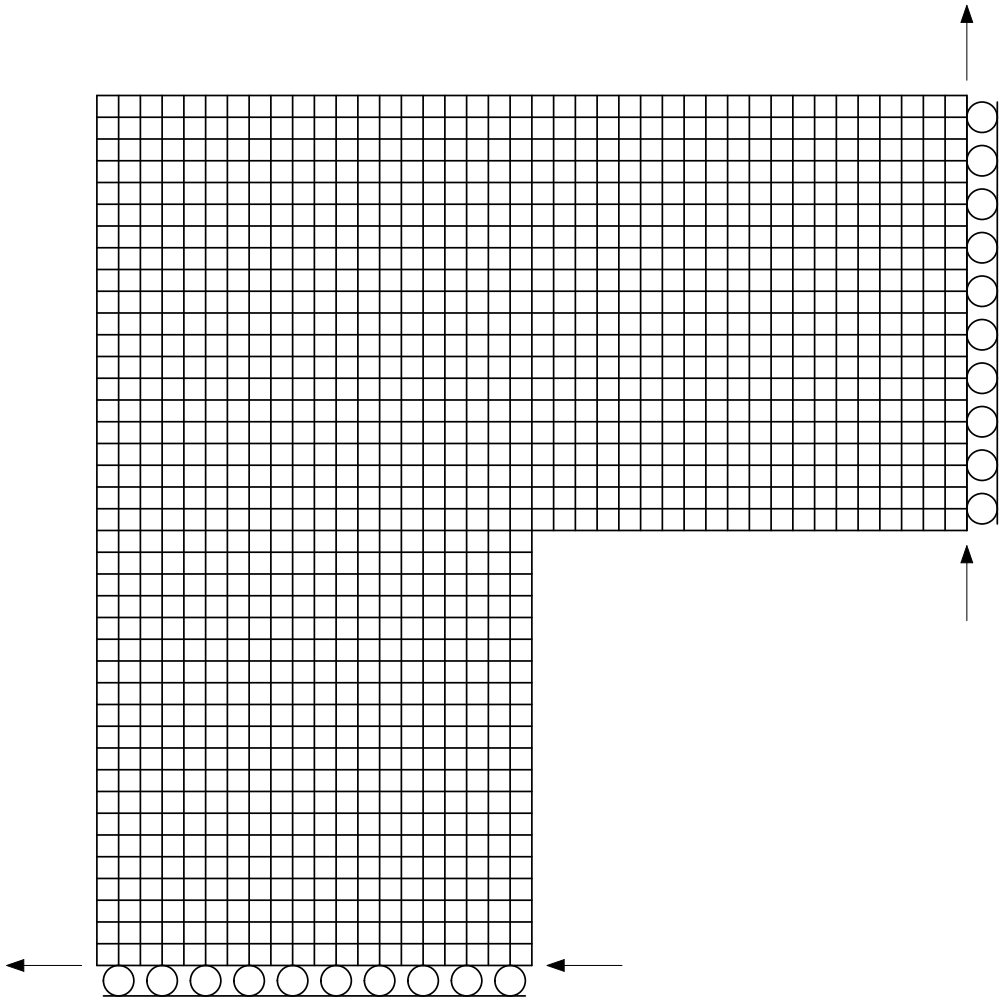

Figure 6.1: Schematic representation of the undeformed configuration of the macro-specimen.

6.1.2 Microstructural Model

Once initialized the macroscopic model, we need now to define the representative volume element and assign it to the integration points. A fiber-reinforced matrix is studied in the present work as micro-model, consisted of non-aligned fiber elements. A volume fraction of 5% is adopted for the fibers, with random geometry and distribution into the RVE. The stochastic modeling of the fiber geometry is produced after processing a number of CNT geometries from scanning electron microscope images according to [7]. The produced fibers are then placed in the micro-specimen at random position and direction. More specifically, a random point is generated as starting point and an angle denoting the fiber axis. If the generated fiber lies within the micro-specimen the procedure continues with the next location step or else a number of specified attempts is performed until the produced fiber is completely surrounded by the representative volume. If the process surpasses the prescribed number of

attempts, a new set of random point and angle is generated and so forth. The following figure constitutes a schematic representation of the produced RVE, containing 5% volume fraction of reinforcing fibers, and the finite element discretization.

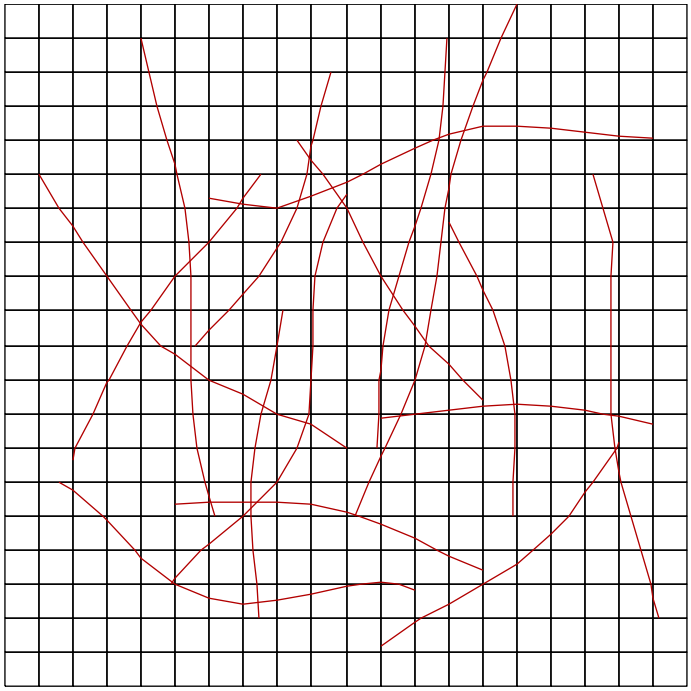

Figure 6.2: Microstructural cell.

The matrix behavior is discribed by a linear elastic material with Young's modulus and Poisson's ration being 3 MPa and 0.35 respectively while a full-bond model is implemented for the interaction between fiber and polymer. Fibers are discretized with beam elements of hollow cylindrical cross section with equivalent section properties given by

$$A_{eq} = \frac{\pi}{4}\left[(d+t)^2 - (d-t)^2\right]$$

$$I_{eq} = \frac{\pi}{32}\left[(d+t)^2 - (d-t)^2\right]$$

with d being the equivalent diameter, where a value of 18 nm is adopted in the framework of the present work, and is calculated according to [7] for wall thickness t equal to 0.35 nm.

Now the procedure is transfered to the micro level where the above microstructural cell (figure 6.2) is initialized for both linear and periodic displacements and the computed tangent moduli is the assigned to every integration point for the initialization of the macroscopic stiffness matrix. As depicted in the following results, a stiffer response is obtained in the case of linear displacements in comparison with periodic deformation with the difference though being indiscernible.

$$C_{Linear} = \begin{bmatrix} 6.9225E+09 & 2.2862E+09 & 1.7152E+08 \\ 2.2862E+09 & 1.0670E+10 & 1.0460E+09 \\ 1.7152E+08 & 1.0460E+09 & 3.0342E+09 \end{bmatrix}$$

$$C_{Periodic} = \begin{bmatrix} 6.9052E+09 & 2.2807E+09 & 1.7114E+08 \\ 2.2807E+09 & 1.0667E+10 & 1.0441E+09 \\ 1.7114E+08 & 1.0441E+09 & 3.0304E+09 \end{bmatrix}$$

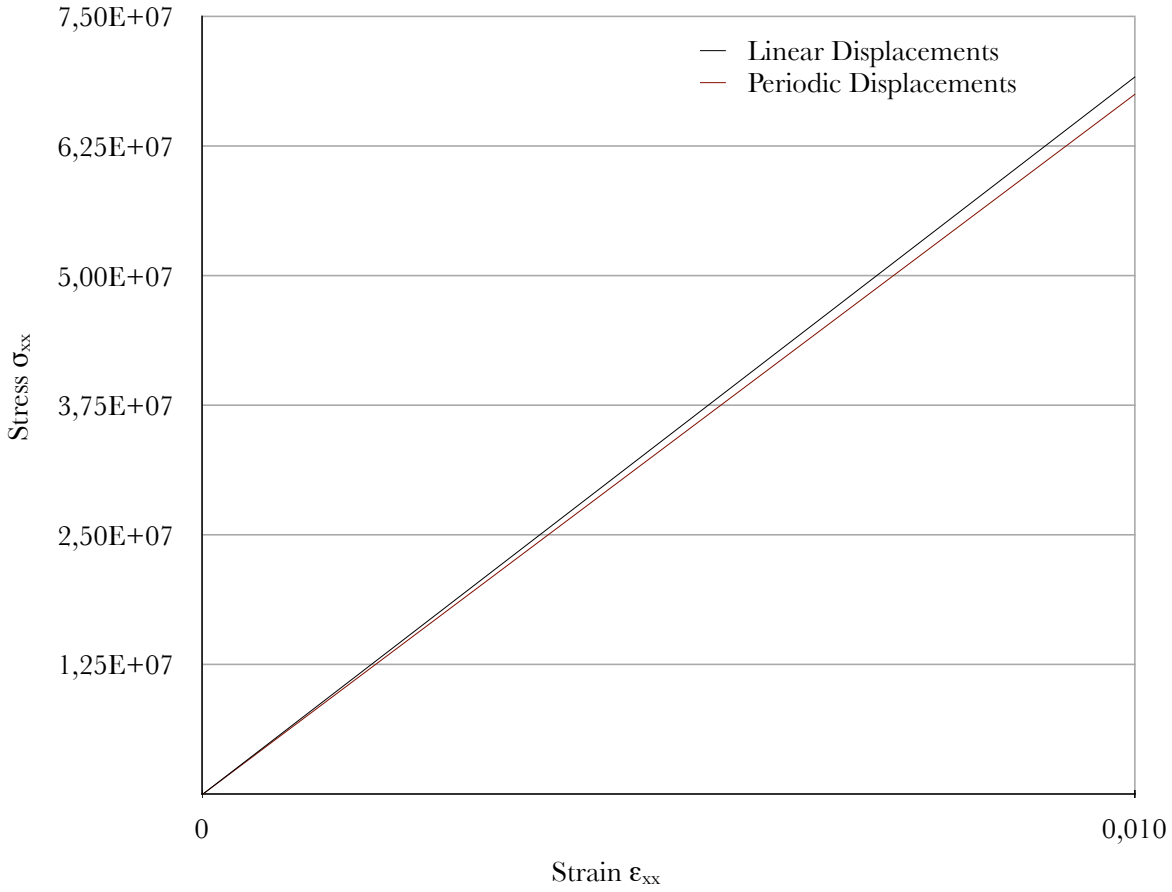

Figure 6.3: Macroscopic stress-strain curves ($\sigma_{xx} - \epsilon_{xx}$) for analyses with linear and periodic displacements.

This difference in the calculated macroscopic stiffness for the two schemes of boundary conditions is better depicted in figure 6.3 in terms of strain-stress curves. Now, the above constitutive matrices are assigned to the integration-points in order to complete the initialization of the macro-model and the procedure returns to the macro-level.

6.1.3 Macroscopic Response

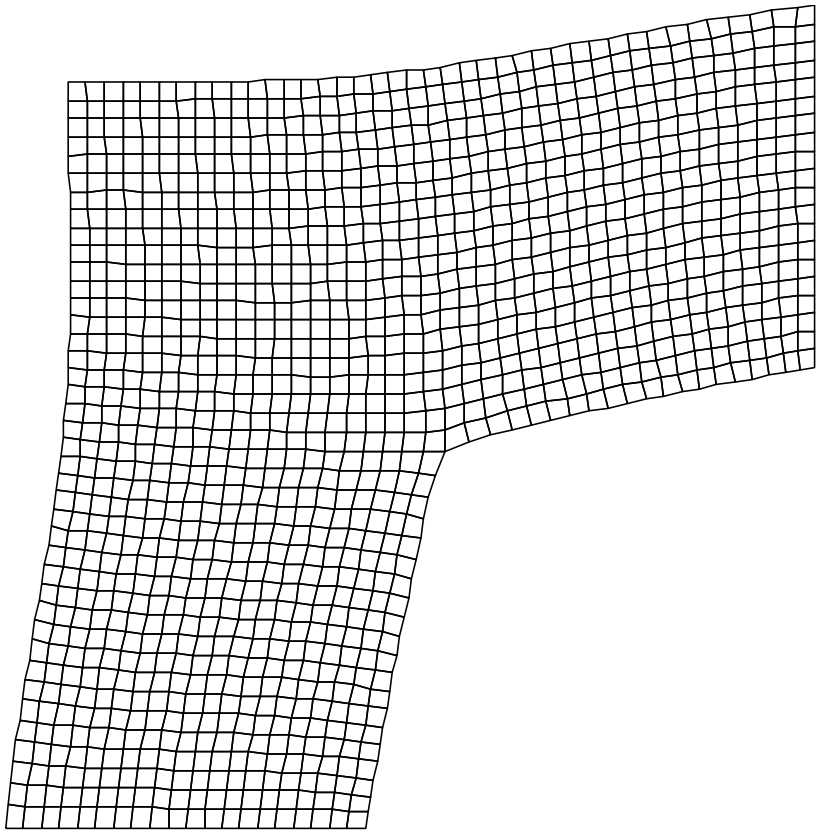

Figure 6.4: Schematic representation of the deformed configuration of the macro-specimen.

Due to the imperceptible difference between the computed macro-stiffness, the obtained deformed configurations for the load illustrated in figure 6.1 are almost identical for both types of boundary conditions according to figure 6.4.

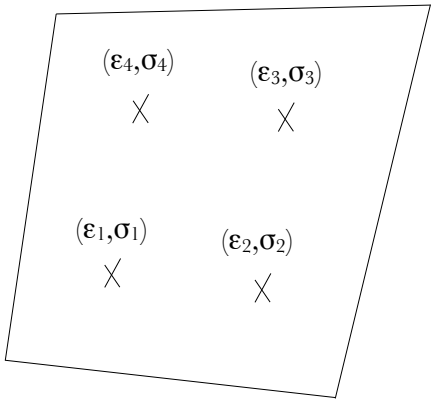

Figure 6.5: Deformed element of the inside corner.

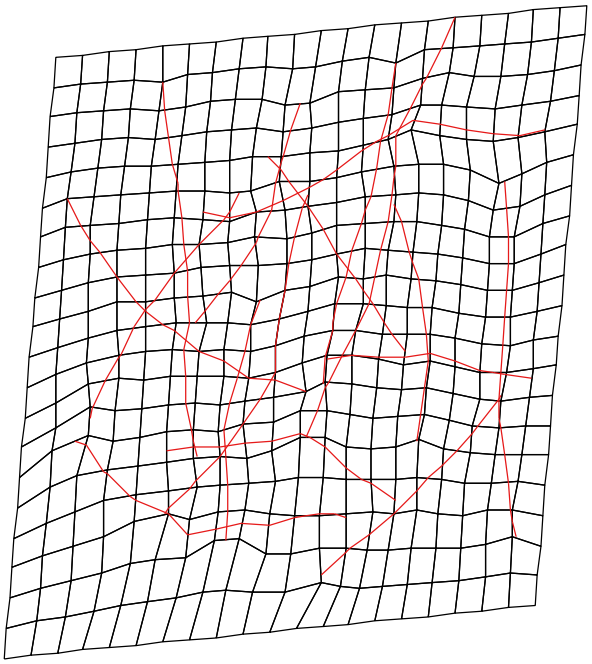

Figure 6.6: Deformed microstructural cell of Gauss-point (1).

$$\epsilon_1 = \begin{bmatrix} 9.7245E-09 \\ 7.6745E-08 \\ 1.0057E-07 \end{bmatrix} \quad \sigma_1 = \begin{bmatrix} 2.6002E+02 \\ 9.4632E+02 \\ 3.8709E+02 \end{bmatrix} \qquad \epsilon_2 = \begin{bmatrix} 9.7245E-09 \\ 1.7015E-07 \\ 1.9351E-07 \end{bmatrix} \quad \sigma_2 = \begin{bmatrix} 4.8950E+02 \\ 2.0401E+03 \\ 7.6678E+02 \end{bmatrix}$$

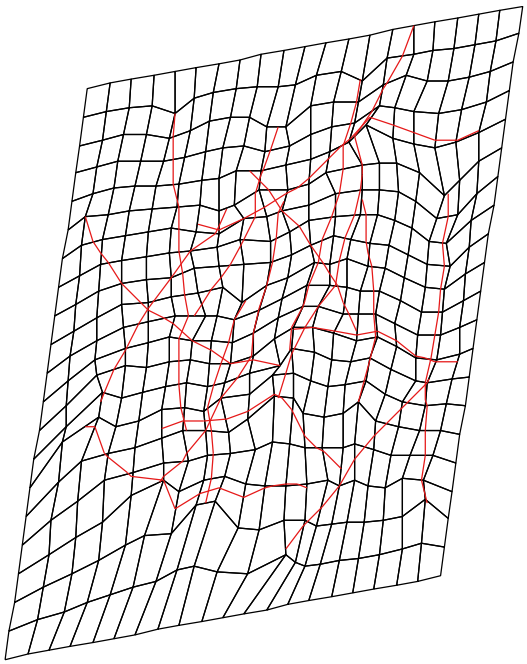

Figure 6.7: Deformed microstructural cell of Gauss-point (2).

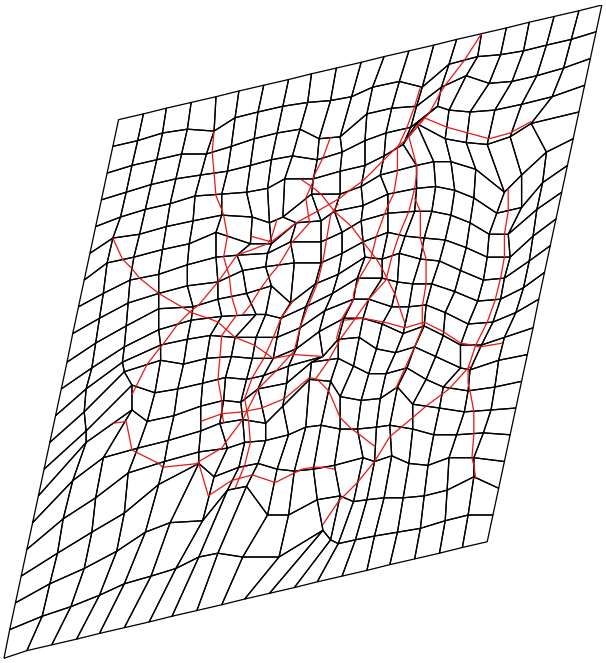

Figure 6.8: Deformed microstructural cell of Gauss-point (3).

$$\epsilon_3 = \begin{bmatrix} 1.0266E-07 \\ 1.7015E-07 \\ 2.8691E-07 \end{bmatrix} \quad \sigma_3 = \begin{bmatrix} 1.1489E+03 \\ 2.3503E+03 \\ 1.0661E+03 \end{bmatrix} \qquad \epsilon_4 = \begin{bmatrix} 1.0266E-07 \\ 7.6745E-08 \\ 1.9397E-07 \end{bmatrix} \quad \sigma_4 = \begin{bmatrix} 9.1942E+02 \\ 1.2565E+03 \\ 6.8643E+02 \end{bmatrix}$$

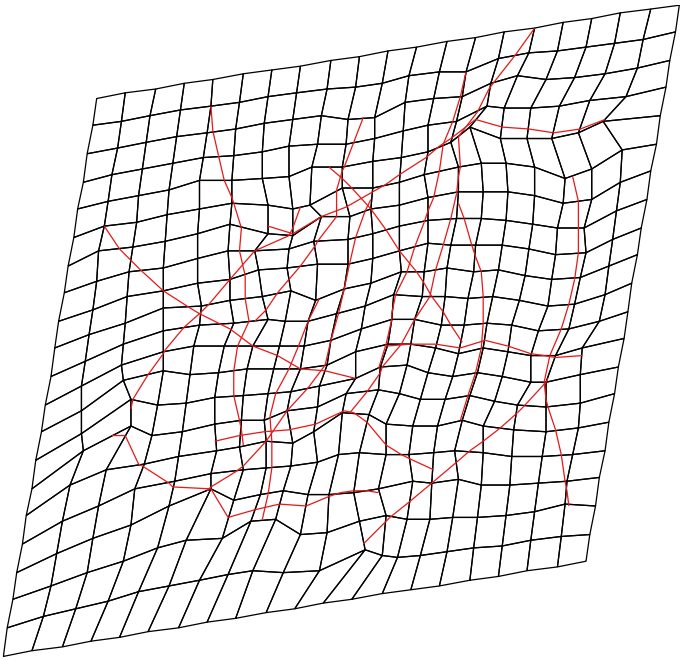

Figure 6.9: Deformed microstructural cell of Gauss-point (4).

Figure 6.5 depicts the deformation state of the element located at the inside corner of the macroscopic domain along with its integration points. In the next figures (6.6 - 6.9), the deformed configuration of each Gauss-point is schematically represented and the corresponding strain and stress vectors are given respectively.

It is now obvious from the above figures, and the stress and strain tensors as well, that the RVEs in the upper part of the examined element are mainly subjected to tension in the direction of x-axis, while for the RVEs of the lower part, the tension along the y-axis is dominant. Furthermore, combining the deformed configuration of figures 6.5 and 6.6 we verify the expected deformation which is mainly consisted in shear stress, according to the biggest strain value of γ_{xy} for the Gauss-point (3). This confirms the conclusion that the method realistically describes the deformation modes of the microstructure.

The following figures represent the boundary nodal tractions for two of the faces of the RVE, namely the left and bottom faces, for linear displacements as boundary conditions.

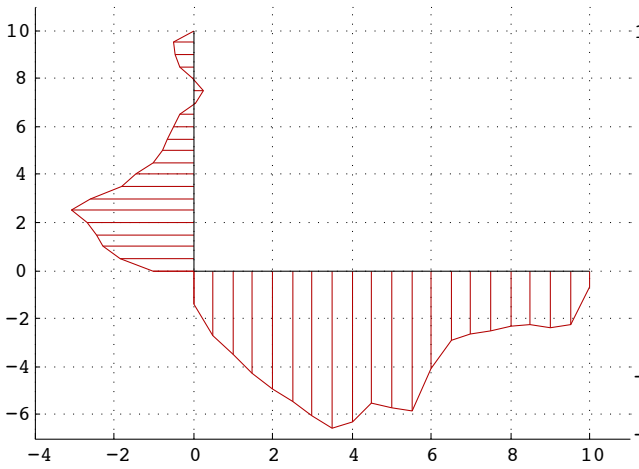

Figure 6.10: Normal nodal forces - RVE (1)

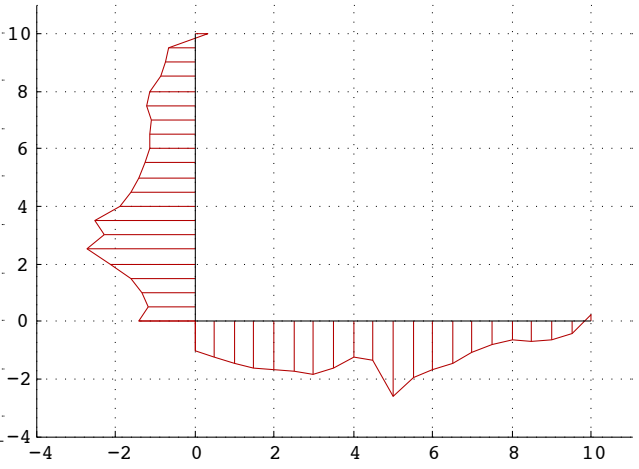

Figure 6.11: Shear nodal forces - RVE (1)

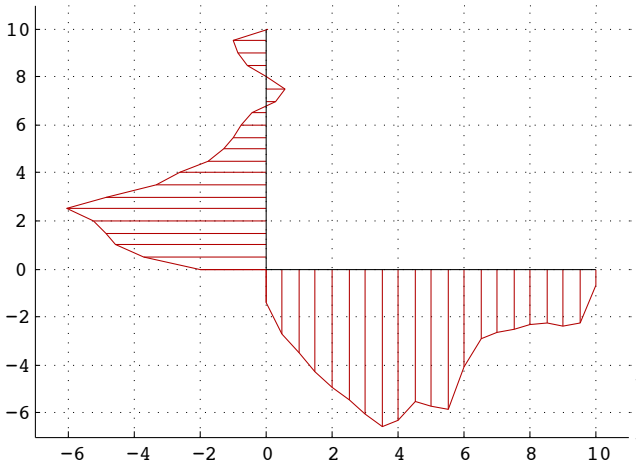

Figure 6.12: Normal nodal forces - RVE (2)

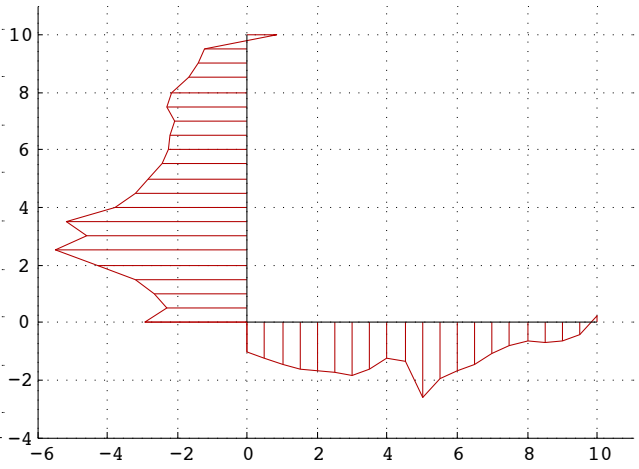

Figure 6.13: Shear nodal forces - RVE (2)

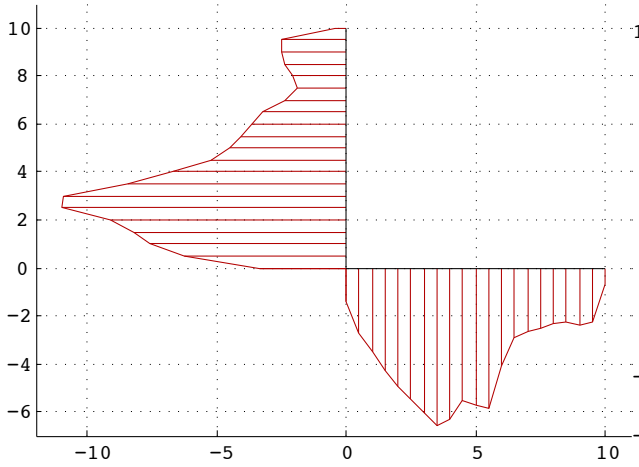

Figure 6.14: Normal nodal forces - RVE (3)

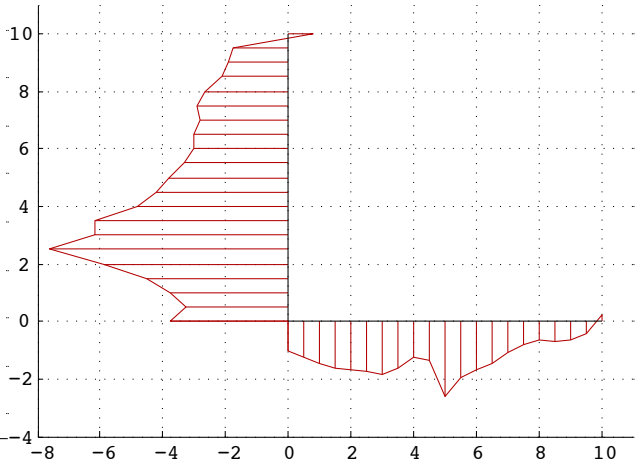

Figure 6.15: Shear nodal forces - RVE (3)

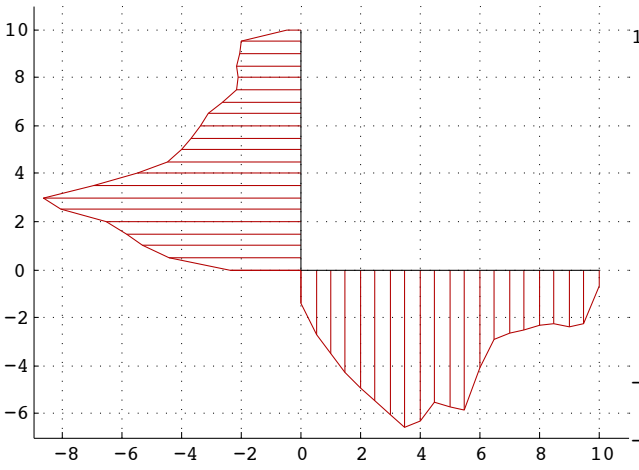

Figure 6.16: Normal nodal forces - RVE (4)

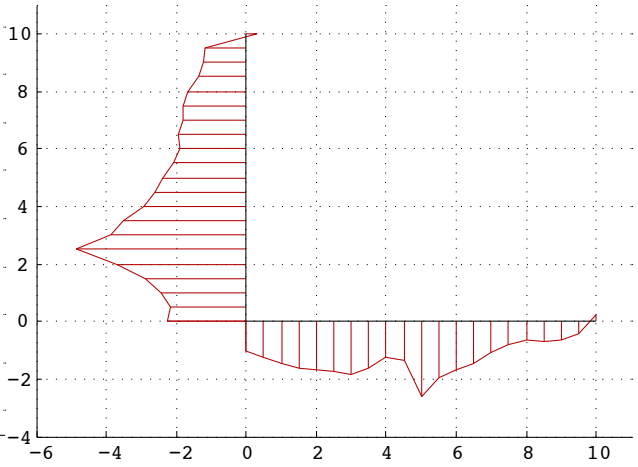

Figure 6.17: Shear nodal forces - RVE (4)

A significant observation of the above figures consists in the influence of the fiber over the stiffness and its distribution within the representative volume element. More specifically, the charts of the nodal forces, placed at the left side of the previous figures, present a peak in both the bottom and the left side in the same boundary points for all the microstructures. Combining now these representations with the microstructural cell, as illustrated in figure 6.2, it becomes evident that the influence of the fibers placed on the left-bottom corner is schematically verified through these graphs for both examined sides of the RVE.

At this point, it should be noted that for the sake of completeness, all numerical analyses are performed for linear and periodic displacements as well. A comparison of their obtained results is performed in this section in order to highlight the influence of the boundary conditions in the framework of a multiscale approach. However, according to the scope of the present work, only the case of linear displacements will be discussed in the following sections since the attention is not concentrated on the solution techniques but most in the influence of the microstructural effects upon the macroscopic quantities.

6.2 Deformation Modes

This section is concentrated on the overall behavior of the representative volume element and the influence of the microstructural effects over the averaged macroscopic quantities. The response of the previously presented microstructural cell is examined for the three deformation modes, that is for ϵ_x, ϵ_y and γ_{xy}, taking into account the interfacial shear strength model of fiber elements and incorporating the elastoplastic constitutive model of the surrounding matrix. The following tables present the implemented values of the microstructural problem for both the polymer

Properties of Polymer	
Young's Modulus	3 MPa
Poisson's Ratio	0.35

Table 6.1: Properties of Polymer

and the fiber elements

Properties of Fibers	
Length	0.5 - 0.7 μm
Diameter	18 nm
Wall Thickness	0.35 nm
Cross Section	Pipe Profile
Number of Fibers	16
Volume Fraction	5%
Young's Modulus	1 TPa
Interfacial Shear Strength	0 MPa 20 MPa 50 and ∞ MPa

Table 6.2: Properties of Fibers

As denoted in table 6.2, the influence of the interfacial shear strength over the RVE's overall response is investigated using two different values, namely 20 and 50 MPa, as well as the fully bonded model (Shear Strength $\rightarrow \infty$) and the neat surrounding polymer (Shear Strength $\rightarrow 0$).

6.2.1 Normal Strain in X-direction

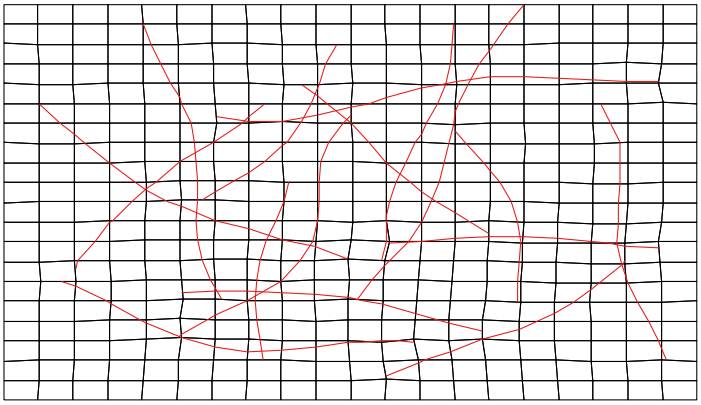

Figure 6.18: Deformed configuration of the RVE for ϵ_{xx}

Linear Elastic Polymer

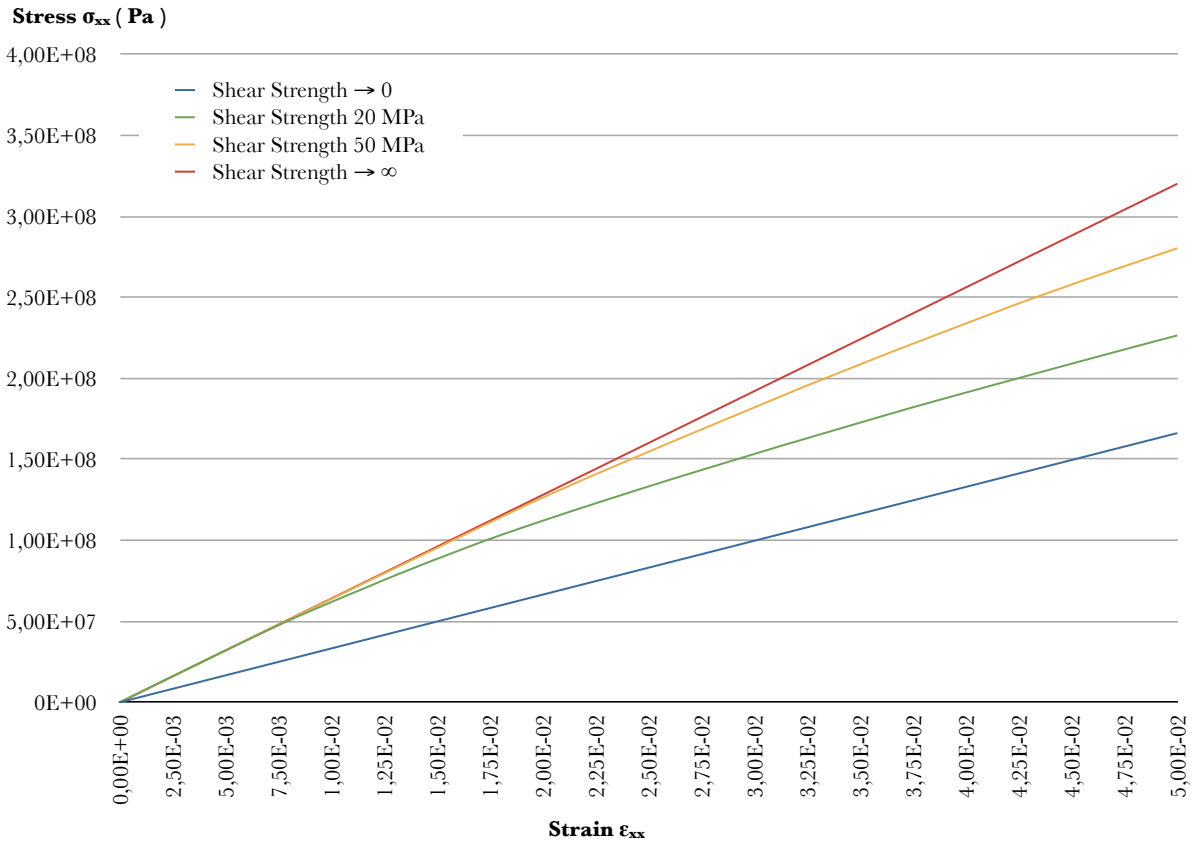

Figure 6.19: Stress-strain curve ($\sigma_{xx} - \epsilon_{xx}$) considering linear elastic polymer

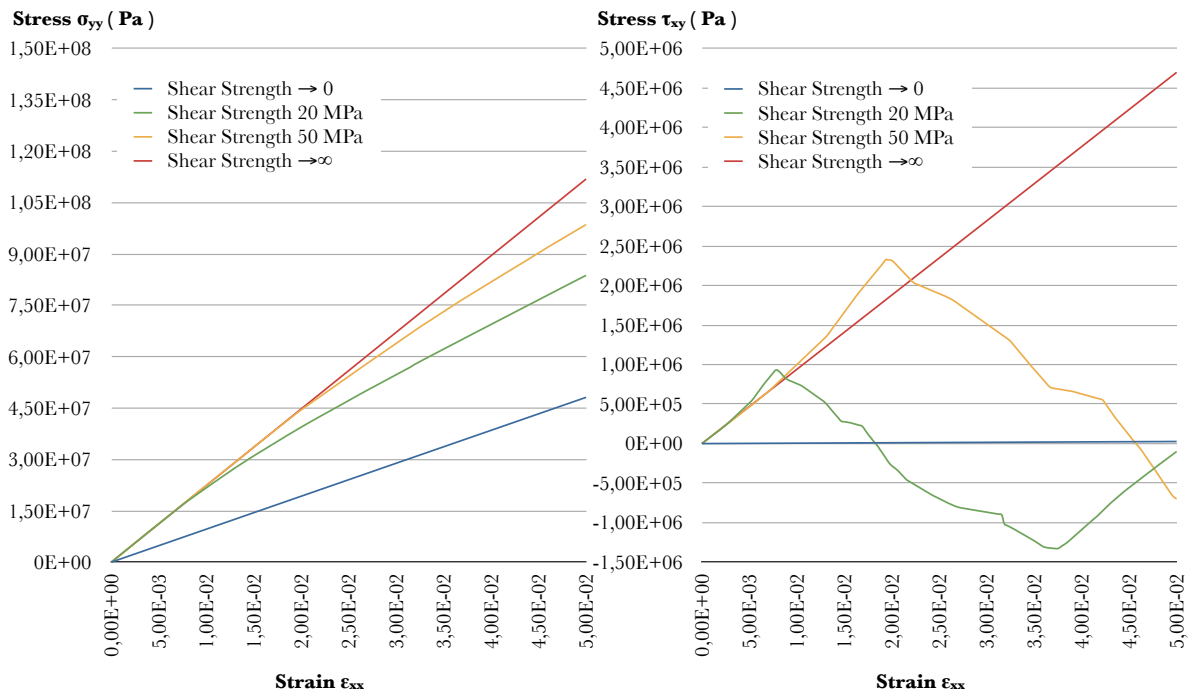

Figure 6.20: Stress-strain curves $(\sigma_{yy} - \epsilon_{xx})$ and $(\tau_{xy} - \epsilon_{xx})$ considering linear elastic polymer

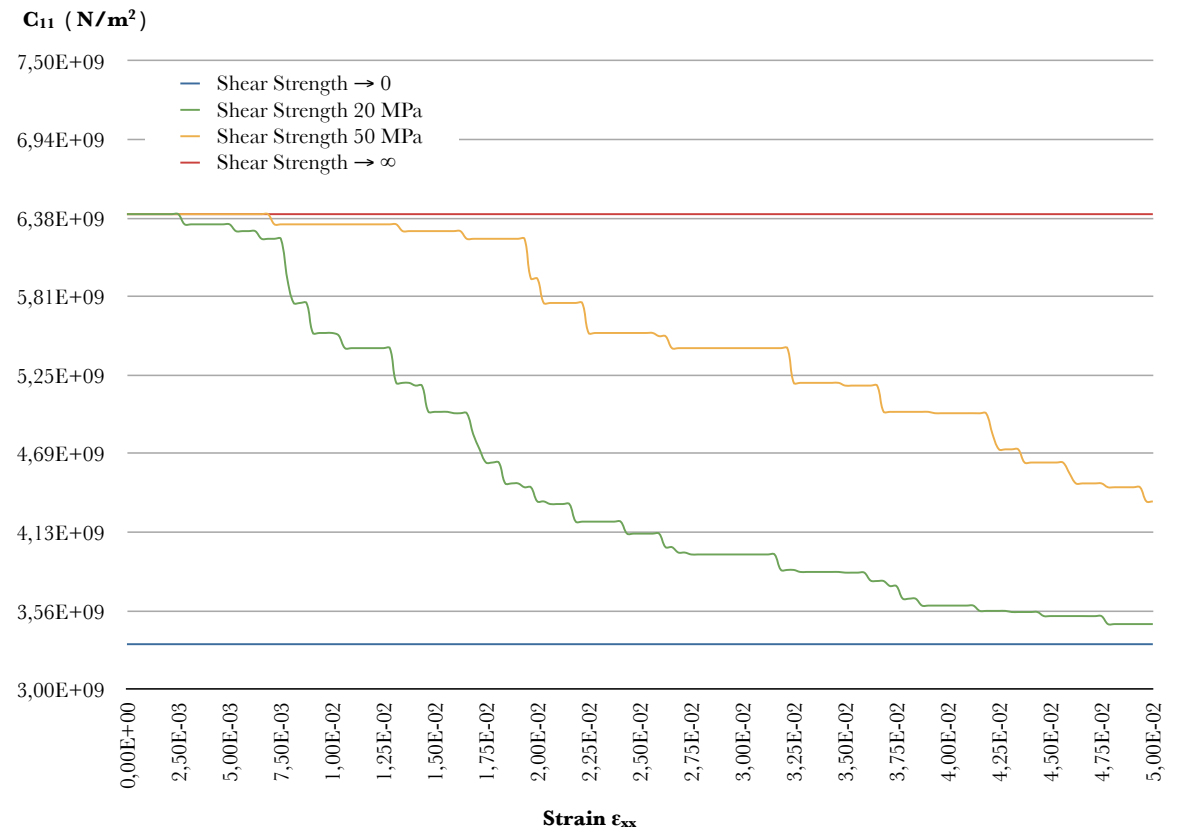

Figure 6.21: Variation of C_{11} component considering linear elastic polymer

As depicted in figures 6.19 - 6.21, the obtained strength of the RVE varies between the two extreme values, namely those of the neat polymer (Shear Strength $\rightarrow 0$) and the fully bonded fibers (Shear Strength $\rightarrow \infty$). The bond slip effect offers thus a significant contribution to the RVE's overall strength. More specifically, a meagre interfacial shear strength leads to an averaged normal stress σ_x of 166.2 MPa where the reinforcing fibers are unable to tranfer axial forces and as a result only through the bending and shear rigidies are considered to contribute to final strength. On the other hand, a fully bonded model gives almost the double averaged stress σ_x, that is 320.1 MPa, and an also significant contribution to the other stress components σ_y and τ_{xy} (figure 6.20).

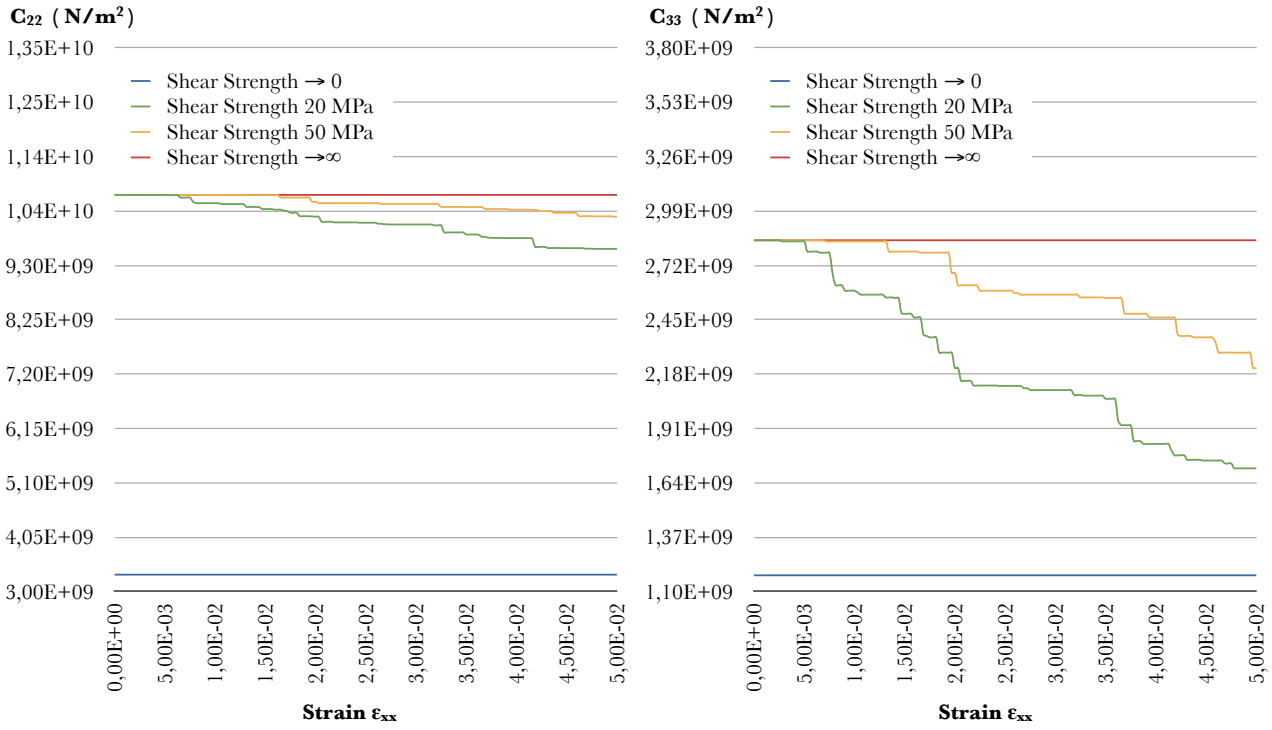

Figure 6.22: Variation of C_{22} and C_{33} components considering linear elastic polymer

Figures 6.21 and 6.22 represent the variation of the constitutive components in relation with the strain increment ϵ_x. In combination with the corresponding stress-strain curves, it becomes evident the both the neat polymer and the fully bonded model constitute the lower and upper strength limits respectively, caracterized by linear elastic response of the entire microstructure.

Furthermore, we observe that even a low value of shear strength, that is 20 MPa, does not cause a failure to all the embedded fibers, but only to a part of them. Their random geometry and direction contribute to the activation of the bending and shear strengths apart from the axial, and hence a group of fibers, namely those having a vertical or better a non-horizontal direction, remains fully bonded and provides the remaining strength to the microstructural cell. However, the insignificant contribution of the bending and shear rigidies is better illustrated in figure 6.22 where the constitutive component C_{11} for shear strength of 20 MPa has almost reached its lower value of 3.32 GPa.

Elasto-Plastic Polymer

Similarly, the following figures depict the stress-strain curves and the variation of the constitutive components of the RVE only this time the behavior of the surrounding material is described by an elasto-plastic model.

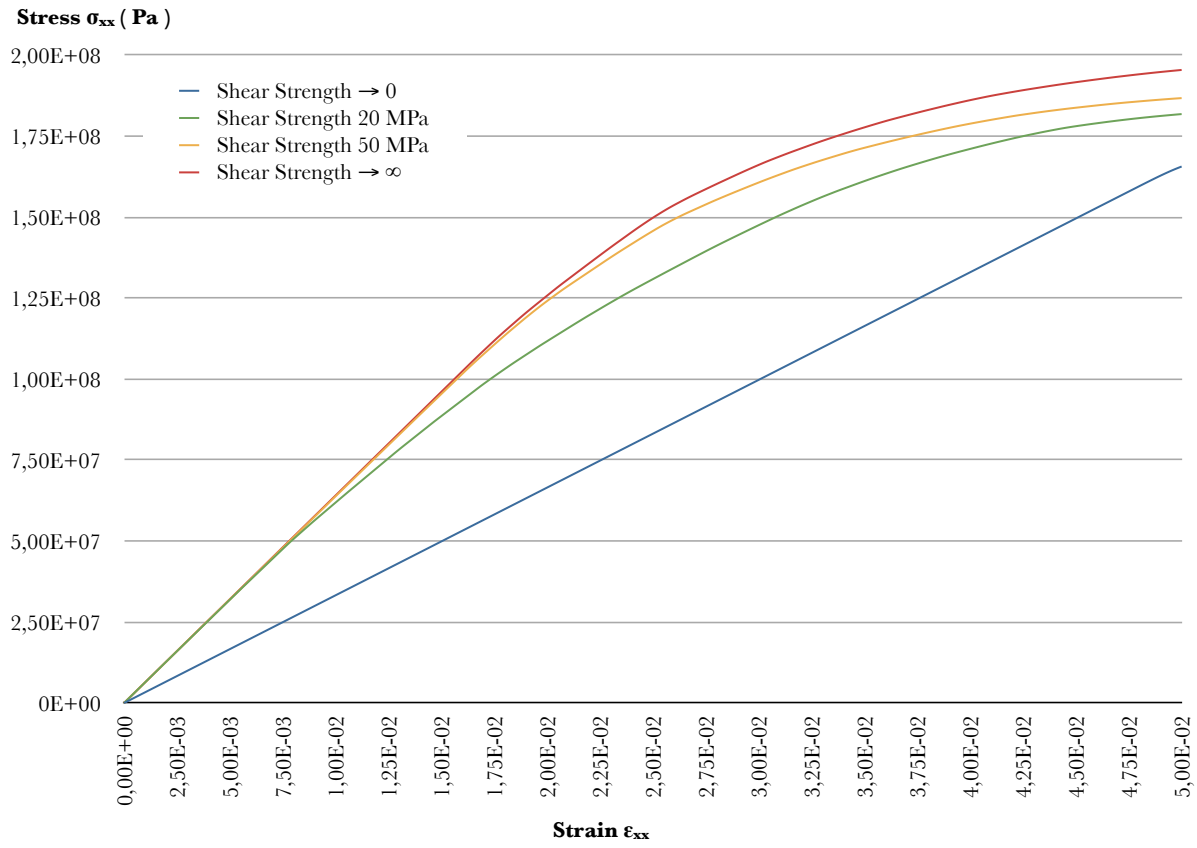

Figure 6.23: Stress-strain curve ($\sigma_{xx} - \epsilon_{xx}$) considering elasto-plastic polymer

In the case of the neat polymer, an almost linear behavior is obtained and the ($\sigma_{xx} - \epsilon_{xx}$) curve seems to be identical with the corresponding curve of the linear elastic polymer. However, a plastic region is developed in the front end of the cell, causing thus a reduction of the overall strength which is better illustrated from the variation of the C_{11} component in figure 6.25. Combining now the curves of shear strength of 20 MPa, we notice that in both cases, a part of fibers enters the slip state at a strain value of 0.75 %. Moreover, a further loss of strength occurs for the elasto-plastic model which becomes noticeable at strain values above 1.5 %. A similar behavior is obtained for shear strength of 50 MPa where the influence of the slip coincides with the plastification of the boundary regions of the RVE. Nonetheless, the influence of the plastic regions is the determinant factor for the overall strength and consequently, the slip effect is not fully performed. This can be better demonstrated through the comparison of yellow and red curves which represent the shear strength of 50 MPa and the fully bonded model. It is thus illustrated that the polymer non-linearity constitutes a significant factor even in a fully bonded reinforced material.

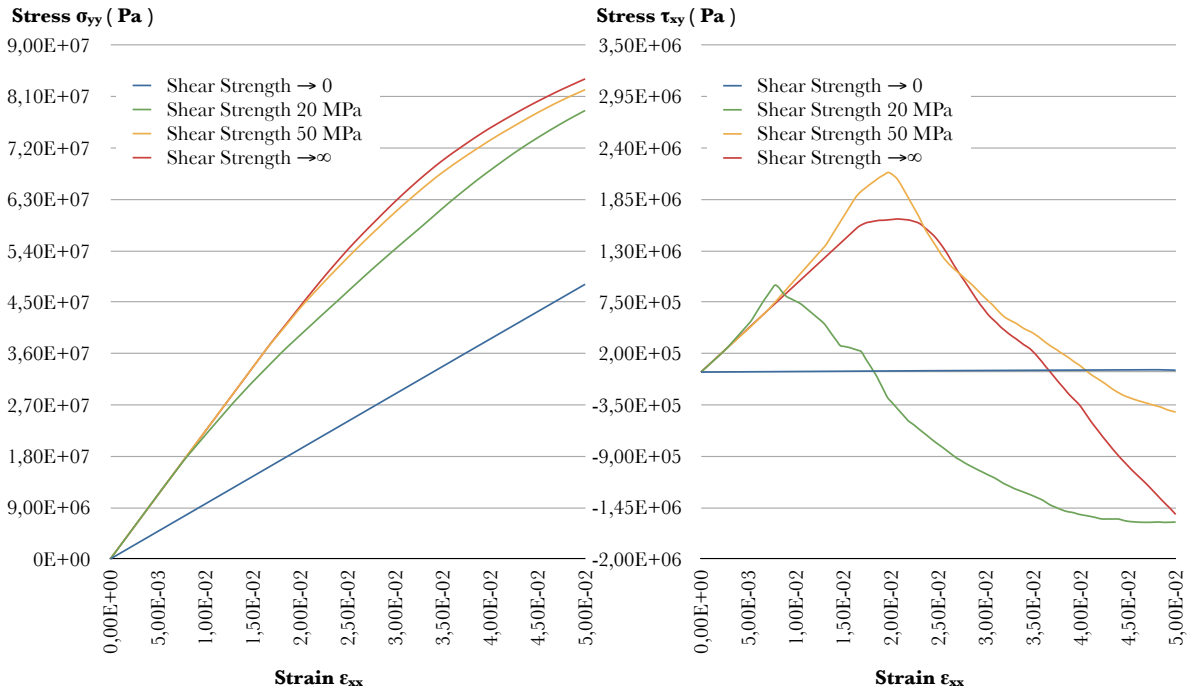

Figure 6.24: Stress-strain curves $(\sigma_{yy} - \epsilon_{xx})$ and $(\tau_{xy} - \epsilon_{xx})$ considering elasto-plastic polymer

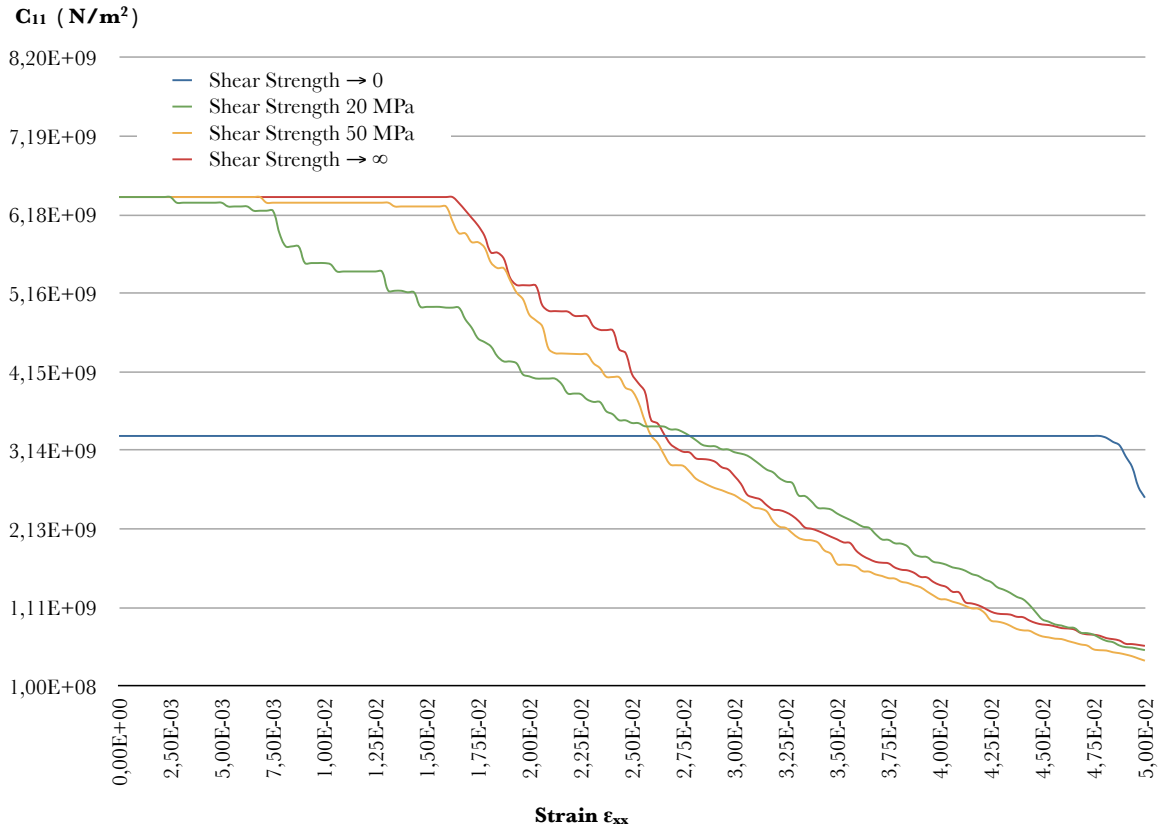

Figure 6.25: Variation of C_{11} component considering elasto-plastic polymer

This can be batter demonstrated through figure 6.25, in terms of variation of the C_{11} component. More specifically, the constitutive element C_{11} appears to be mainly influenced by the non-linear behavior of the polymer leading thus to widely lower values in comparison with the neat polume response.

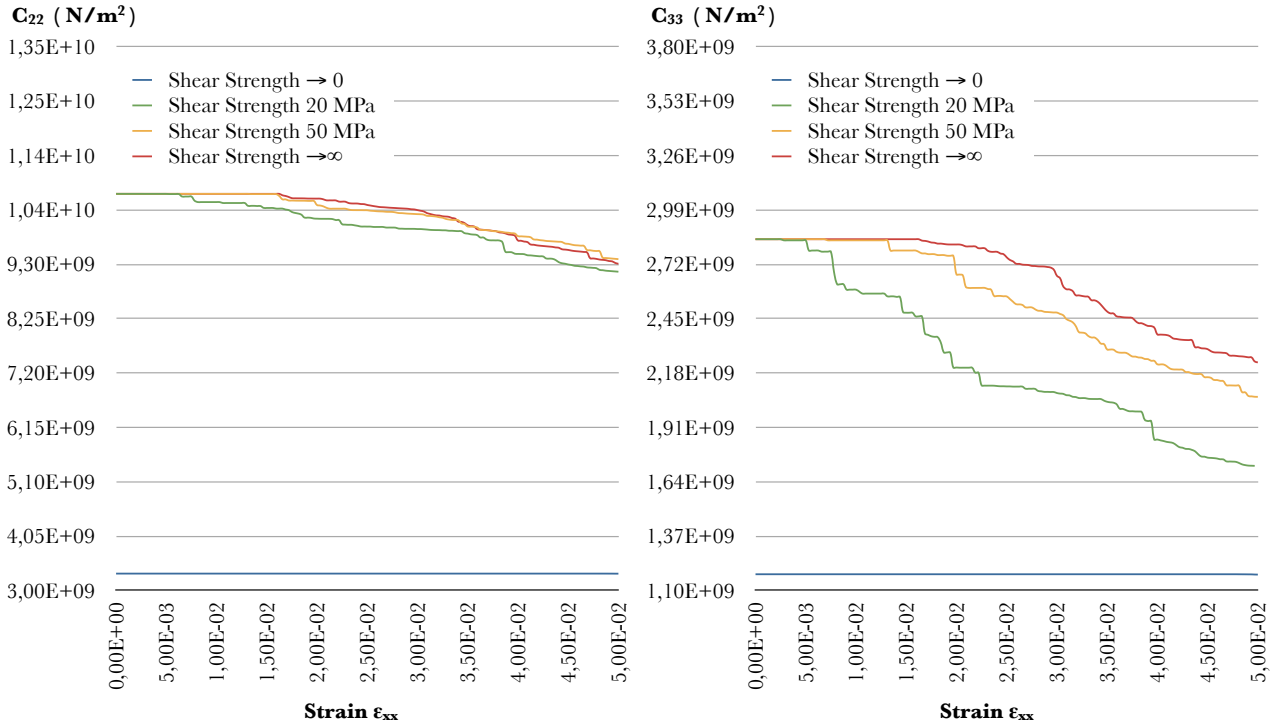

Figure 6.26: Variation of C_{22} and C_{33} components considering elasto-plastic polymer

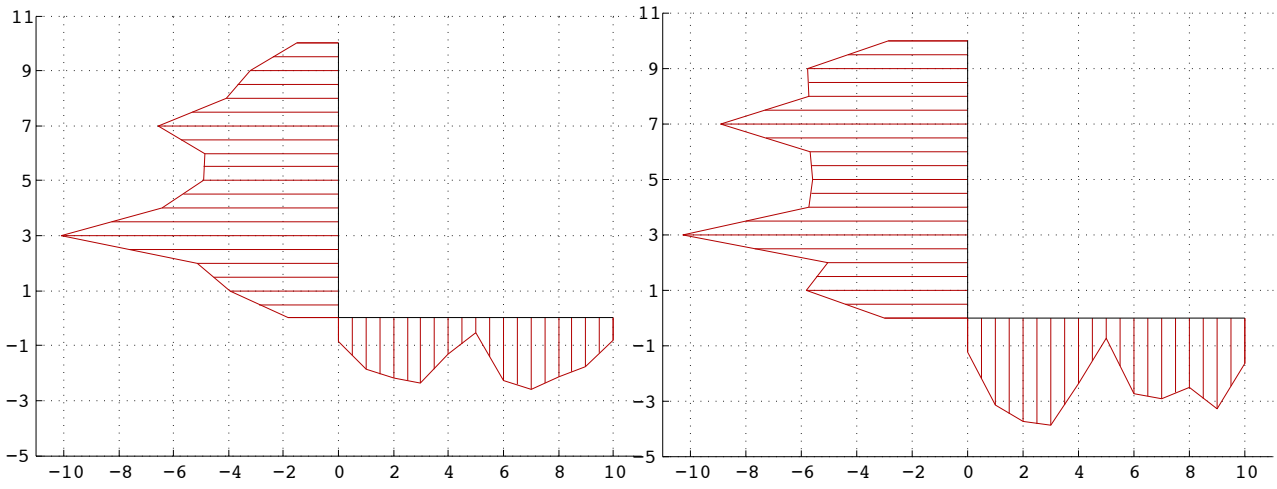

Figure 6.27: Normal nodal forces - Fully bonded model for linear elastic and elasto-plastic polymer behavior respectively.

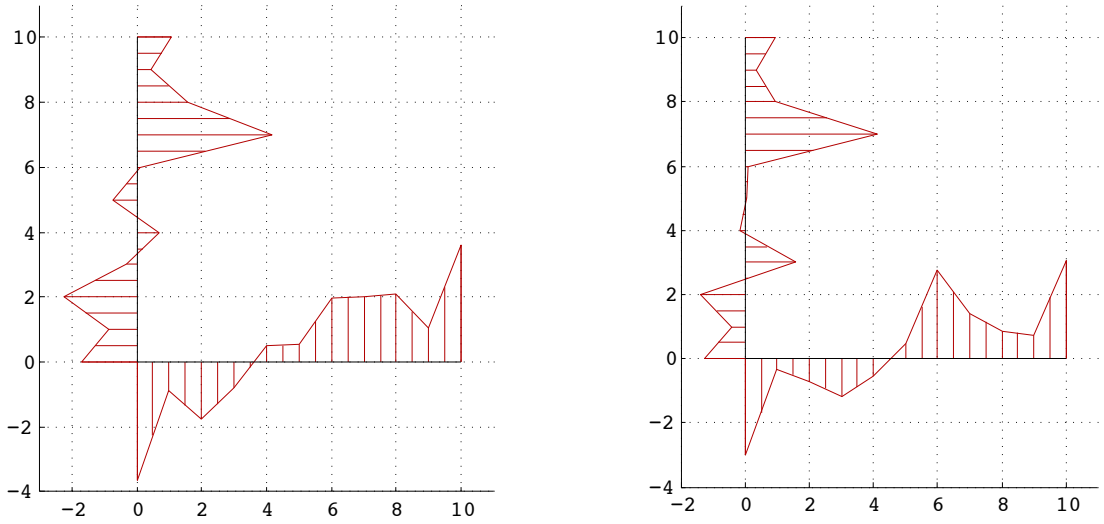

Figure 6.28: Shear nodal forces - Full bond model for linear elastic and elasto-plastic polymer behavior respectively.

Figures 6.27 and 6.28 depict the stiffness distribution over the boundary of the RVE, in terms of normal and shear nodal forces. The developed plastic region in the case of elasto-plastic polymer behavior becomes noticeable through the normal forces distribution. The reinforcing fibers generate a nonuniform displacement field leading thus to the plastification of non-reinforced regions and consequenlty to the limitation of the boundary stiffness and the overall strength.

6.2.2 Normal Strain in Y-direction

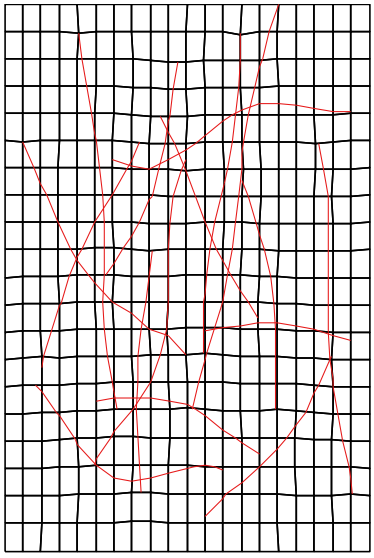

Figure 6.29: Deformed configuration of the RVE for ϵ_{yy}

Linear Elastic Polymer

As depicted in the following stress-strain curve, an identical behavior with the strain mode in x-direction is obtained for the neat polymer, leading to a final strength of 166 MPa while for the other cases a significant difference is noticed in the overall response. More specifically, a full bond model of the reinforcing fibers leads to a strength of 532 MPa for normal strain in y-direction versus 320 MPa for normal strain in x-direction. It becomes now evident that the fiber distribution and especially the direction of their axes is a determinant factor for the distribution of the overall stiffness and consequently for the strength of the RVE. Furthermore, the fact that the major part of the fibers is placed along the y axis, means a more noticeable influence of the slip effect over the RVE's response.

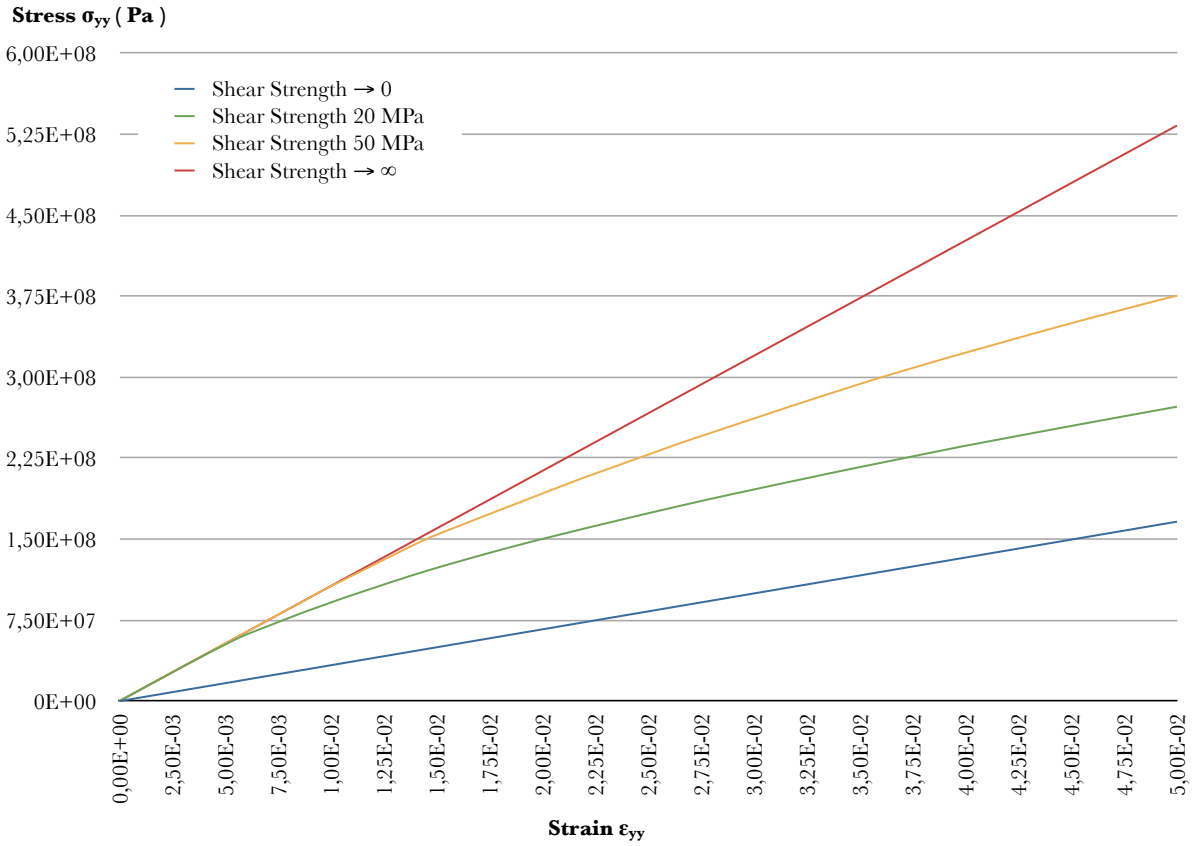

Figure 6.30: Stress-strain curve ($\sigma_{yy} - \epsilon_{yy}$) considering linear elastic polymer

Concretely, the model of 20 MPa shear strength reaches a normal stress of 272 MPa while for the first mode, the corresponding stress is 226 MPa. Thus, we observe a loss factor of 0.48 for the mode of y-direction and 0.29 for the mode of x-direction. Almost half of the full bond model strength is lost due to the slip effect making thus clear the contribution of random geometry and direction of the reinforcing fibers to the overall response. Figure 6.30 illustrates clearly this loss of strength in terms of stress-strain curves, namely between red and green curve.

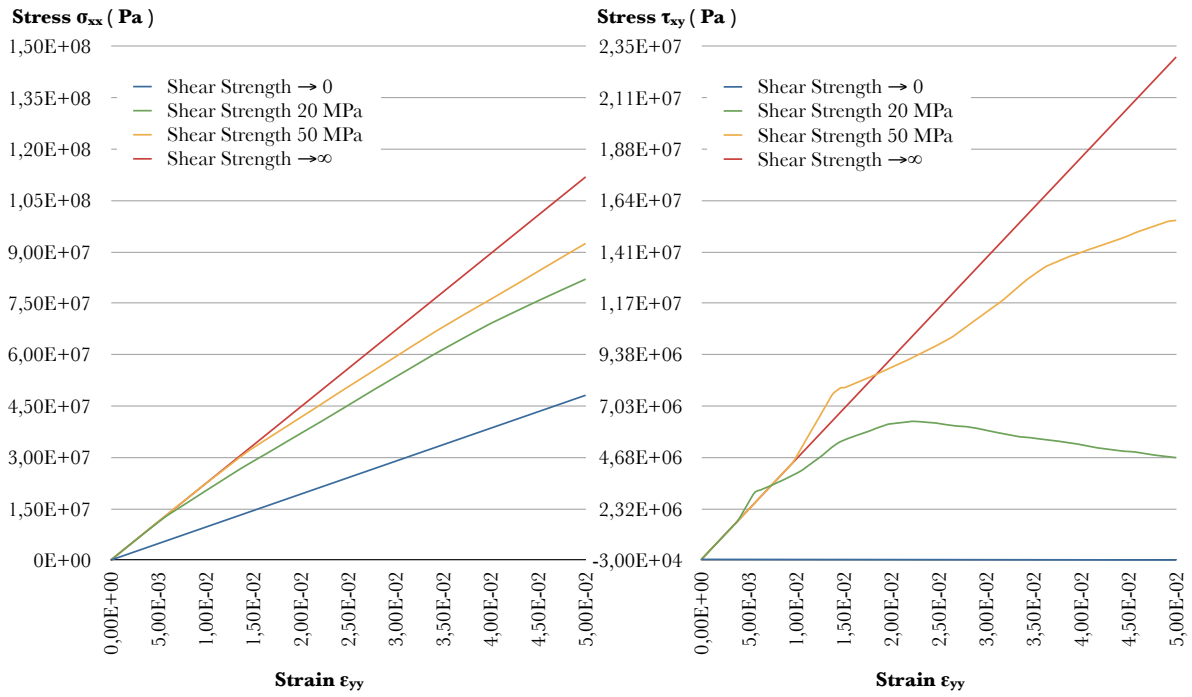

Figure 6.31: Stress-strain curves $(\sigma_{xx} - \epsilon_{yy})$ and $(\tau_{xy} - \epsilon_{yy})$ considering linear elastic polymer.

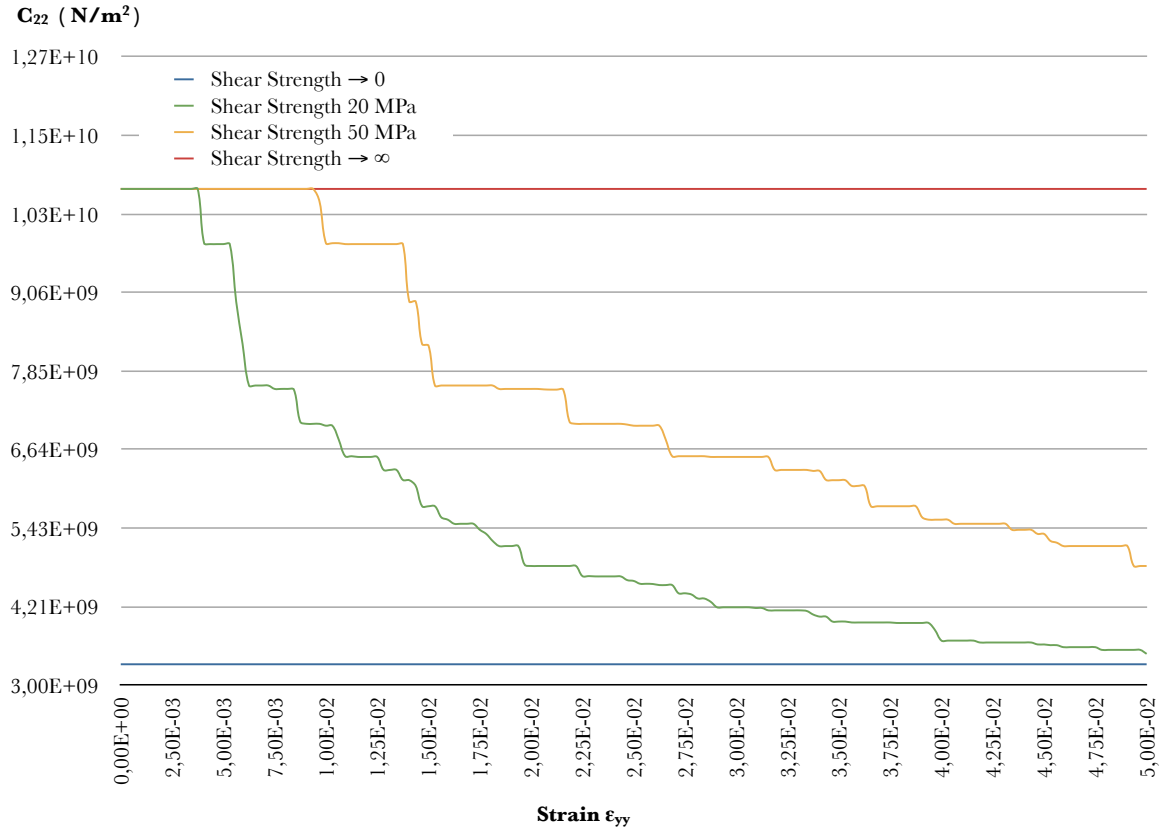

Figure 6.32: Variation of C_{22} component considering linear elastic polymer

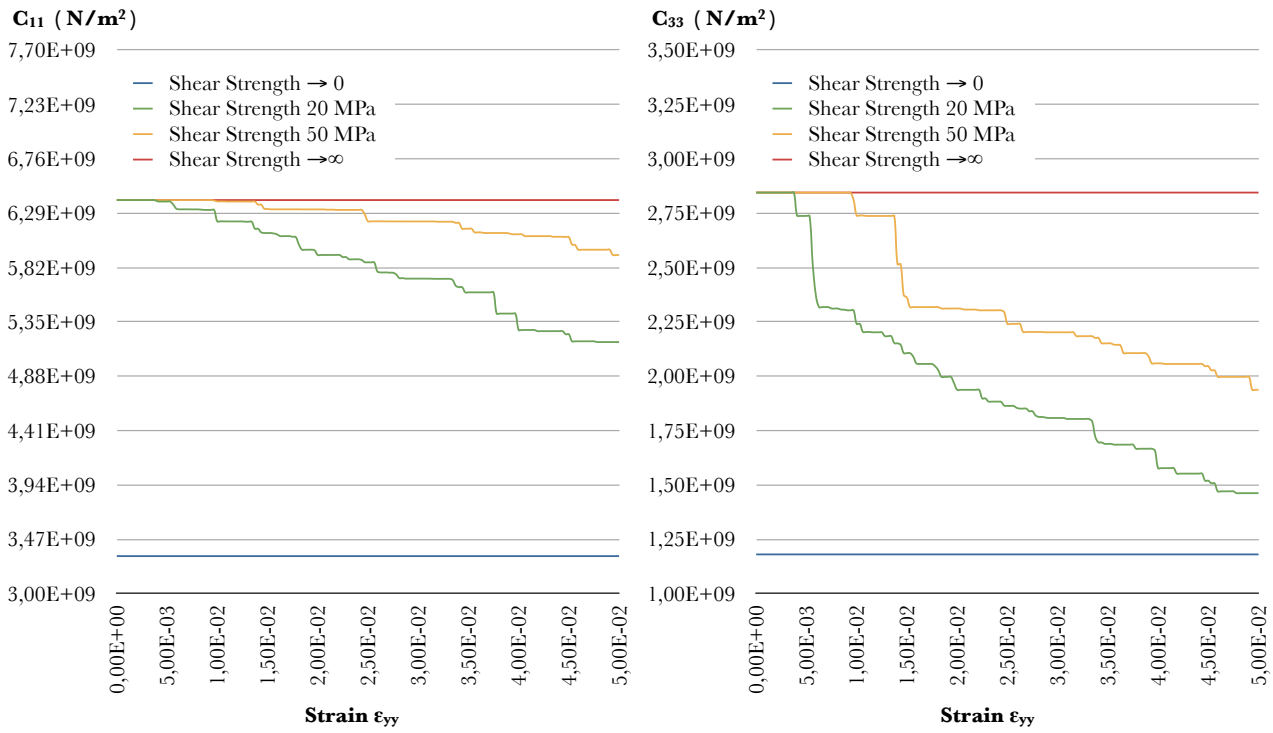

Figure 6.33: Variation of C_{11} and C_{33} components considering linear elastic polymer

Elasto-plastic Polymer

As demonstrated through the previous modal analysis, a plastic region is expected to be generated along the direction of the imposed strain, namely at the bottom and the top of the RVE for the case of normal strain in y-direction. The following stress-strain curve, in terms of σ_{yy} and ϵ_{yy} respectively, depicts this behavior and hence the contribution of the fibers. A full bond model and even those of shear strength of 20 and 50 MPa lead to a reduction of the strength due to the fact that the reinforcement is concentrated in the center of the RVE generating thus a nonuniform distribution of the stiffness. As a result, the imposed displacement field has a greater effect on non-reinforced regions and specifically on the displaced boundaries. In terms of loss of strength, for the full bond model the strength is reduced from 532 MPa to 262.8 MPa or 50.6 % while for a slight bond model, that is shear strength of 20 MPa, the correspoding loss percentage is 25.1 %, namely from 272 MPa to 203.7 MPa.

Consequently, not only the random shape but mainly the spatial distribution of the reinforcing fibers is the determinant factor of the RVE's strength and overall response. In addition, a more uniform distribution of the reinforcing components and hence of the total stiffness, leads to a more effective performance of the representative volume. Now, a similar conclusion can be drawn for the other stress components whose variation is illustrated in the following figures (6.34 and 6.35).

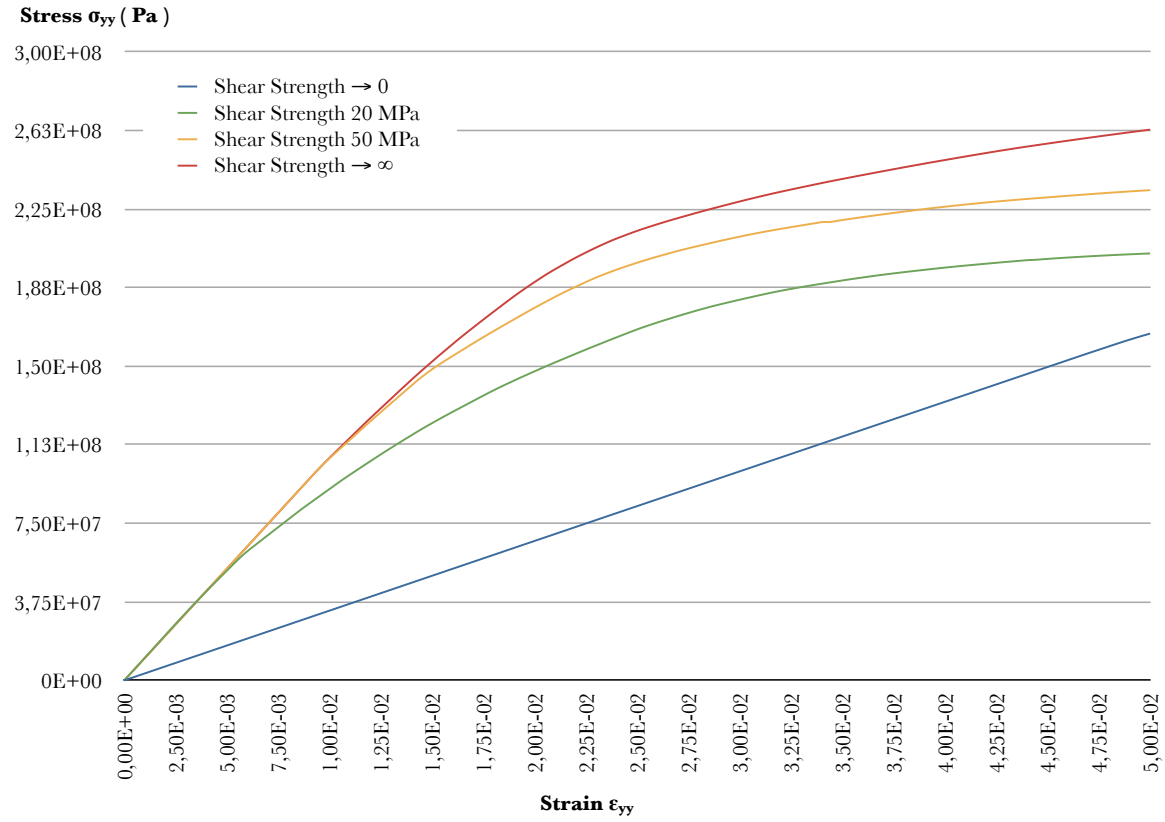

Figure 6.34: Stress-strain curve ($\sigma_{yy} - \epsilon_{yy}$) considering elasto-plastic polymer

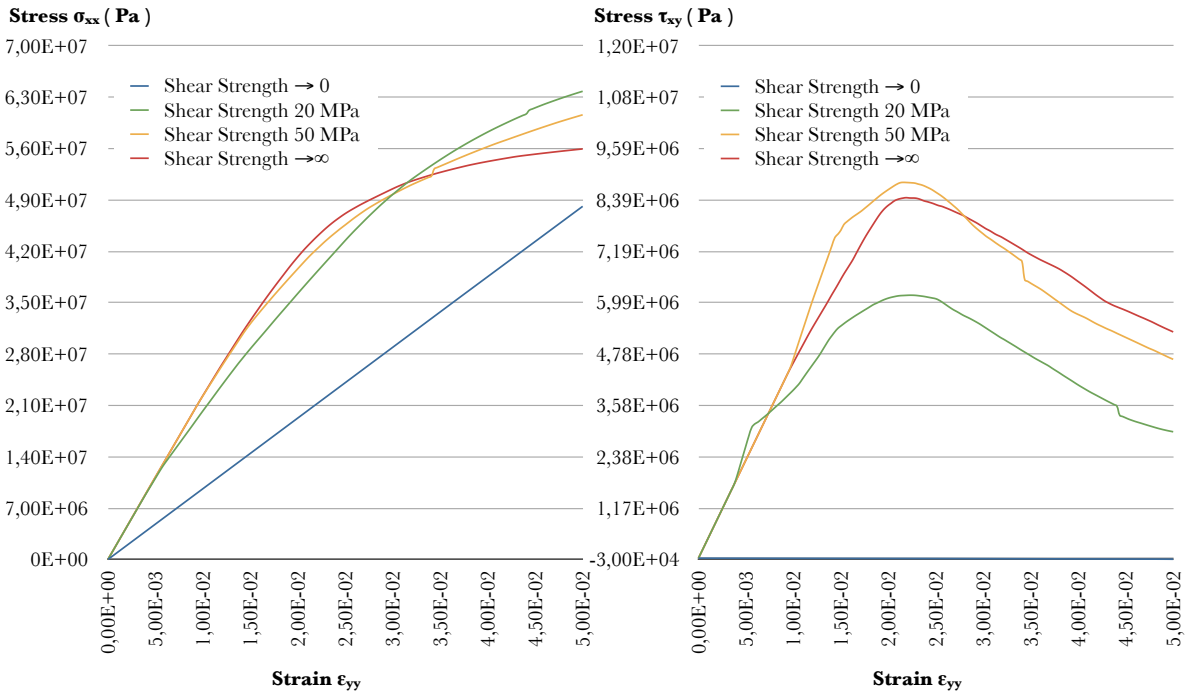

Figure 6.35: Stress-strain curves ($\sigma_{xx} - \epsilon_{yy}$) and ($\tau_{xy} - \epsilon_{yy}$) considering elasto-plastic polymer

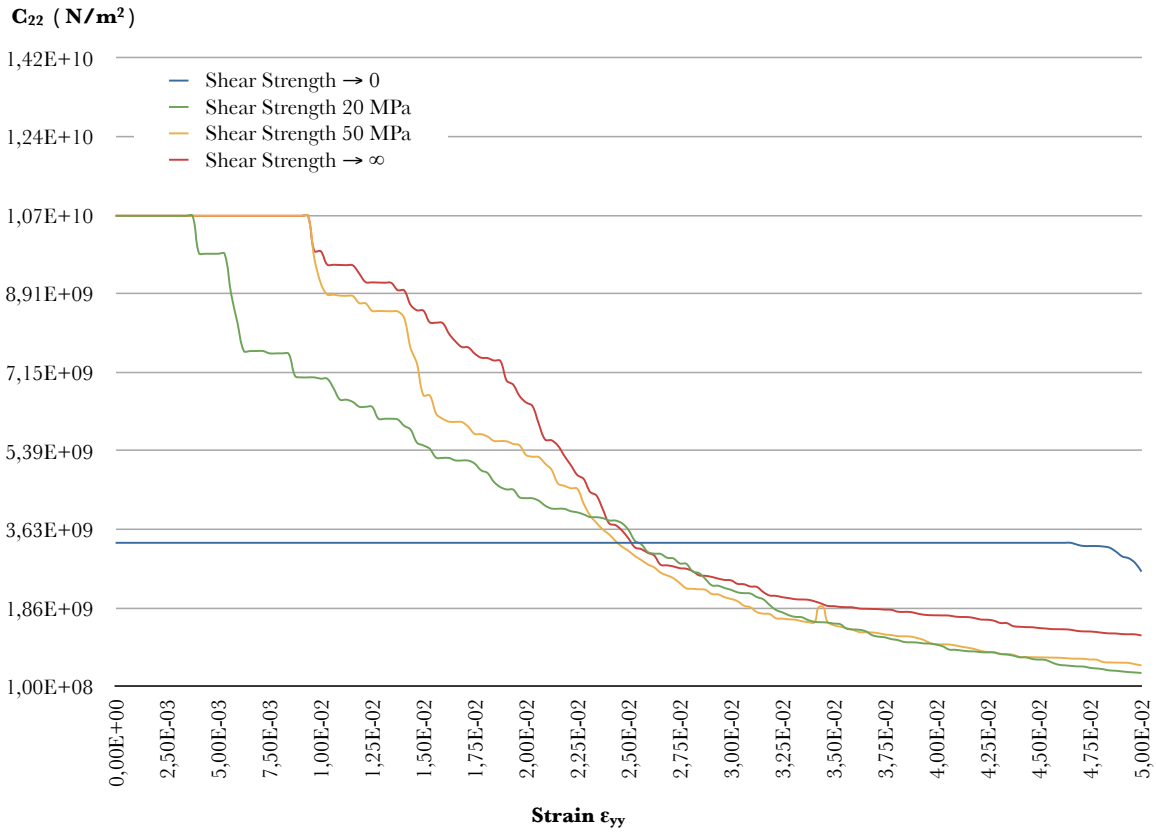

Figure 6.36: Variation of C_{22} component considering elasto-plastic polymer

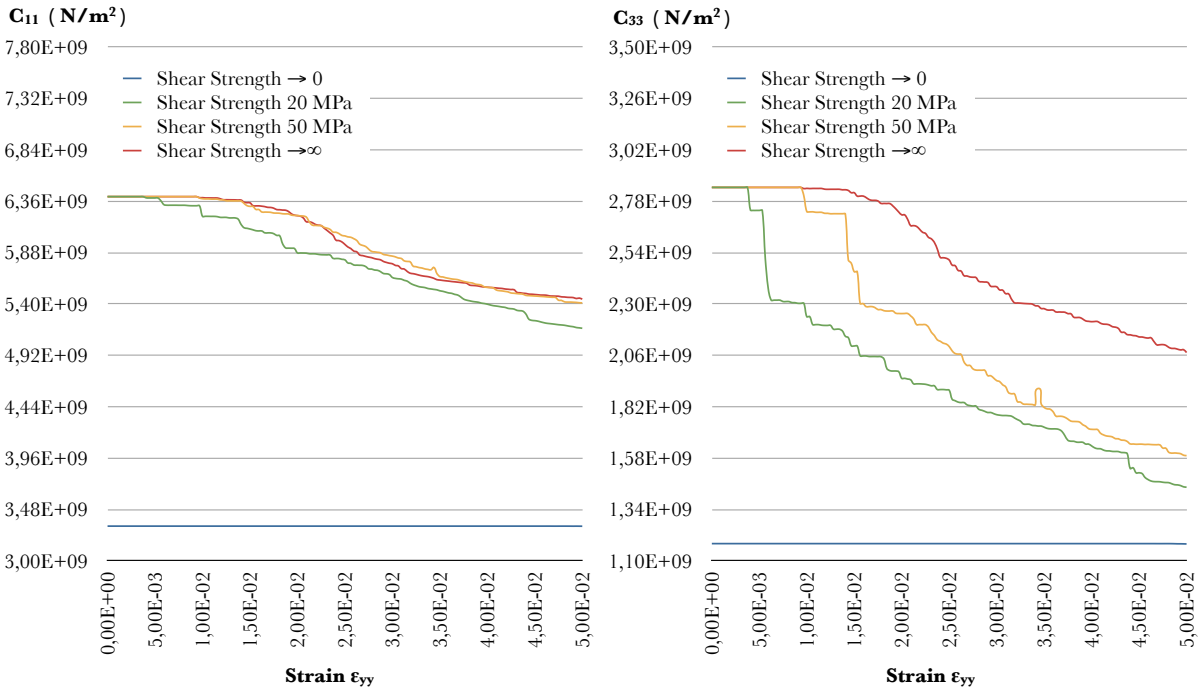

Figure 6.37: Variation of C_{11} and C_{33} components considering elasto-plastic polymer

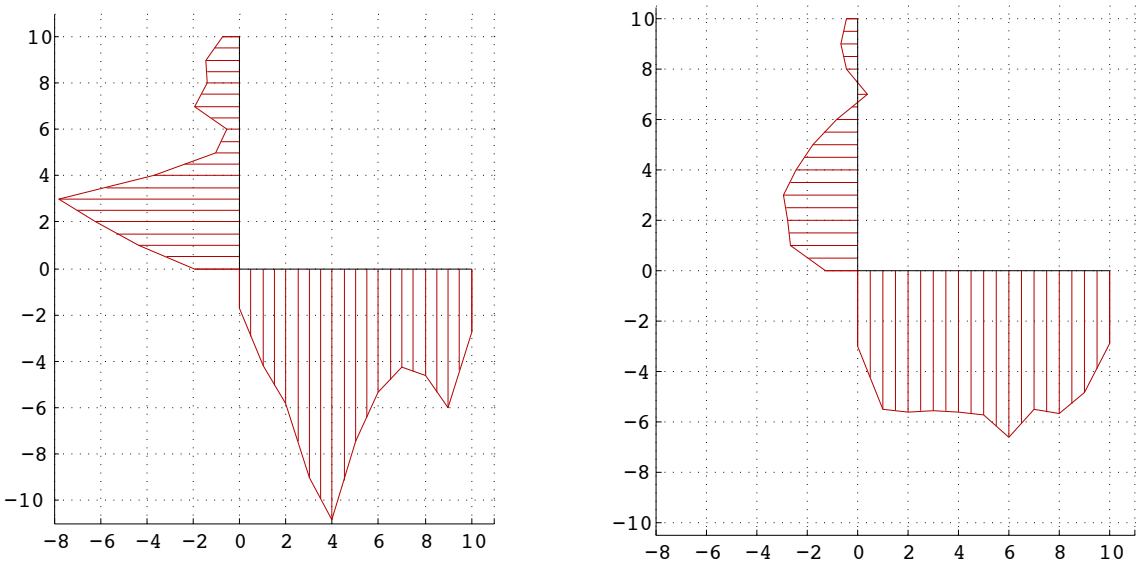

Figure 6.38: Normal nodal forces - Fully bonded model for linear elastic and elasto-plastic polymer behavior respectively.

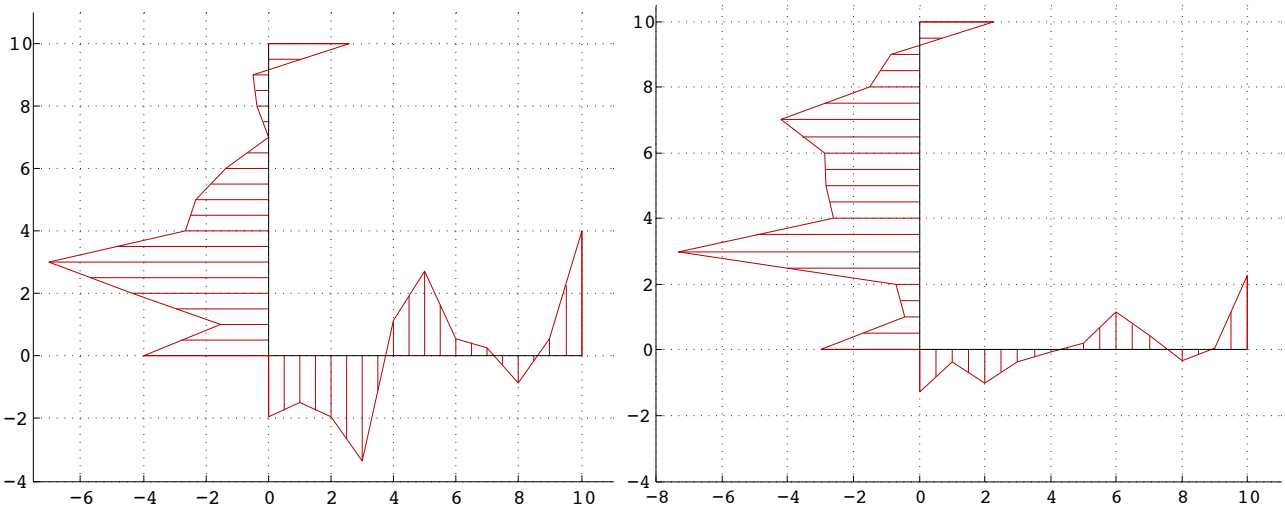

Figure 6.39: Shear nodal forces - Fully bonded model for linear elastic and elasto-plastic polymer behavior respectively.

It becomes evident through figure 6.39 that elasto-plastic behavior of the polymer leads to the plastification of the entire boundary of the bottom side, making thus unnoticeable the contribution of the fibers, even if they are in a full-bond state. Furthermore, only the corner regions of the bottom side remain in the elastic domain, since there is no reinforcement at the left and right sides, along y-axis. Hence, the higher percentage of fibers along y-axis leads to this limitation of the strength, as also illustrated in figure 6.34.

6.2.3 Numerical Results

The results of the above performed analyses are presented in the following tables in terms of normal and shear stresses. They are dived in two parts, one for the case of linear elastic model of the surrounding polymer and one for elasto-plastic behaviour. Each part presents the stress components σ_{xx}, σ_{yy} and τ_{xy} for the four cases of shear strength and for normal strains in both x and y directions.

Linear Elastic Polymer

	Normal Stress σ_{xx} (MPa)	Normal Stress σ_{yy} (MPa)	Shear Stress τ_{xy} (MPa)
Normal Strain in x-direction			
Shear Strength $\rightarrow 0$	166.169	48.116	0.026
Shear Strength 20 MPa	226.493	83.738	-0.100
Shear Strength 50 MPa	280.263	98.558	-0.702
Shear Strength $\rightarrow \infty$	320.107	111.864	4.697
Normal Strain in y-direction			
Shear Strength $\rightarrow 0$	48.116	116.169	-0.026
Shear Strength 20 MPa	82.018	272.628	4.569
Shear Strength 50 MPa	92.458	375.462	15.529
Shear Strength $\rightarrow \infty$	111.864	532.953	23.011

Table 6.3: Numerical Results for Linear Elastic Polymer

It becomes now clear, in numerical terms, that the RVE's response varies significantly under the influence of non-linear effects concerning the microstructural components and their mechanical interaction. Apart from the loss of strength due to the interfacial mechanism, the microstructural behavior is directly dependent on the random nature of its model. As already mentioned, and illustrated in figures of nodal forces, the non-reinforced faces of the representative volume are intensively stressed compared to the interior of the structure, leading thus to the inability of further loading, since the boundary nodes define the overall moduli. On the other hand, a face reinforced cell, or even a more uniform reinforcement, would lead to a significantly higher strength, preventing the plastification of the faces.

Elasto-plastic Polymer

	Normal Stress σ_{xx} (MPa)	Normal Stress σ_{yy} (MPa)	Shear Stress τ_{xy} (MPa)
Normal Strain in x-direction			
Shear Strength $\to 0$	165.589	48.108	0.019
Shear Strength 20 MPa	181.775	78.557	-1.605
Shear Strength 50 MPa	186.701	82.207	-0.428
Shear Strength $\to \infty$	195.394	84.096	-1.524
Normal Strain in y-direction			
Shear Strength $\to 0$	48.116	165.514	-0.025
Shear Strength 20 MPa	63.797	203.764	2.960
Shear Strength 50 MPa	60.589	233.976	4.657
Shear Strength $\to \infty$	55.941	262.853	5.298

Table 6.4: Numerical Results for Elasto-plastic Polymer

Chapter 7

Conclusions and Recommendations

This chapter summarizes the conclusions with regard to the investigated first-order homogenization method in the framework of the multi-scale approach and concurrently recommends some future reasearch perspectives and directions.

7.1 Conclusions

The objective of this thesis was the code development of a multi-scale modelling technique, a necessity that derives from the complex property relations of heterogeneous materials. It is evident that performing straightforward parametric experimental measurements on a number of material samples is a hardly feasible task. Furthermore, it is also impossible to follow a brute force approach and generate a finite element mesh that accurately represents the microstructure and enables the numerical computation of the response of a macroscopic structural component within a reasonable amount of time on todays computational systems. Consequently, the examined first-order homogenization scheme constitutes a powerful strategy which can adequately serve the above purposes.

The most significant points of this technique, according to the developments of the present work, can be summarized in the following observations:

i. There is no need for constitutive assumption on the macrolevel of the structure but only the mechanical properties of the microscopic components are required. According to the assumptions of the method, the macroscopic constitutive behavior is computed through the microscale boundary value problem. Moreover, this can be easily achieved in the framework of the finite element analysis, in terms of boundary stiffness and nodal forces, as illustrated in Chapter 2.

ii. The formulation of the method enables the incorporation of all kinds of non-linear effects. The separated and concurrently nested nature of the scales allows the modelling of heterogeneous structures under large deformations, in contrast with other homogenization approaches and techniques, where various difficulties derive from their incorporation.

iii. In this thesis the developed multi-scale method was implemented in a finite element analysis however, any appropriate solution technique may be applied. In addition, this technique is not limited to the continuum mechanics field since it enables the non-continuum modelling of the microstructure.

iv. The solution of a microscale boundary value problem for every integration point of the macroscale constitutes a demanding computational task, in terms of volume data and time, leading thus to the necessity of reduction techniques.

v. The randomness concerning geometry, orientation and distribution of the reinforcing fibers is a significant and determinant component of the microstructural and material properties as well, and should be taken into account for the sake of modelling completeness.

7.2 Future Reasearch Proposals

According to the investigated matters in the framework of this thesis, the recommended directions of a future expansion of this work can be divided into two classes, namely those concerning some solution techniques and those concentrated on the microstructural modelling.

The proposals of the first class are summarized in the following points:

i. The implementation of a fully nested multi-scale solution scheme in the case of complex and large-scale structures constitutes a forbidden method in terms of computational cost and time. The solution of a non-linear boundary value problem for every integration point is obviously a rather expensive computational task and as a result the implementation of reduction techniques becomes a necessity. Concretely, a selective usage, where non-critical regions are modelled by continuum closed-form homogenized constitutive relations (or by the constitutive tangents derived from the microstructure in case an incremental update of these tangents can be omitted, e.g. if the material hardly evolves or unloads) while in critical regions a multi-scale analysis of the microstructure is fully performed, could lead to a remarkable time-reduced solution scheme.

ii. Similarly, the time reduction of the solution procedure can be achieved with the implementation of parallel computation techniques. The RVE boundary value problems can be separately solved using parallel programming procedures.

iii. A completetely different solution technique can be employed, not only at the level of the cell but also at the macrostructure. Techniques that take into account cracks and crack propagation (X-FEM) or the implementation of the Element Free Galerkin (EFG) method would be also interesting research topics.

On the other hand, the microstructural modelling proposals include:

i. The investigation of nonlinear phenomena, such as buckling of the reinforcing fibers. Incorporation of the nonlinear behavior of the equivalent beam elements, combined with the already examined bond-stress nonlinear model would lead to notable observations concerning the effectiveness of the reinforcement.

ii. The randomness at the level of the integration point. In the present work the investigated RVE is common for all integration points and takes into account the random geometry, distribution and length of the reinforcing fibers for a given volume fraction. A future work could include a totally random microstructure for every Gauss-point where furthermore, the volume fraction and the diameter of the fibers are also arbitrary variables.

Bibliography

[1] J. Fish, T. Belytschko, *A First Course in Finite Elements*. John Wiley & Sons, 2007

[2] V. G. Kouznetsova, *Computational homogenization for the multi-scale analysis of multi-phase materials*. TU Eindhoven, 2002.

[3] C. Miehe, A. Koch, *Computational micro-to-macro transitions of discretized microstructures undergoing small strains*. Springer-Verlag, 2002.

[4] M. A. Crisfield, *Non-Linear Finite Element Analysis of Solids and Structures, Essentials, Volume 1*. John Wiley & Sons, 1996.

[5] M. A. Crisfield, *Non-Linear Finite Element Analysis of Solids and Structures, Advanced Topics, Volume 2*. John Wiley & Sons, 1997.

[6] R. de Borst, M.A. Crisfield, J.C. Remmers, C.V. Verhoose, *Non-Linear Finite Element Analysis of Solids and Structures*. John Wiley & Sons, 2012.

[7] D. N. Savvas, V. Papadopoulos, M. Papadrakakis, *The effect of interfacial shear strength on damping behavior of carbon nanotube reinforced composites*. Elsevier, 2012.

[8] O. C. Zienkiewicz and R. L. Taylor, *The Finite Element Method for Solid and Structural Mechanics*. Butterworth-Heinemann, 6 edition, 2005.

[9] Μ. Παπαδρακακης, *Ανάλυση Φορέων με τη Μέθοδο των Πεπερασμένων Στοιχείων*. Παπασωτηρίου, 2001.

[10] Μ. Παπαδρακάκης, *Πλαστική Ανάλυση Ραβδωτών Φορέων, Σύγχρονες Μέθοδοι*. Εκδόσεις ΕΜΠ, 2011.

[11] O. C. Zienkiewicz, R. L. Taylor, and J. Z. Zhu, *The Finite Element Method: Its Basis and Fundamentals*. Butterworth-Heinemann, 2005.

[12] P. Wriggers, S. O. Moftah, *Mesoscale models for concrete: Homogenisation and damage behaviour*. Elsevier, 2006.

[13] F. Feyel, J. L. Chaboche, *FE^2 multiscale approach for modelling the elastoviscoplastic behaviour of long fibre SiC/Ti composite materials*. Elsevier, 1998.

[14] H. G. Kwak, F. C. Filippou, *Finite Element Analysis of Reinforced Concrete Structures under Monotonic Loads*. University of California, Berkeley, 1990.

[15] K. J. Bathe, *Finite Element Procedures in Engineering Analysis*. Prentice-Hall, 1982.

[16] J. N. Reddy, *An Introduction to Nonlinear Finite Element Analysis*. Oxford University Press, 2004.